FUNCTIONALISED POLYMER FIBRES FOR ORTHOPAEDIC INTERFACIAL TISSUE ENGINEERING AND OTHER BIOMEDICAL APPLICATIONS

Gabriel Mecklenburg

Imperial College London

submitted in accordance with the requirements for the degree of MASTER OF PHILOSPOHY

DEPARTMENT OF MATERIALS, IMPERIAL COLLEGE LONDON

APRIL 2014

Declaration of originality

I, Gabriel Mecklenburg, hereby declare that this thesis and the work reported herein was composed by and originated entirely from me. Information derived from the published and unpublished work of others has been acknowledged in the text and references are given in the list of sources.

Copyright declaration

Abstract

Tissue engineering is a promising approach for the regeneration of a variety of human tissues, where traditional surgical repairs produce inadequate results or appropriate transplant material is in scarce supply. In orthopaedic tissue engineering, the regeneration of the bone/soft tissue interface is of special interest. However, this requires the creation of biomaterial scaffolds with controlled gradients of biochemical cues, in addition to mimicking the microstructure of the natural tissue. For this purpose, a scheme for the covalent immobilisation of biomolecule gradients on aligned synthetic nanofibre scaffolds created via electrospinning was devised. Surface-initiated atom transfer radical polymerisation allows for the controlled growth of a polymer brush containing reactive functional groups on the scaffold surface, specifically poly (glycidyl methacrylate) (PGMA), which contains epoxy groups that can conjugate to biomolecules via nucleophiles such as amines or thiols.

A PGMA-based biomolecule attachment scheme in a 2D model system was optimised. Creating a brush with a larger inter-chain spacing (by the replacement of a fraction of the ATRP initiator with an inactive molecule), as well as improving its water-swellability by incorporation of a water-soluble monomer (hydroxyethyl methacrylate, HEMA), were shown to increase the amount of peptide that could be bound to the polymer surface. Initial results indicate that this system can be used to create covalently immobilised gradients of biomolecules on aligned electrospun scaffolds.

The versatility of the ATRP-based functionalistion approach was further demonstrated by creation of brushes of Poly (2-Methacryloyloxyethyl phosphorylcholine) (PMPC) on electrospun polymer fibres. Due to PMPC's excellent haemocompatibility, these materials show great promise in vascular tissue engineering.

Contents

List of figures

List of abbreviations

ACL	Anterior cruciate ligament
ATR-FTIR	Attenuated total reflection Fourier transform infrared
ATRP	Atom transfer radical polymerization
BIBB	2-Bromo-isobutyryl bromide
BMSC	Bone marrow stromal cell
Bpy	2,2'-Bipyridyl
Dapsone-MA	Dapsone-methacrylate
diH_2O	Deionized water
DIPEA	of N,N-Diisopropylethylamine

DMF	Dimethylformamide
DMSO	Dimethyl sulfoxide
DTT	Dithiothreitol
ECM	Extracellular matrix
Fmoc	9-fluorenylmethyloxycarbonyl
Fluorescein-NHS	Fluorescein N-hydroxysuccinimide ester
GAG	Glycosaminoglycan
GMA	Glycidyl methacrylate
GPC	Gel permeation chromatography
HBTU	2-(1H-benzotriazol-1-yl)-1,1,3,3,-tetramethyluronium hexafluorophosphate
HCCA	4-hydroxy-α-cynocinnamic acid
HEMA	(Hydroxyethyl)methacrylate
NMR	Nuclear magnetic resonance
OTS	Octadecyl trichlorosilane
PBS	Phosphate buffered saline
PCL	Poly (ε-caprolactone)
PEO	Poly (ethylene oxide)
PGA	Poly (D,L-glycolic acid)
PGMA	Poly (glycidyl methacrylate)
PIB	Propionyl isobromide
PLA	Poly (D,L-lactic acid)
PLCL	Poly (D,L-lactic acid-co-caprolactone)
PLGA	Poly (D,L-lactic-co-glycolic acid)
PLLA	Poly (L-lactic acid)
PγGA	Poly (γ-glutamic acid)
PMDETA	N,N,N',N'',N''-pentamethyldiethylenetriamine
PMPC	Poly (2-Methacryloyloxyethyl phosphorylcholine)
SAM	Self-assembled monolayer
SEM	Scanning electron microscopy
TEOS	Triethoxy octylsilane
TFA	Trifluoroacetic acid
TIS	Triisopropylsilane

Acknowledgements

There are a number of people that I would like to thank for their invaluable support during my project.

Firstly I am grateful to my supervisors, Prof Molly Stevens and Dr Iain Dunlop, for the opportunity to conduct research in such a stimulating environment under their excellent guidance.

Many people both within and outside the group have helped me in countless ways. Dr Lesley Chow has been a great help both in planning my project and resolving any issues that have arisen along the way and by generally taking me under her wing.

Furthermore I would like to thank Dr Seth McCullen for his introduction to electrospinning and his generous offers of help throughout the months, Dr Jonathan Weaver for his indispensable insight into chemical synthesis, Dr Anthony Callanan for help with the design of the electrospinning setup, Dr Stéphane Kena-Cohen for help with ellipsometry and Dr Min Tang for help with GPC.

I would like to thank Prof Anthony Bull, Mr Andrew Wallace, Mr Peter Reilly, Prof Roger Emery and Dr Toby Baring for their input on the surgical and biomechanical aspects of my project.

Additionally, all the members of the Stevens Group have had a part in making these months enjoyable, both by always lending an open ear for discussions and by creating a wonderfully stimulating atmosphere both in and out of the work place.

I would also like to gratefully acknowledge the work done by the technicians who maintain the instruments throughout the department and are always at hand with help and advice.

Finally I express my gratitude to EPSRC for the funding provided.

1 Introduction

1.1 Motivation

Versatile methods for the modification of the surface functionality of synthetic materials is of great importance in a range of medical fields. Where these materials come into contact with the human body, tailoring the surface property allows one to adjust the body's response in a controlled fashion. The work presented in this thesis centers on the development of such a versatile surface modification system for polyesters, a commonly used class of synthetic polymers for biomedical applications.

Most directly, this work was motivated by the need for novel ways of creating tissue engineering scaffolds with gradient properties for orthopaedic applications. Repair of interfaces in the musculoskeletal system between bone and soft tissues such as ligaments, tendons and cartilage remains an important challenge in this field.[1–3] Prominent examples of this are surgical interventions after tears of the supraspinatus tendon located in the shoulder's rotator cuff and the anterior cruciate ligament (ACL) in the knee. Supraspinatus tendon tears are present in roughly 30% of the population over the age of 60,[4] and, extrapolating from 2002 figures for New York State,[5] 160,000 repair procedures are performed annually in the USA. Similarly, figures for annual ACL repair procedures range from 60,000-175,000.[6] Both ACL and rotator cuff injuries are associated with a loss of soft tissue around the tear, which makes it difficult or sometimes impossible to directly suture the torn ends together with satisfactory results.[7,8] Autografts can provide satisfactory outcomes for ACL repair, although they may be associated with donor site morbidity.[7] For rotator cuff repair, where no universally accepted choice of graft material exists, re-failure rates between 11% and 94% are reported, depending on factors such as tear size, patient age etc.[5] A common theme in unsatisfactory repair outcomes is that the complex native interface, which is made up of a series of distinct tissue types in order to create a strong bond with a gradual transition in properties is not usually re-established by traditional repair techniques.[9,10]

To avoid the problems associated with auto- and allografts, such as limited availability, unfavourable immune response or donor site morbidity,[10] it is desirable to create artificial scaffolds which stimulate re-growth of the natural tissue , while degrading over time. Importantly, since the graft would ideally convert the damaged site to its pre-injury state over time, long-term outcomes should significantly improve. Such tissue engineering approaches have traditionally focussed on a single tissue type, i.e. have attempted to recreate only tendon/ligament.[11,12] Recently however, the field of interfacial tissue engineering has begun to attract more attention, as the shortfalls of simpler approaches are now coming to light (see section1.3.4). A scaffold for regeneration of the tendon/ligament-bone interface should fulfil the following conditions:

- Appropriate mechanical properties to sustain loads similar to the native tissue. The modulus and failure stress of the supraspinatus tendon can reach up to 270 and 16 MPa respectively.
- A microstructure that mimics the physical makeup of the extracellular matrix (ECM) of the different tissues. Bone and tendon/ligament ECM are made up of a network of collagen fibrils ranging from 100-500nm in diameter with varying degrees of alignment.
- Biodegradability over time-scales comparable to the rate of tissue neoformation.
- A pattern of biochemical signals guiding cells towards the phenotype relevant to the different tissues.

Electrospinning is a technique that is widely studied for applications in tendon/ligament tissue engineering due to the fact that constructs which mimic the aligned nanofibrous ECM of the tendon/ligament substance can easily be created, which has been shown to result in desirable cell behaviour.[13,14] Poly (ε-caprolactone) (PCL) is chosen as a material for initial trials due to its biocompatibility and biodegradability (as attested by FDA approval), adequate mechanical properties and relatively low cost. Alternatives such as polylactide (PLA) with different mechanical properties and degradation rates will

subsequently be investigated. Both have previously been used in biodegradable devices such as sutures and fixation screws as well as a number of tissue engineering studies.[15–17]

Like most synthetic materials, PCL and PLA in their unaltered form are not recognized well by cells, which means that tissue neo-formation is not stimulated to a significant extent. Using the living radical polymerization technique of atom transfer radical polymerization (ATRP), reactive polymer brushes with well-defined functionality and molecular weight distribution can be grown from initiators previously immobilized on the fibre surface. Living radical polymerization techniques have recently attracted much attention in a wide variety of fields due to their controllability and versatility.[18] We have chosen to investigate and subsequently adapt the modification route previously described for a PCL film system by Xu *et al.*[19], who used polymer brushes containing epoxy groups to immobilize biomolecules. By increasing the spacing of the polymer brush, and incorporating a water-soluble monomer, a sparser, swellable brush can be created, which will allow biomolecules to more easily attach along the whole length of the brush.

Furthermore, by building on the "controlled filling method" described by e.g. Shi *et al*.[20], where gradual immersion in a biomolecule solution resulted in formation of a biochemical gradient on a fibrous scaffold, it will in principle be possible to create distinct regions with specific bioactivity as required for an interfacial tissue engineering construct. A schematic depiction of the implantation of such a biphasic scaffold is seen in Figure 1.

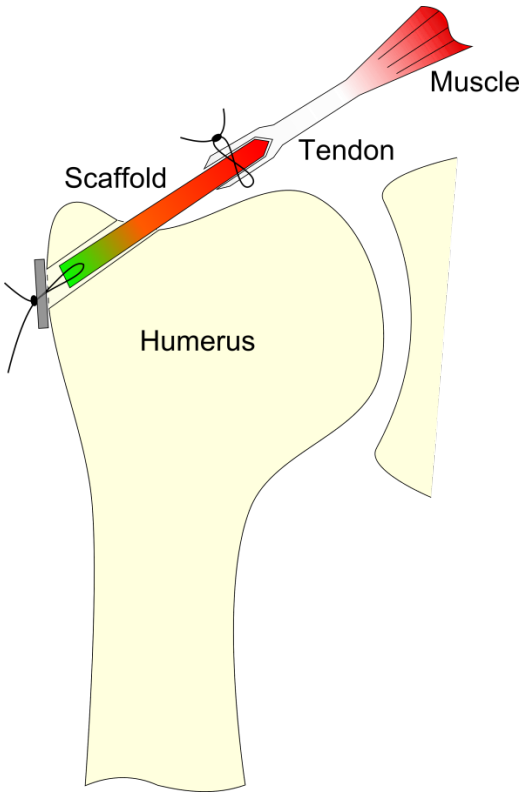

Figure 1: Concept of an artificial interpositional supraspinatus graft. Red denotes tenogenic, green osteogenic bioactivity of the scaffold.

While the main areas of application of the scaffolds developed in this project were envisioned to be in rotator cuff and ACL repair, it is worth bearing in mind that fibrous biomaterials with tailorable surface properties could find application in many biomedical applications, including outside of tissue engineering. The usefulness of the functionalization platform described here rests largely on the highly diverse range of methacrylate-monomers that are available, and which can be immobilised on polyester fibres with only minor modifications to the manufacturing methods.

Two such studies will be described in the final chapters of this thesis:

- Creation of brushes of a zwitterionic polymer, PMPC, to create highly haemocompatible electrospun scaffolds for cardiovascular tissue engineering.

- Evaluation of the feasibility of creating brushes of a polymerised antibacterial drug, dapsone, on polymer surfaces.

1.1.1 Scope of the thesis

The work in this project focuses on the development of a well-controlled functionalization scheme for the creation of biochemical gradients on electrospun scaffolds composed of biodegradable polyesters such as PCL, focussing on applications in orthopaedic interfacial tissue engineering. The key enabling technology developed is a well-controlled 2D model, which can be used to rapidly optimise reaction conditions for a new monomer system, before translation into functionalization of a fibrous 3D material.

Based on an initial scheme, whereby PGMA brushes are used for immobilisation of biomolecules onto PCL surfaces through free amine/thiol groups, an optimised attachment scheme was created and evaluated it in both 2D and 3D model systems. Additionally presented are exploratory results relating to (a) the creation of covalently bound biomolecule gradients on electrospun PCL scaffolds, and (b) two unrelated polymer-brush systems for biomedical applications.

1.1.1.1 Functionalization of polymer films (model system)

In order to characterize the functionalization scheme, it is desirable to use a system that is easier to analyze than the complex three-dimensional environment of the electrospun scaffold. After significant exploratory work, a robust system was established, based on short-chain PCL covalently immobilised onto silicon wafers via an isocyanate-terminated silane. The ability of ellipsometry to measure film thicknesses with nanometer accuracy allows accurate monitoring of reaction progress at each step, and of subsequent biomolecule incorporation efficiency. This system is then used to optimise the reaction parameters for surface initiated ATRP of:

- Simple PGMA brushes;
- PGMA brushes co-polymerised with water-soluble PHEMA to create a water swellable brush;

- The above brushes grown from surfaces on which a fraction of the initiator molecules is replaced with inert molecules to create a sparser brush.

The efficiency of covalent incorporation of a variety of amine- and thiol-functionalised molecules into these brushes is then evaluated and compared.

1.1.1.2 Functionalization of electrospun samples

Based on the data gained by a thorough exploration of parameter space using the 2D model system, appropriate conditions for functionalization of fibrous polymer scaffolds have been determined. This part of the project builds on previous work carried out in the group by Dr Seth McCullen, who has established procedures for creating fibrous meshes with varying diameter and degree of alignment of fibres. Proof-of-concept studies for the feasibility of this approach have been carried out successfully using a fluorescent model molecule. One alternative graft polymer system was also evaluated, which has shown promise in the 2D model.

1.1.1.3 Biomolecule gradients on fibrous scaffolds

The aim of the project was to create a fibrous scaffold that is able to direct cell behaviour towards recreation of the native tendon/ligament-bone interface. The concept of the creation of a scaffold containing smooth gradients of osteogenic and tenogenic bioactive agents created by gradual immersion of scaffolds previously activated for biomolecule attachment by graft polymerization is depicted schematically in Figure 2. While this has not been completed, preliminary results demonstrating the covalent immobilisation of a gradient of a fluorescent model molecule are presented.

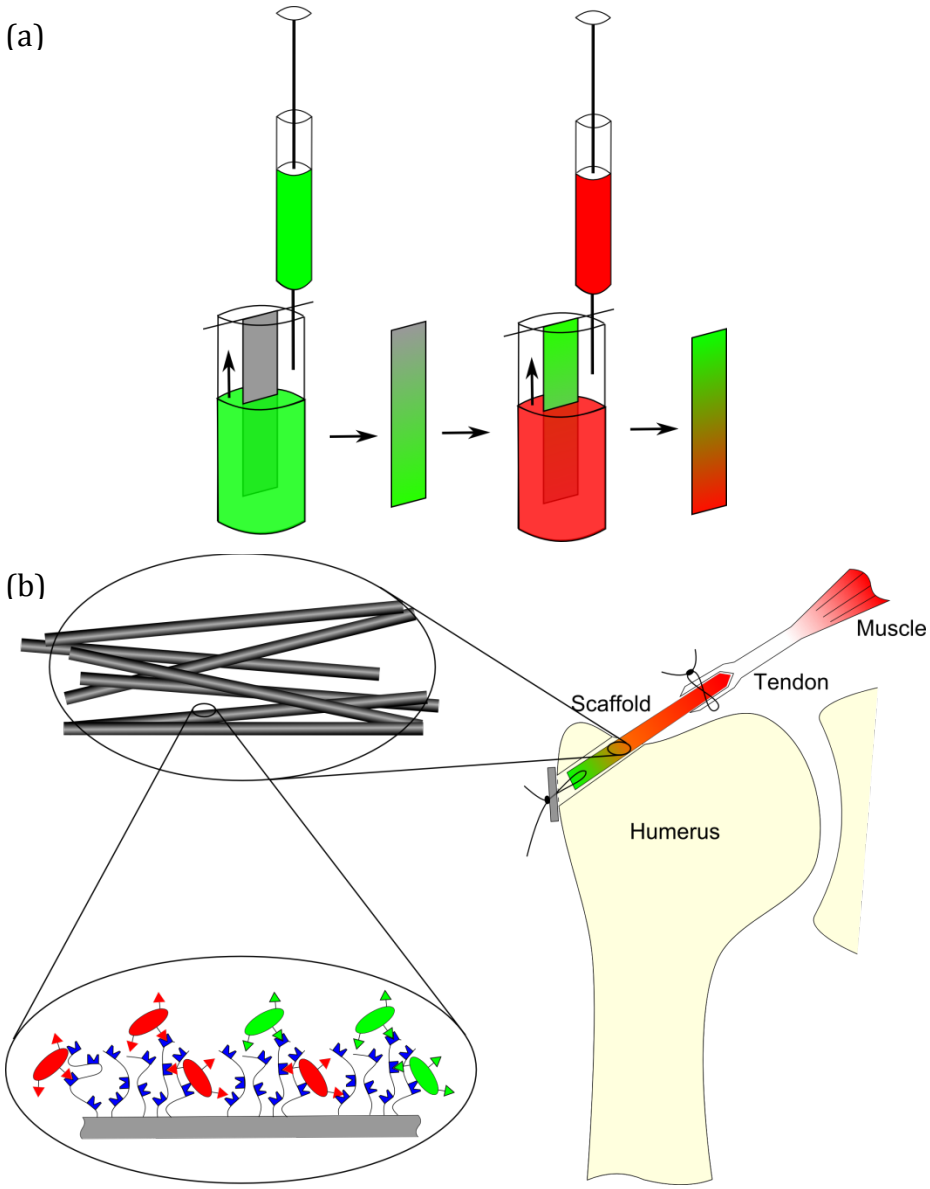

Figure 2: Schematics depicting (a) dual gradient creation by the "controlled filling method" and (b) graft implantation for rotator cuff repair. Red denotes biomolecules with tenogenic, green with osteogenic activity.

1.2 Structure, biology and biomechanics of tendon/ligament

Any attempt at engineering the bone-tendon/ligament system needs to be founded on knowledge about the structure and biomechanics of both the bulk tissues and the interface. The information below refers mainly to the supraspinatus-bone complex, but applies very similarly to the anterior cruciate ligament (ACL) and other tendons and ligaments in the body. Tendons act to transmit forces from muscles to bone, while ligaments stabilize joints by linking bone to bone. This means that ligaments tend to be somewhat more compliant than tendon to provide flexibility to the joint and absorb the energy of sudden impacts.

1.2.1 Tendon proper

The structure of the tendon proper has been described in great detail; for a review see e.g. M. Benjamin,[21] on which most of the following description is based. High failure stress and elastic modulus are necessary for tendon to fulfil its structural functions, with exact values depending on the location in the body and within each tendon/ligament.[22] For the supraspinatus tendon, the tensile failure stress reaches 16 MPa and the modulus 270 MPa in the strongest part of the tissue, while in other regions of the same tendon, these can be as low as 4 and 50 MPa respectively.[23] These properties result from an extracellular matrix (ECM) consisting of highly aligned type I collagen fibrils 100-500 nm in diameter[24] arranged in a hierarchical fashion into fascicles (as depicted in Figure 3), which provides high stiffness, while preventing crack propagation.

The bulk of the cell population of mature tendon consists of a sparse distribution of tenocytes, a specialized type of fibroblasts. They are aligned in rows with their long axes parallel to the collagen fibrils. Populations of progenitor and stem cells exist which provide the tendon with limited regenerative potential.[25] Healing is often also aided by migration of cells from the surrounding tissues into the tendon.[24] Despite the limited regenerative potential provided by the native cell population, positive *in vivo* results have

been reported for implantation of tissue engineering scaffolds without prior *ex vivo* cell seeding.[26]

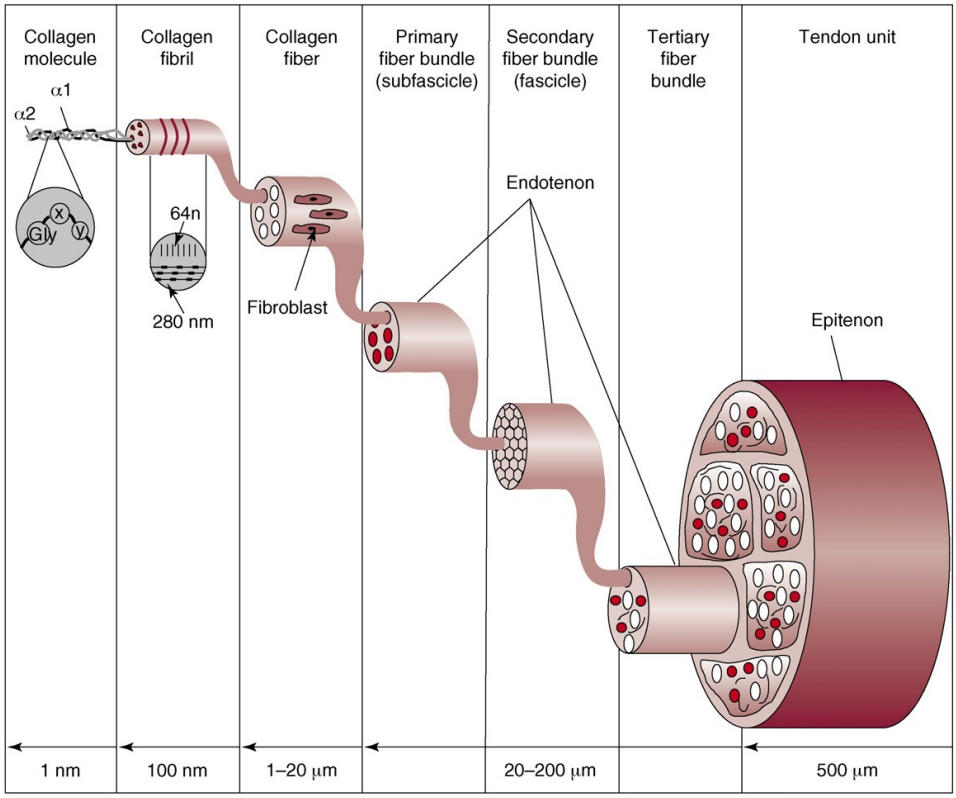

Figure 3: Hierarchical structure of tendon. Reproduced from Liu et al.[27]

1.2.2 Enthesis

Tendons and ligaments attach to the underlying bone via a complex interface called the enthesis. The type to be discussed here, which is relevant to the supraspinatus tendon and ACL, is a direct (or fibrocartilaginous) enthesis. At other locations, tendons or ligaments attach via indirect (or fibrous) entheses.[1]

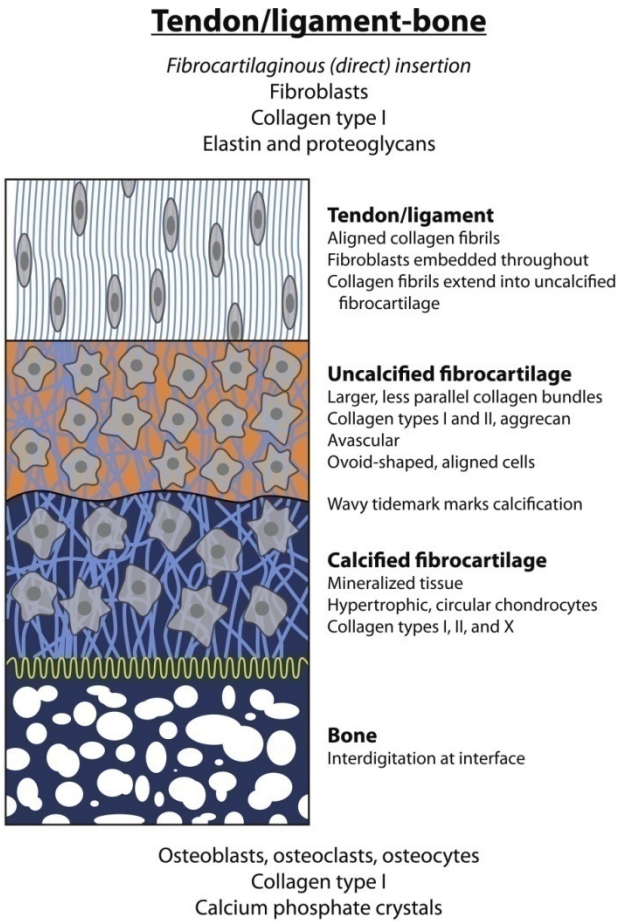

Figure 4: (a) Structure of a direct enthesis. Reproduced from Yang et al.[1]

The structure of a direct enthesis is depicted schematically in Figure 4. It acts to dissipate the stress concentration associated with a hard-soft interface via a gradual transition from the tendon proper to bone via uncalcified and calcified fibrocartilage layers. Fibrocartilage also shows greater resistance to bending loads than tendon or ligament tissue and thus acts to protect it much like the grommet does on an electrical socket. Continuous collagen fibres, which extend into the underlying cancellous bone as "Sharpey's fibres" and a jagged interface between bone and calcified fibrocartilage create a strong bond. The cell population transitions from tenocytes in the tendon proper to chondrocytes in the calcified fibrocartilage via an ovoid-shaped cell-type in the uncalcified layer.[1] While the fibrocartilage layers contain collagen type II and large proteoglycans such as aggrecan,[28,29] bone consists again of a network of collagen type I fibres. In bone, the hierarchical collagen fibre structure in combination with nano-scale calcium phosphate crystals gives bone the high compressive strength and fracture toughness required for its structural functions. The cell population,

consisting of osteoblasts, osteoclasts and osteocytes, is significantly more active than the one found in tendon or ligament. This means that bone has a significantly greater healing potential.[1,30] It should be noted that the enthesis of the supraspinatus extends over a very large distance of ca. 2 cm, compared to less than 1 mm at most other locations in the body.[31] This is due to the fact that the larger range of motion of the shoulder joint exerts larger than usual bending forces on the enthesis of the supraspinatus tendon.

Guided by knowledge of the enthesis structure and biochemical makeup, potential biomimetic approaches could build on e.g. the changing collagen fibre alignment or the gradients in ECM makeup. Osteogenic and tenogenic biochemical signals such as growth factors are another potential handle. In the next section previous attempts that have been made at regenerating tendon/ligament tissue are discussed. The limited range of dedicated attempts at recreating the interface is outlined in section 1.3.4.

1.3 Tendon/Ligament Tissue Engineering

The common theme in tissue engineering is to supply cells with an environment which provides appropriate behavioural instructions to stimulate the formation of new tissue. The scaffold should direct cell behaviour via physical as well as chemical cues while degrading at a rate matched to the rate of tissue formation.[32] The field of tendon and ligament tissue engineering has been extensively reviewed by a number of authors.[5,27,33–35] Overall, mixed success has been reported in the use of tissue engineering approaches to repair of the two most common targets: The anterior cruciate ligament[36] and the tendons of the rotator cuff.[37] There certainly appears to be no silver bullet approach that manages to clearly outperform traditional repairs in a clinical setting, indicating there is significant scope for further research. As discussed in the introduction, a successful tissue engineering construct needs to mimic mictrostructure, mechanical properties, and the biochemical extracellular environment. As such, tendon/ligament tissue engineering approaches tend to focus on:

- Mimicking the fibrillar structure of the collagen ECM (aligned within the tendon, gradually transitioning to random within bone);

- Providing adequate tensile support, mainly through the use of aligned fibres;
- Seeding with representative cell types, often MSCs;
- Provision of relevant biochemical cues for tenogenic and osteogenic differentiaton, supplied in different areas of the scaffold;
- Mechanical stimulation to mimic normal tendon loading.

Here, the advantages and disadvantages of the various materials used are discussed, with a second section reviewing the use of electrospun synthetic biodegradable polymers. Non-regenerative approaches using non-degradable materials will not be discussed. This is followed by discussion of the use of mechanical stimuli, and an extensive review of different approaches used for the creation of gradient biomaterials for orthopaedic interfacial tissue engineering.

1.3.1 Materials choices

An obvious choice for a scaffold material is type I collagen, as it comprises most of the native ECM, thus providing relevant biochemical cues. Going even further, decellularized tissue may be used, which is thought to provide many of the desired physical and biochemical cues to cells without complicated materials engineering. However, these materials suffer from a number of significant disadvantages. Low strength and rapid, unpredictable degradation compared to e.g. polyesters (see below), both of which can only be improved to a minor extent by artificial crosslinking,[33] mean they are not ideally suited as interpositional grafts. Additionally, many processing steps denature natural proteins, reducing or eliminating their bioactivity. Decellularized tissue also carries the risk of disease transmission and an inflammatory immune reaction due to its natural origin. Another negative effect of this natural origin is that the exact composition of the scaffolds will be unknown and is likely to vary between batches.[5] Nevertheless, collagen gels[33,38] or the somewhat stronger sponge-form[39] are used, commonly for *in vitro* studies of cell behaviour. In tissue engineering applications, it is commonly used in combination with a stronger, but less bioactive material such as silk.[40] Decellularized tissue is the most commonly

implanted non-autograft material. Despite this, clinical trials have shown mainly ambivalent results, although GraftJacket™ (decellularized human dermis) has shown some promise.[33,41,42]

An interesting material that has recently been developed comprises electrochemically aligned collagen fibrils. These show significant promise, both in terms of matching mechanical properties of relevant tissues, and tenogenic differentiation of hMSCs.[43] This might raise new interest in the use of natural materials, which have been largely replaced by synthetic polymers in recent studies.

The problems of batch-to-batch variation, limited availability, low strength and immunogenicity can be circumvented by fabricating scaffolds from synthetic bioresorbable polymers. In contrast to natural materials, they offer greater flexibility in terms of processing and sterilization as well as tightly controllable degradation rates and mechanical properties. Widely studied are poly (D,L-glycolic acid) (PGA), poly (D,L-lactic acid) (PLA), poly (L-lactic acid) (PLLA) and poly (ε-caprolactone) (PCL). In vivo degradation occurs via random hydrolytic chain scission throughout these materials with degradation products being processed through natural metabolic pathways. The time until the strength of the polymer is lost ranges from 1-2 months for PGA and PLA to 6 months for PLLA and up to 2-3 years for PCL. Tailoring of degradation rates and mechanical properties can be achieved by copolymerization.[44] While there are no clinical studies available to date, some limited success has been reported using *in vitro* and animal models for scaffolds based on all of the above-mentioned polymers.[14,45–49]

1.3.2 Electrospinning-based approaches

A range of constructs based on electrospun synthetic polymer fibres have been studied in the context of tendon/ligament tissue engineering, although only relatively simple systems have progressed to the stage of *in vivo* testing. The reader is referred to a recent review of the use of electrospinning for use in orthopaedic tissue engineering for further reading on the topic.[50]

However, even these simple systems show significant promise: Randomly oriented mats of PGA resulted in significantly enhanced stiffness when used to reinforce the repair site in a rodent model of rotator cuff repair when compared to surgical repair on its own at four weeks.[26] However, complete degradation in the same time-frame is likely to make this material unsuitable for use in humans. Another group has created a hierarchically structured construct by twisting and braiding electrospun PCL fibre bundles. The scaffold was reported to sustain the tenocyte phenotype *in vivo* and stimulate ingrowth of tendon-like tissue in a mouse Achilles tendon repair model.[51] Another study demonstrated that the addition of MSCs to electrospun PGA scaffolds results in significantly greater strength, and restoration of a more natural microstructure when compared to unseeded controls in a rabbit rotator cuff injury model. [52]

In related *in vitro* studies, aligned sub-micron sized fibres have been shown to cause tendon progenitor cells to express tendon-specific biomarkers,[53] while another group demonstrated that larger aligned microfibers might indeed be even more tenogenic than nanofibres. [54] Similarly, tenocytes encapsulated in a hydrogel surrounding aligned PCL/PLA copolymer (denoted PLCL) fibres maintained viability and phenotype for four weeks.[55] Electrospun fibres have furthermore been combined with a knitted fabric (by electrospinning onto the fabric) for improved construct porosity and mechanical properties. Random PLA/PGA copolymer (denote PLGA) on knitted PLGA was shown to sustain bone marrow stromal cell (BMSC) proliferation[46] and aligned PLCL on knitted silk or PLGA was shown to promote differentiation of BMSCs into tenocyte-like cells and tendon-specific extracellular matrix elaboration *in vitro*.[14] More recently, more complex electrospinning-based microstructures have been explored: so-called “nanoyarns”, consisting of electrospun nanofibrils that are twisted into larger fibres and arranged into an aligned, macroporous structure. This was achieved by electrospinning directly into a water vortex, followed by winding the resulting twisted fibres onto a rotating mandrel to achieve alignment. When compared to both aligned and randomly oriented electrospun fibre mats, these nanoyarns (consisting of co-spun collagen and P(LLA-co-CL)) were shown to

improve tenocyte proliferation and infiltration, as well as expression on tendon-specific ECM. [56]

Relatively few attempts have been made at incorporating biochemical signals. The knitted/electrospun PLGA hybrid scaffold described above was shown to yield improved results when basic fibroblast growth factor was encapsulated in the electrospun fibres.[57] Growth and differentiation factor 5 added to the culture medium was also shown to promote the tenocyte phenotype when adipose derived stem cells were cultured on randomly oriented PLGA mats.[58] Another group used less well-defined, but more realistic biochemical cues in the form of tendon-derived ECM. Coating electrospun scaffolds with this material resulted in enhanced tenogenic differentiation of stem cells, as well as increased collagen I production.[59]

Tendon/ligament tissue engineering approaches based on electrospun synthetic polymer constructs have shown significant promise in *in vitro* and *in vivo* studies, although there are currently no constructs that have made the transition to the clinic.[27,33,60,61] The incorporation of spatial patterns of mechanical and biochemical cues can be expected to be a powerful tool in the process of achieving this goal. Work relating to different methods for incorporating these gradients is reviewed in a later section.

1.3.3 Effect of mechanical stimuli

While not directly a topic addressed by this project, a key tool used in tendon/ligament tissue engineering is mechanical stimulation. In the natural environment, tendon cells are constantly exposed to tensile stress, which can therefore be expected to have a significant influence on maintaining the relevant cell phenotype. Indeed it has been shown that mechanical loading results in more tendon-like tissue-engineered constructs, and that removal of the mechanical load results in the loss of tendon differentiation markers and an increase of inflammation.[62] Especially when combined with microstructural clues (by way of aligned fibrous scaffolds), mechanical stimulation can be a powerful tool in guiding MSCs towards developing a tissue engineering scaffold into a tendon-like construct.[63] For further information on this aspect, the reader

is directed to a comprehensive review of the effect of mechanical stimulation on cell differentiation in both 2D and 3D systems.[64]

1.3.4 Graded/Stratified Materials and Interfacial Tissue Engineering

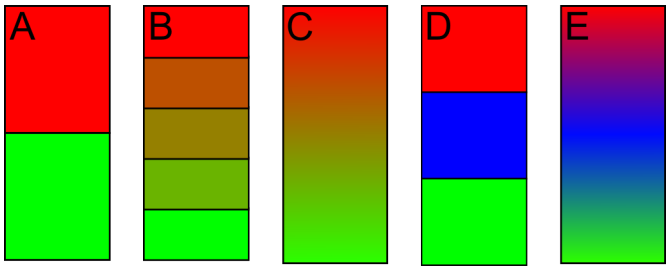

Figure 5: Some possible scaffold concepts for orthopaedic interface tissue engineering. A: bilayered, B: multilayered (two biomolecules), C: gradient (two biomolecules), D: trilayered (three biomolecules), E: gradient (three biomolecules).

For many potential tissue engineering applications the incorporation of gradients or stratification of physical and/or biochemical cues is likely to be highly advantageous. Especially for orthopaedic interface tissue engineering, where multiple tissue types with good integration between each other are to be created within a single construct, it is thought to be crucially important.[1–3] The ultimate goal is a graft that re-establishes the full *in vivo* functionality of the injured site.[1–3,65,66] For this, inclusion of a osteogenic region, which gradually transitions into a soft-tissue region is critical: It has for example been shown that the inclusion of the enthesis in decellularised grafts used for rotator cuff repair in a rat model significantly improves strength and restores a more natural microstructure when compared to grafts that lack this osteogenic region.[67]

In recent studies it has been successfully shown in this context that distinct relevant cell populations can be maintained in the same scaffold given the right physical and chemical stimuli.[2,68] For the purpose of this thesis, the focus will lie mainly on incorporation of bioactive agents, but physical cues are also briefly discussed. For a wider overview of recent progress in this field the reader is referred to a number of review articles, which describe the varied attempts at engineering the tendon/bone interface.[65,69–74]

One important distinction to note here is that between gradient and stratified scaffolds. Some examples are schematically depicted in Figure 5. Ideally, scaffolds would include smooth gradients of two or three relevant

biochemical factors (C and E) to recreate the smooth transition in properties found in the native enthesis. However, simple stratified scaffolds (A and D) are often used instead due to the relative ease of manufacture. Multilayered approaches (B) lie between these two in terms of complexity.

There have been a number of theoretical studies into the effectiveness of different biochemical gradients in directing cell populations towards tendon/ligament- or bone-like phenotype and ECM elaboration in a spatially defined manner. Inkjet patterning of BMP-2 and fibroblast growth factor 2 was used to direct stem cell fate towards osteoblasts and tenocytes respectively.[75] A gradient of Runx2-encoding retrovirus was shown to effect transdifferentiation of fibroblasts into osteoblasts in a dose-dependent manner along the gradient with associated changes in mineral deposition *in vivo*.[2] Another group evaluated the effect of combined gradients in stiffness and coating with different matrix proteins. It was found that stiff fibronectin-coated substrate regions promoted osteogenic stem cell differentiation, while collagen-coated substrates, especially those of intermediate stiffness promoted tenogenic differentiation.[76] Very relevantly, covalently immobilised gradient of alendronate, a drug commonly prescribed for osteoporosis and similar bone-diseases, on PCL membrane showed increased osteogenic differentiation as a function of alendronate concentration.[77] This might be a very relevant candidate for the creation of the osteogenic region of the scaffold proposed in this project.

A prominent contribution to the field of interfacial tissue engineering has been made by Helen Lu's group, which has developed a triphasic scaffold to be used as a graft collar during autograft procedures for regeneration of the ACL enthesis. The three distinct strata were: fibroblast-seeded knitted PLGA for ligament, chondrocytes-seeded sintered PLGA microspheres for fibrocartilage and an osteoblast-seeded composite of bioglass and PLGA microspheres for bone regeneration. Cell type and elaboration of ECM specific to the different tissues were maintained in a spatially defined manner, although only to a limited extent. In related work, co-culture of adjacent osteoblast and fibroblast populations resulted in a fibrocartilage-like cell type at the interface.[68,78,79] Some groups have attempted to create bone-ligament-bone constructs to completely replace the

need for other graft sources. Using joined bone-like and ligament-like constructs created by scaffold-less *in vitro* culture of BMSCs, near-native strength was achieved in an MCL-defect animal model.[80] Another group used heparin gel to deliver fibrochondrocytes in combination with bone morphogenetic protein 2 and fibroblasts to distinct regions of a porous PLCL scaffold created by particulate-leaching. Biochemical and mechanical properties characteristic of the enthesis and the ligament proper developed in the two regions after implantation.[81]

Several groups have focused on gradients through the thickness (rather than along the length) of electrospun mats, which would be of great use for creating osteochondral tissue engineering constructs, as reviewed previously.[82,83] One relatively simple approach is the joining of collagen scaffolds with different mineral and glycosaminoglycan content to create a biomimetic bi-layered scaffold.[84] Similarly, simple sequential deposition of electrospun fibres can create through-thickness mechanical (alignment) and biochemical (encapsulation) gradients.[85] When combining this approach with the co-spinning of polymers with different degradation rates, tailored sequential time-release can be achieved in these through-thickness stratified scaffolds.[86] Even more complex scaffolds can be created using the stratified approach: One group has for example developed a stacked bioglass-hydrogel-electrospun fibre scaffold for engineering of the osteochondral interface. However, biological validation of this approach is still lacking.[87] Fundamentally however, no stratified scaffold will ever truly mimic the gradient interface found between bone and soft tissues in the body.

For a smoother transition in properties, Eriksen *et al*. used a combination of twin-screw extrusion and electrospinning to create smooth through-thickness gradients of calcium phosphate crystals encapsulated in PCL fibres by varying the amount of mineral mixed into the electrospinning solution over time.[88] The group similarly showed the effectiveness of this approach for protein encapsulation.[89] In another approach, a PLGA microsphere scaffold with a continuous gradient in osteogenic and chondrogenic factors was created for regeneration of the bone-cartilage interface. Comparison to a blank scaffold

showed improved bone & cartilage regeneration.[90] While these developments are promising for the field of osteochondral tissue engineering, they are less likely to be applicable to the bone/tendon interface.

Some progress has also been made towards incorporating gradients along the length of electrospun mats, which is relevant for recreation of the tendon/enthesis structure, where properties vary along the direction of collagen fibre alignment. In an attempt to mimic the organization of collagen fibres at the enthesis, scaffolds with a gradual change from aligned to random fibre architecture were created.[47] Interestingly, different groups have managed, by gradual immersion of scaffolds in a solution containing the bioactive agent, to create gradients of calcium phosphate on PLGA and PCL[91] as well as physisorbed gradients of fibronectin on poly (methylglutarimide).[20] In fact, mineral gradients on electrospun scaffolds showed improved bone formation on mineralised side.[92] Furthermore, it has been shown that the incorporation of brittle mineral components into electrospun scaffolds does not necessarily result in a decrease in toughness.[93]

However, these physisorbed gradients cannot be expected to be maintained over the long time-scales required for tendon-repair *in vivo* due to diffusive effects. Nevertheless, this gradual immersion approach could be a powerful tool for the creation of stable gradients when combined with covalent post-functionalization methods as discussed in section 1.4.2., which will form the basis of work carried out in this project. Such an approach (based on carbodiimide chemistry) has already proven effective for a particulate-leached silk fibroin scaffold in a different context,[94] and its extension to electrospun scaffolds is expected to be a valuable tool.

1.4 Polymer Functionalization

In this section, the different approaches employed in order to bestow biological activity to tissue engineering scaffolds will be discussed with a focus on covalent attachment of biomolecules on fibrous matrices. Methods for physical entrapment, which is limited with regard to sustaining spatial patterns of bioactivity by diffusion, have been reviewed by e.g. Lee *et al.*[95] The reader is

referred to a number of recent reviews for further information on the topics discussed below.[60,96,97]

1.4.1 Functionalization prior to fabrication

Functional moieties can be incorporated by chemical modification of the polymer chains prior to scaffold fabrication. For example, one group has incorporated amine-reactive pentafluorophenyl esters into PCL fibres for one-step immobilization of biomolecules. This was achieved by blending a polymer bearing these functional groups into the PCL electrospinning solution.[98] However, the disadvantage of this and similar approaches is the significant amount of reactive groups remaining in the bulk, which may lead to problems when they are released during scaffold degradation *in vivo*. As a way of circumventing this issue, it has recently been shown that blending peptide-grafted polymer chains into polymer solutions prior to electrospinning can lead to field-driven accumulation of the bioactive peptide on the fibre surface of both polyethylene oxide[99] and PLGA.[100] While this approach is promising in its own right, biomolecule gradients can only be created through the thickness, rather than along the length of scaffolds, making it less suitable for reproducing the enthesis.

1.4.2 Post-fabrication functionalization

Scaffold functionalization after fabrication can be achieved through attachment of linking agents such as graft polymers and bifunctional cross-linkers (see below) after the creation of a distribution of reactive groups (most commonly amine, carboxyl or amine groups) on the scaffold surface. The latter can be achieved through plasma treatment, UV/gamma irradiation or wet chemical routes. For electrospun meshes, wet chemical methods are preferable due to the combination of surface-specificity (unlike irradiatiation) and an ability to penetrate the whole scaffold (unlike plasma treatments).[101] The most common wet chemical methods create functional groups by breaking the ester bond present in e.g. the widely used polyesters PCL, PLA and PGA. This is usually achieved by hydrolysis or aminolyis. It should be noted at this point that while base-catalyzed hydrolysis of polyesters is confined to the fibre surface, acid-

catalyzed hydrolysis as well as aminolysis (unless a relatively bulky amine is chosen) tend to result in bulk degradation.[102] A good overview of the chemical immobilisation of small peptide cell binding fragments can be found in *Delaittre et al.*[103]

1.4.2.1 Cross-linkers

A common class of linking agents are (hetero)-bifunctional cross-linkers. The term cross-linker as used in this context signifies a molecule containing two moieties that are able to create a covalent bond to a certain functional group, typically with high reactivity under even relatively mild conditions. This concept is depicted in Figure 6.

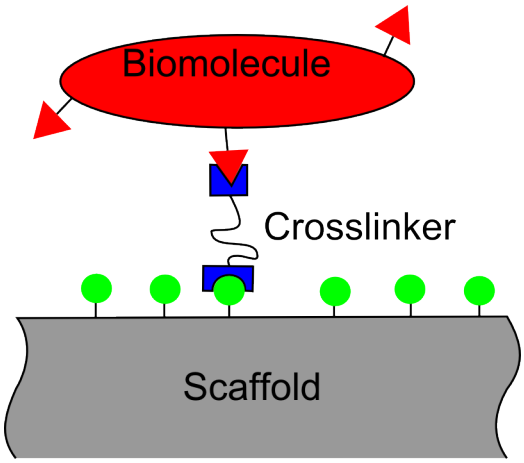

Figure 6: Concept drawing of post-functionalization with a hetero-bifunctional cross-linker. Green circles and red triangles denote different functional groups.

A variety of commercial molecules exist which can cross-link different combinations of functional groups typically found on biomolecules and pre-activated scaffolds, namely amine, thiol and carboxylic acid groups. Glutaraldehyde is an amine-reactive bifunctional crosslinking molecule, which has been used to e.g. immobilize gelatine, collagen and chitosan onto aminolyzed PCL films.[104] Despite its advantages of high reactivity and uncomplicated chemistry, concerns about the potential toxicity of glutaraldehyde-cross-linked scaffolds remain.[105] A popular approach is to use carbodiimide chemistry to link amines and carboxylic acid groups. This has been used to functionalize a variety of aminolyzed or hydrolyzed polyester scaffolds with different biomolecules.[106–108] Cross-linkers containing maleimide groups can react with thiol-groups and

are therefore specific to cysteine residues in peptide molecules. They are however affected by rapid degradation in aqueous conditions.[109,110] More recently, "click"-chemistry has been employed to effectively functionalise PLA surfaces with antibacterial quaternized poly(2-(dimethylamino)ethyl methacrylate).[111]

1.4.2.2 Graft polymerization

An alternative method involves the use of surface graft polymerization. After pre-activation of the scaffold surface, polymer brushes are grown from the surface, essentially creating a covalently linked core-shell structure. The grafting-based approach has gained prominence due to the recent advances in living radical polymerization techniques such as atom transfer radical polymerization (ATRP), which allow creation of polymer brushes with low polydispersity, well-defined molecular weight and a range of well-controlled architectures.[18]

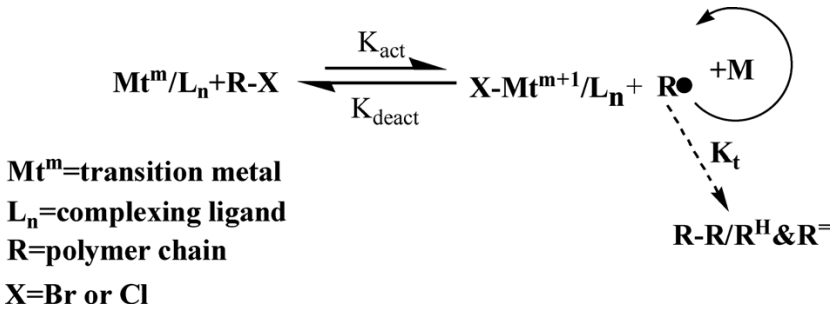

Figure 7: Mechanism of ATRP. Reproduced from Jiang et al. (2013)

The grafting approach can provide a greater density of functional groups than the maximum achievable on a flat surface or by attachment of polymer chains previously created in solution.[112] Biomolecules may also profit from attachment to a flexible polymer brush rather than directly to the rigid scaffold surface, since the hydrated polymer-brush environment more reminiscent of the native ECM may limit denaturation and make the molecules more accessible to cells. The method is very flexible due to the possibility of using (combinations of) monomers from a large library of molecules with a range of functionalities. This introduces a facile handle for tailoring the amount of available attachment sites and the properties of the immediate environment of the biomolecules and attached cells. Furthermore, it could potentially allow added functionality, such

as pH- or temperature-responsiveness (enabling the creation of "smart" biomaterials[113]) or antifouling properties to be incorporated.

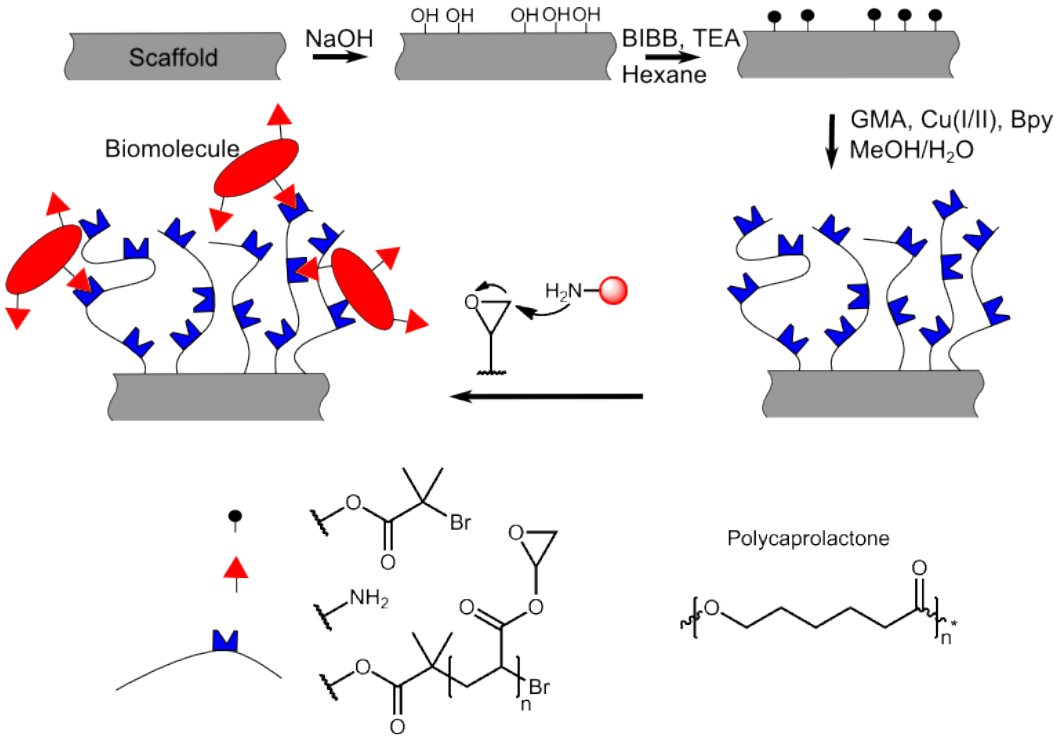

Figure 8: Concept drawing of a post-functionalization scheme involving surface graft polymerization.

In some cases, the shell is only used to alter the surface chemistry of the scaffolds. Examples include grafting of poly (acrylic acid) to increase the hydrophilicity of PLLA scaffolds[114] or the creation of bactericidal polyurethane fibre mats.[115] In other work, poly(oligo(ethylene glycol) methacrylate) (POEGMA) brushes on PCL were shown to override any influence of surface topology on cell behavior allowing materials processing modifications without any impact on cell adhesion.[116] Similarly, POEGMA brushes shown to improve hemocompatibility of styrene-b-(ethylene-co-butylene)-b-styrene elastomer,[117] as were poly(ethylene glycol) methacrylate (PEGMA) brushes grown on electrospun polycarbonateurethane fibres.[118] Outside the biomedical realm, PGMA brushes grafted onto regenerated cellulose, followed by derivitisation with diethylamine, used to create effective ion exchange membranes.[119]

More importantly in the context of this project, biomolecules can be immobilized in analogy to approaches employing cross-linker molecules by incorporating reactive moieties into the brush polymer. A very thorough review

of recent work on biomolecule immobilisation via graft polymer brushes has been compiled by *Jiang et al*. [120] Common functional groups incorporated into the polymer brush for subsequent conjugation to groups on the biomolecules to be immobilised include epoxy, carboxyl, hydroxyl, cationic, aldehyde, and primary amine groups. Various chemistries based on these groups have been used to immobilised anything from short peptide fragments to complete proteins and DNA strands on a range of polymer and inorganic surfaces.

One such simple approach (as depicted in Figure 8) based on reaction between epoxy-groups in the poly (glycidyl methacrylate) (PGMA) brushes and free amines in biomolecules has previously been demonstrated for PCL films.[19] This pathway will form the starting point for this project. In a closely related fashion, surface-initiated PGMA brushes were also used to create a variety of biosensors: A gold electrode was first modified by consecutive surface initiated ATRP of ferrocenylmethyl methacrylate (FMMA) and GMA. Tumour necrosis factor alpha (TNF-α) antibody was then coupled to the PGMA segment via an aqueous carbodiimide coupling reaction. Aided by the FMMA component, this made for an effective electrochemical biosensor for TNF-α.[121] For a similar purpose, poly(poly(ethylene glycol) monomethacrylate) brushes were conjugated to carcinoembryonic antigen antibodies via EDC/NHS chemistry.[122]

An interesting approach not based on living radical polymerization was the use of enzyme-catalyzed grafting of silicon-based polymers to incorporate both epoxy and glutaraldehyde moieties onto electrospun polystyrene fibres for biomolecule attachment.[123]

More sophisticated approaches can be used to improve the coupling specificity or to make the coating responsive to an external stimulus such as pH, temperature or UV light. Yao *et al.* have developed a varied range of such systems based on electrospinning, (surface graft) living radical polymerization and "click chemistry" (certain bonding schemes with high specificity and yield as well as other desirable traits).[124] Another group has used PLCL nanofibres modified with a layer of thermo-responsive polymer (of poly(N-isopropylacrylamide) (PNIPAM)) for temperature-controlled drug-release.[125] Brushes of this material

have also been shown to release bovine serum albumin from the surface of porous PCL membranes[126] and to detach cell sheets from the culture surface with the correct temperature trigger.[127]

Copolymerisation also adds an interesting avenue for improving the performance of surface-bound polymer brushes. A random copolymer of PGMA and poly(2-(diethylamino)ethyl methacrylate) (PDEAEMA) for example has been shown to improve the amount of bound biomolecules, since the PDEAEMA's amino groups catalyse the epoxy ring opening reaction.[128] Furthermore, by block-copolymerising PGMA with a highly biocompatible polymer such as PMPC, the overall biocompatibility of a synthetic construct can be significantly improved, and non-specific protein binding reduced.[129]

A very important aspect to consider for biomolecule attachment is choosing a bonding reaction which would act only at a certain, well-defined point within the molecule, resulting in its presentation in a bioactive conformation. A range of chemistries that can be exploited to this end has been reviewed by Rao *et al.*[130] – this will be further discussed in section 3.2.4.

There has been great interest in the surface modification of biologically relevant materials in recent years. Among these, surface graft polymerization approaches offer good control and a versatile range of potential functionalities via the wide range of (combinations of) monomers that can be employed. The aim of this project is to develop a tool-box of such approaches for modification of electrospun biodegradable polyesters for interfacial tissue engineering approaches. As a starting point the approach based on epoxy-amine coupling developed on PCL films by Xu *et al.*[19] will be used, which is shown in Figure 8. This approach is then built on by modifying the brush and biomolecule attachment conditions in such a way as to maximise incorporation of the biomolecule into the brush.

1.5 Deep vein diseases and tissue engineering approaches

This section will very briefly touch upon the subject of diseases of the deep veins in the leg, and possible tissue engineering approaches as it relates to section 0. Vascular tissue engineering presents different challenges to

orthopaedic tissue engineering: One of the key challenges here is haemocompatibility. However, the versatility of the ATRP-based functionalization approach discussed above means that it can be adapted to this task: Instead of using a polymer brush to immobilise biomolecules, a simple brush of a haemocompatible polymer can be grown on the surface of an engineering polymer (such as PCL) to reduce the danger of negative effects when implanted in a blood-contacting location.

Chronic venous disease of the lower limbs manifests in in adequate blood flow to regions of the leg, which, if untreated, can result in symptoms ranging from manageable (swelling, varicose veins), to the dangerous (chronic ulcers and open wounds). The scale of this problem is significant: In a study conducted amongst 18-65 year olds in Scotland, varicose veins were present in 40 percent of men and 16% of women, while 7% of men and 16% of women presented with ankle oedema. Active and healed venous leg ulcers were found in about 1% of the population. All of these symptoms increase in frequency and severity with age.[131,132]

A central cause for these conditions are malfunctioning venous valves, which prevent adequate blood circulation. As such, surgical treatments that could restore normal function to the valves of the lower limb deep veins and thus prevent venous reflux would be highly beneficial.

Ideally this would take the form of a tissue engineering construct, which closely mimics the mechanical properties, microstructure, and biochemical cues found in the venous valve and surrounding venous tissue. To date, only few attempts have been made to achieve this. The few trials that have been carried out largely used decellularised ECM scaffolds. It has for example been shown that it is possible to fully decellularise human venous allografts containing venous valves, and subsequently re-seed them with human endothelial cells.[133] In a similar *in vivo* study, decellularised canine venous valve constructs were seeded with endothelial progenitor cells and subsequently reimplanted. The implanted constructs were shown to cause significantly different flow patterns than the natural, unaltered veins, but were able to restore some function to the vein.[134]

As discussed in previous sections, a more well-controlled approach would use functionalised synthetic materials to create the tissue engineering construct, rather than relying on decellularised natural materials. In fact, electrospun fibrous samples have been evaluated with some success as candidates for cardiovascular tissue engineering.[135–137]

However, one key problem with the use of synthetics in blood-contacting environments, especially in complex geometries such as the venous valve, is the formation of blood clots. To circumvent this, synthetic polymers can be modified with haemocompatible surface layers. One candidate for this layer is Poly(2-Methacryloyloxyethyl phosphorylcholine) (PMPC). The zwitterionic side-chains on the polymer chain mimic chemical structures found in the cell membrane, and have been shown to dramatically improve the haemocompatibility of artificial materials.[138,139] It has additionally been shown that PMPC is compatible with surface-initiated ATRP[140,141] – as such, brushes of this haemocompatible material can be grown from initiators immobilised on the surface of a synthetic scaffold. In fact, this approach has been demonstrated for PCL membranes, albeit not for electrospun scaffolds.

2 Methods

2.1 Preparation of 2D samples for subsequent functionalization

2.1.1 Silicon cleaning

Silicon wafer fragments (500 µm thickness, 100 orientation, reclaim grade, p-type B-doped, 0-100 Ωcm^{-1} wafers purchased from Compart Technology (Peterborough, UK)) were used as the substrate for various 2D model systems to explore the effect of varying reaction conditions during the functionalization process in a highly controlled manner. Nanometer-thin films with very low roughness can be manufactured on this substrate, which makes it a suitable system for surface-sensitive and thin-film analysis techniques.[142] Monocrystalline silicon is also a highly suitable system for ellipsometric measurements (see section 2.6).[143]

The cleaning protocol to remove any organic or other surface contaminations was as follows: The wafer fragments (ca. 1x1cm) were sonicated in acetone for two minutes, and rinsed with ethanol (absolute, Sigma) and deionized water (diH_2O, from an Ondeo Pur1te Select water purifier). The fragments were then immersed in piranha solution (a 3:1 mixture of concentrated sulphuric acid and 30% hydrogen peroxide) for one hour, rinsed thoroughly with deionized water (diH_2O, from an Ondeo Pur1te Select water purifier) and dried under a Nitrogen stream.

2.1.2 Spin coating to create PCL-coated Silicon chips

Spin coating can be used to easily create polymer films with nanometer-scale roughness. Two different silanization procedures were employed to render the fragments hydrophobic for better bonding to the PCL film. Following a protocol previously developed by a group member to yield very smooth coatings of intermediate hydrophobicity, silicon chips were immersed in a 2% solution of triethoxyoctylsilane (TEOS, 97.5%, Sigma) in absolute ethanol at 70-75^{0}C for 1h. They were then rinsed with ethanol and diH_2O, followed by drying under vacuum. Secondly, to create highly hydrophobic self-assembled monolayers, a previously established protocol[144] was followed. Chips were immersed in a 2 mM solution of octadecyl-trichlorosilane (OTS, 90%, Sigma) in anhydrous

hexadecane (Sigma) overnight prior to rinsing with dichloromethane, ethanol and diH_2O and drying under vacuum.

The spin-coating itself was performed, unless otherwise stated, as follows (on a Laurell WS-650SZ-6NPP/LITE spin coater): 50µl of a solution of PCL (M_n = 10 kDa or 70-90 kDa, Sigma) in 1,1,2,2-tetrachloroethane (99.8%, Sigma) were deposited onto the silicon. A spinning speed of 6000 rpm with an acceleration of 400 rpm/s and a hold time of 10 s was used.

2.1.3 APTES monolayers on Silicon chips

Silicon chips were coated with (3-aminopropyl)-triethoxysilane (APTES, 98%, Sigma) using a vapour-phase protocol. Clean and dry chips were arranged in a grease-free plastic desiccator, placed on a glass dish to prevent agitation when the desiccator is opened. In the center of the glass dish, a glass vial was placed, in which 10ml hexane (dried over 3Å molecular sieves, which were baked at 200C for 2h, Sigma) were mixed together with 0.25ml of APTES.

The desiccator was then pumped for 5 minutes to create a sufficient APTES vapour (with the hexane acting as a carrier gas) and then left for 90 minutes, during which the APTES bonds covalently to the silicon surface. After the desiccator was vented, the samples were stored until further use.

Ellipsometric measurements revealed sub-nanometer film thickness, indicative of successful deposition of a silane monolayer.

2.1.4 Covalently immobilized PCL on Silicon

To covalently bond PCL to silicon, 3-Isocyanatopropyltrimethoxysilane (ICTS, 95%, Sigma) was covalently attached to the silicon surface. The isocyano-groups of the ICTS can subsequently react with the hydroxyl end-groups of the PCL.

For this, a solution-coating protocol was chosen. Toluene (dried over 3Å molecular sieve, baked at 200C) and triethylamine (TEA, 99%, Sigma) were added to an oven-dry round bottom flask and degased by bubbling nitrogen for 5min. ICTS was then added while maintaining Nitrogen pressure in the vessel.

In the meantime, one clean silicon chip (or two chips, back-to-back) were placed in an oven-dry test tube, which was sealed and purged using Nitrogen for 2 minutes. The ICTS solution was then added to each test tube using an oven-dry, gas-tight syringe. The process was carried out with the following amounts per test tube: 5ml toluene, 1.7 µl TEA, 640µl ICTS.

The samples were left in solution for 90mins, after which they were cleaned in dry toluene, dried under a nitrogen stream, and used immediately for attachment of the PCL film.

2.1.5 Covalent attachment of PCL to silicon

PCL was attached to the ICTS-coated silicon samples (prepared as described above) from the melt.

A clean and dry glass dish was coated evenly with granules of PCL (10kDa, Sigma). The silicon chips were placed on the granules with the smooth, shiny side contacting the polymer, the dish covered with aluminium foil and placed in an oven at 150°C overnight.

The samples were then removed from the melt, placed in a vial containing dichloromethane (DCM, Sigma) and placed on an orbital shaker for 2 hours to dissolve away all but the covalently attached PCL chains. The samples were then cleaned successively using DCM, ethanol, and diH_2O, and subsequently dried under a nitrogen stream and stored for future use.

Ellipsometeric measurements yielded film thicknesses of 10±1nm. These were measured for each individual sample and subsequently subtracted to yield the thickness of polymer brushes grown on these surfaces.

2.2 Electrospinning

Electrospinning of PCL was performed on the custom-made apparatus depicted in Figure 9. Polymer solution (15%w/v in 1,1,1,3,3,3-hexafluoroisopropanol (99%, Sigma)) was ejected at a constant flow rate of 3 ml/h using a syringe pump. A high voltage of 15 kV was applied to a blunted needle tip at a distance of 15 cm to a rotating grounded collector. The technique and the mechanism behind formation of nanofibres have been described in detail

by e.g. Li *et al.*[145] Briefly, the large electric field causes instabilities in the ejected polymer solution droplet, resulting in the formation of a jet, which is further drawn into a thin fibre under the influence of the field. The rotating mandrel can be used to create fibre mats with varying degrees of alignment by adjusting the linear velocity of the collector surface between 0 and 15 m/s. As depicted in Figure 9, a fanner can be introduced between pump and collector to move the needle (connected to the syringe via flexible tubing) back and forth along the width of the mandrel, resulting in a more even thickness of the fibre mat. The polymer jet was protected from air flow and, to an extent, from stray fields by an acrylic box as depicted. A detailed description of the apparatus design will be given in section 3.1. Samples were cut from the fibre mat for functionalization and further analysis.

Simultaneous electrospinning of PCL and poly (ethylene oxide) (PEO, Mn = 200 kDa with 200-500 ppm BHT, Sigma) was also carried out, using one syringe on each side of the mandrel. PEO was spun from a 5%w/v solution in 10% ethanol/90%diH_2.

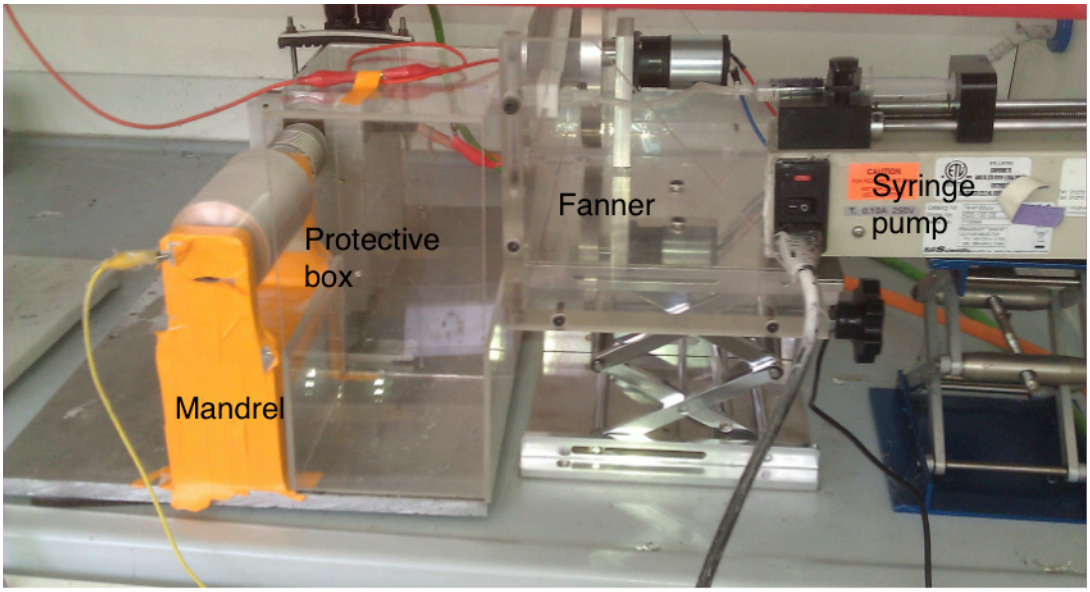

Figure 9: Photograph of electrospinning apparatus.

2.3 Functionalization: Films and fibrous scaffolds

The functionalization of PCL films and fibres was performed according to modified versions of the protocol described by Xu *et al.*[19]

2.3.1 Initiator attachment

For some samples, the first step involved immersion of the PCL-coated Si chips or fibrous PCL scaffolds in aqueous NaOH or HCl solutions of different molarities for different lengths of time to increase the number of hydroxyl groups on the polymer surface. Washing was carried out with diH_2O. Other samples, notably those where APTES or PCL were covalently bound to the silicon surface, were used as is.

The initiator molecule, 2-bromo-isobutyryl bromide (BIBB, 98%, Sigma), was attached to the PCL's exposed hydroxyl groups (or NH_2 groups in the case of APTES) by immersion of the samples in a mixture of BIBB and triethylamine (99%, Sigma) at a 1:1 molar ratio in hexane (dried over baked molecular sieve (3Å pore size)) after degassing by bubbling nitrogen. The samples were left in solution for 1.5h and then rinsed with hexane followed ethanol and diH_2O.

The concentrations of BIBB and triethylamine in hexane used were:

- 2 mmol in 5 ml per film sample
- 0.2 mmol in 100 ml for uniform fibrous samples after hydrolysis
- 1 mmol in 65 ml for gradient fibrous samples.

Other 2D samples were created with a mixed surface coverage of BIBB and propionyl bromide (PIB, 97%, Sigma), which creates a lower density of available initiators on the samples surface. Samples were created using v/v ratios of BIBB:PIB of 1:9, 2:8 and 0:10. In addition, the same protocol was used to create electrospun PCL fibres with a 2:8 ratio of BIBB:PIB on electrospun fibres that have not undergone any hydrolysis.

2.3.2 Growth of brushes based on GMA and HEMA

Surface-initiated atom transfer radical polymerization (ATRP) of Glycidyl Methacrylate (GMA, 97%, Sigma) off the immobilized BIBB molecules to create covalently attached brushes of Poly (Glycidyl Methacrylate) (PGMA) was carried out under the following conditions: The polymer samples were immersed in a reaction mixture of GMA, CuCl (97%, Sigma), $CuBr_2$(99%, Sigma) and 2,2'-

bipyridine (Bpy, 99%, Sigma) with a molar ratio of 100:1:0.05:2.5, in a volume equal to that of GMA of a 4:1 mixture of methanol and diH_2O. The monomer and solvent were first combined in a round bottom flask and degassed by bubbling nitrogen for 5 minutes. The remaining reactants were then added while maintaining positive nitrogen pressure, and the solution stirred until all solids were completely dissolved.

The solution was then added to vessels containing the samples, previously degassed using positive nitrogen pressure. Fibrous samples were contained within a round-bottom flask and reacted while stirring. Silicon chips were placed individually (or back-to-back) inside sealed test-tubes and reacted without agitation.

After various lengths of reaction time, washing was carried out successively with dimethyl sulfoxide (DMSO, Sigma), ethanol, and diH_2O, followed by drying under a nitrogen stream and subsequently *in vacuo*. Reaction times were 2 hours for all fibrous samples unless otherwise stated.

The trials with the 3D system were carried out using GMA, CuCl (97%, Sigma) and Bpy at a molar ratio of 100:1:2.5. Volume ratios of GMA to the methanol/water mixture were 1:2 and 1:3 for the uniform and gradient samples respectively.

The protocol was further modified for the copolymerisation of GMA with Hydroxyethyl-Methacrylate (HEMA, 99%, Sigma): GMA was replaced with an equal volume of a 1:1 (molarity) mixture of GMA and HEMA, and the solvent system used is a 1:1 v/v mixture of MeOH and diH_2O. All other quantities used remained the same.

As a reference material, bulk PGMA was synthesized via ATRP in solution using ethyl 2-bromoisobutyrate as initiator (with a 20:1:2.5:1 feed ratio of GMA, initiator, Bpy and CuBr) and purified by dissolution in tetrahydrofuran and re-precipitation in diH_2O.

2.3.3 Reaction of GMA-based brushes

In a series of exploratory experiments, various thin-film and electrospun polymer samples with attached GMA-based polymer brushes were immersed in a range of solutions containing molecules designed to react with the GMA's epoxy groups.

1. Thin film samples of PGMA brushes grown on APTES-functionalised silicon surfaces, as well as thin films of PGMA, PHEMA and PGMA-co-HEMA on PCL immobilised on silicon, were immersed in 20mM solutions of two small molecules containing a reactive amine and thiol group respectively: ethanolamine (Sigma, 98%) and 2-mercaptoethanol (Sigma, 99%). Both molecules were dissolved in 0.1M $NaHCO_3$ buffer (adjusted to pH 8 or 10) and samples immersed in solution overnight.

2. Thin films of PGMA-co-HEMA on PCL immobilised on silicon were immersed in a solution of a thiol-containing peptide (CG_3K_3) at 1mg/ml in 0.1M $NaHCO_3$ buffer (adjusted to pH 8) overnight.

3. Electrospun PCL with PGMA brushes grown for 2h were reacted with a model molecule (fluorescein modified to contain a primary amine group, Sigma). This was carried out by immersion in a 0.1mg/ml solution in phosphate buffered saline (PBS) (diluted from a concentrated stock solution in methanol) at room temperature followed by thorough washing in PBS to remove any molecules not covalently attached. Further, type 1 collagen (Sigma) was attached from a 1 mg/ml solution in PBS for 24h with stirring followed by removal of non-bound collagen by exchanging PBS several times over two days.

2.3.4 Growth of brushes based on MPC

ATRP of PMPC brushes was carried out on both thin-film samples (APTES or PCL covalently bound to silicon) and electrospun PCL.

The protocol employed largely mirrored that used for growth of GMA-based brushes. 2-Methacryloyloxyethyl Phosphorylcholine (MPC, 97%, Sigma) was used alongside CuCl, $CuBr_2$ and Bpy in a 33:1:0.05:2.5 feed ratio, and the solvent system employed is 4:1 (v/v) MeOH / diH_2O.

Silicon samples were reduced in size to 0.5cm x 0.5cm to allow for the use of smaller vials and reduced reaction mixture volumes. To each vial were added 92mg of PMPC and 125µl of the remaining reaction mixture, each separately degassed using nitrogen.

2.3.5 Growth of brushes based on dapsone-MA

Dapsone methacrylate monomer was kindly supplied by Luis Roje del Olmo. ATRP of dapsone-MA on APTES and PCL-coated silicon was carried out in a DMSO-based system. Several protocols were employed:

1. To 7.5ml of degassed DMSO were added N,N,N',N"-pentamethyldiethylenetriamine (PMDETA, 99%, Sigma), CuCl and $CuBr_2$ in a 1.3:1:0.2 feed ratio, based on 0.57 mmol CuCl.

2. Experiments were also carried out with a modified feed ratio of 1.1:1:0.02. In each case, the solution was stirred under positive nitrogen pressure until all solids are dissolved.

3. Substituting PMDETA for Tris[2-(dimethylamino)ethyl]amine (Me6TREN, Sigma, 97%), a more active catalyst. Feed ratio 1:0.1:1.3 CuCl:$CuBr_2$:Me6TREN.

4. Attempting to protonate the amine group on the dapsone-MA monomer before carrying out the protocol describe in point 3. This was attempted by:

    a. Dissolving 100mg monomer in 3ml acetone with 1.5ml acetic acid, followed by drying under reduced pressure, filtering, washing with diH_2O and drying in vacuo.

    b. Dissolving 100mg monomer in the minimum amount (ca. 1ml) of TFA, followed by precipitation in ether and drying in vacuo.

In a separate vial, each sample was degased alongside 50mg of dapsone-MA, to which the above reaction solution was then added. Samples were left to react for various lengths of time without agitation.

2.4 Controlled filling method

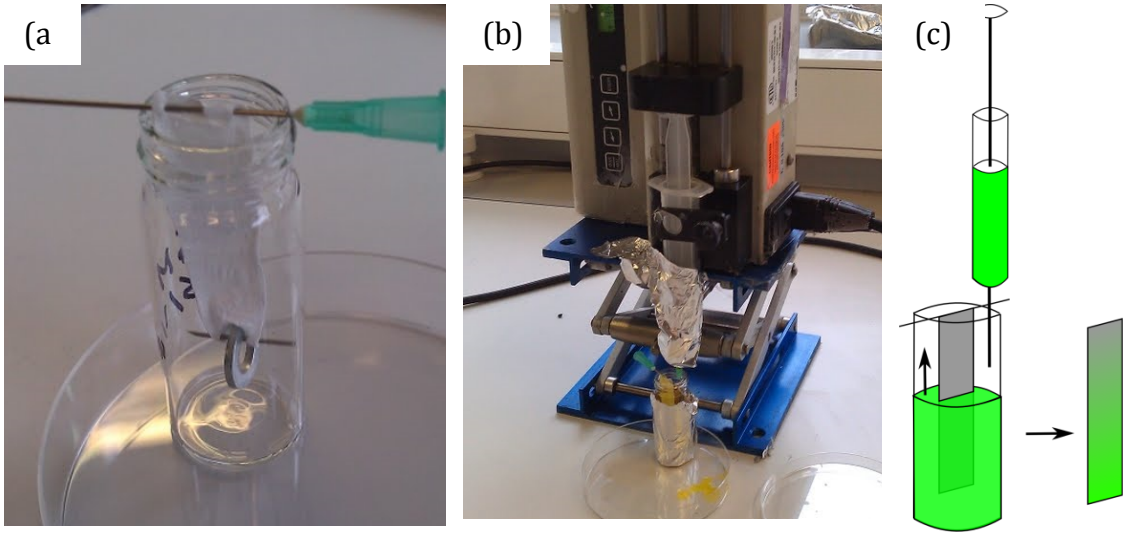

Figure 10: Photographs of (a) the suspended sample and (b) the controlled filling apparatus. (c) Diagram of gradient creation.

First trials of gradient functionalization of were carried out with a simple version of the "controlled filling" apparatus previously employed for mineral[91] and physisorbed protein[20] gradients of electrospun scaffolds as depicted in Figure 10. Strips of electrospun PCL ca. 5x1 cm^2 in size were pre-soaked in PBS to prevent wicking and gradually immersed in the fluorescein-amine solution in a 14 ml glass vial.

2.5 Gel permeation chromatography (GPC)

GPC was used to analyze the molecular weight distribution of a polymer sample. It has been evaluated here as a way of assessing the extent of hydrolysis of fibrous scaffolds. Measurements were carried out in $CHCl_3$ on a Polymer Labs SEC 50 instrument with two Polymer Labs mixed D columns at a flow rate of 1ml/h. Calibration was carried out using two narrow molecular weight polystyrene standards (Polymer Labs, Mixed A and B).

2.6 Ellipsometry

The thickness of thin films can be measured using ellipsometry with an accuracy of up to a few Å under ideal conditions. It should be noted that this represents a significant potential increase in accuracy over the weight-based method for determination of PGMA graft yield employed by Xu *et al.*[19] The

refractive index of the film material is also accessible with this technique. Combined with rapid data acquisition and non-destructiveness, this makes ellipsometry ideal for high-throughput analysis of the various steps of the 2D functionalization scheme. It has previously been used to study a large number of polymer thin film and biological systems and Si wafers have been established as a highly suitable substrate.[143,146]

A full description of ellipsometry theory and applications is found in Tompkins&Irene.[147] Briefly, ellipsometry probes the dielectric properties of a thin film by measuring the change in the polarization state of light that is reflected off the film-substrate system, expressed in terms of the ellipsometric parameters Δ and Ψ. These parameters can be collected at various angles of incidence and/or wavelengths λ as well as averaged over multiple "zones" for more accurate results. Using an appropriate model, film thickness and, if desired, optical properties of the film can be fitted to the experimental data.

Unless otherwise stated, measurements were collected using the following conditions:

Nanofilm EP3 (Accurion, Goettingen, Germany) Angles of incidence 61-75^0 in 2^0 steps, λ = 532 nm (frequency-doubled Nd:YAG laser), 2-zone measurements

Some remarks on the quoted thicknesses from ellipsometric measurements are necessary. To maximise consistency between measurements and to minimize uncertainties in the fitting procedure, as many parameters as possible were kept constant between measurements. Specifically, the thickness of the oxide layer was taken to be 1.8 nm (from initial measurements) in all cases. The refractive index n of both silanes and the PCL film were fitted using a Cauchy model (Equation (1)). However, setting n = 1.5 independently of wavelength λ was sufficiently accurate in almost all cases. The silane layer is generally included in the film measurement of PCL film thickness.

$$n(\lambda) = A + \frac{B}{\lambda^2} \qquad (1)$$

2.7 NMR spectroscopy

Nuclear magnetic resonance (NMR) spectroscopy can be used to quantitatively analyze small amounts of sample material after dissolution. It should be noted that values are averaged over the whole scaffold. Here, ^{1}H-NMR spectroscopy was carried out on a Bruker DRX 400MHz in $CDCl_3$.

2.8 ATR-FTIR spectroscopy

Attenuated total reflection (ATR) Fourier transform infrared (FTIR) spectroscopy yields chemical information about the first several µm of a sample by analyzing the IR absorption spectrum of the evanescent wave created on the outside of a crystal when total internal reflection of a laser beam occurs inside the crystal.[148] For the fibrous scaffolds it can be used to quickly assert the presence of chemical groups after certain reaction steps, but accurate quantitative evaluation of the results is not possible. The technique's usefulness for the film samples has not been evaluated, but is expected to be limited as silicon is not highly reflective in the infrared part of the electromagnetic spectrum. Spectra were acquired on a Thermo Scientific Nicolet iS10 spectrometer with a Golden Gate single reflection diamond ATR attachment. Averaging over 128 acquisitions was performed as well as a software correction for the use of ATR-FTIR in the OMNIC program provided by the manufacturer.

2.9 Scanning electron microscopy (SEM)

SEM is ideally suited to observe changes in the bulk appearance of the fibrous scaffolds such as gross surface degradation or fibre fusion. Length scales of several microns to a few nanometres are easily accessible to study both the overall appearance of the mesh as well as the state of the fibre surface. The models employed were a JEOL JSM-5610LV (JEOL, Tokyo, Japan) and a LEO Gemini 1525 (Zeiss, Hertforshire, UK). The latter may be used for high resolution imaging due to being equipped with a field emission electron gun. The JEOL is used for routine imaging. Samples were sputter-coated with Chromium prior to imaging.

2.10 Light microscopy

The quality of the spin-coated films may be assessed to a certain extent via reflected light microscopy (Zeiss Jenalab). Especially hole-formation was easily observed. Using crossed polarizers, crystallinity and microstructure may be studied. Using fluorescence microscopy (Olympus IX51), the amount and distribution of fluorescently tagged molecules immobilized on the polymer surface can be analyzed in a qualitative or semi-quantitative manner.

2.11 Contact angle measurements

Contact angle measurements are a facile way of determining changes in surface chemistry through their effect on the hydrophilicity of the sample. Significant changes in contact angle can be expected during surface hydrolysis of polyester films due to the increased density of polar hydroxyl groups. Subsequent functionalization steps are also likely to result in a change in surface hydrophobicity. It is also useful in determining the quality of hydrophobic silane coatings on the silicon surface.

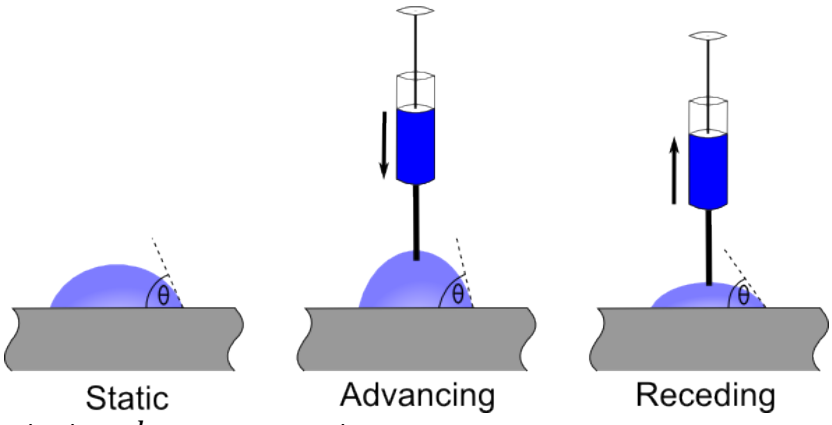

Figure 11: Contact angle measurements.

Three kinds of contact angles were measured as depicted in Figure 11 on a Krüss EasyDrop Standard using diH_2O: Static contact angles were evaluated using 2 µl sessile drops at 4-5 positions on the sample. Fitting was carried out using a formula based on the Young-Laplace equation, while also taking into account distortion of the droplet due to its own weight. For advancing/receding contact angles, 3 measurements were taken while the drop volume is increased/decreased at 10 µl/min with the droplet occupying ~2/3 of the screen at minimum magnification (corresponding to ~30 µl). The needle was kept in the

droplet and lowered or raised to minimize drop shape distortion. Advancing/receding contact angles were determined by fitting a generalized cone section, which yielded better results in this case.

Advancing (and to a lesser extent receding) contact angles are affected by a large degree of inaccuracy due to distortions in drop shape caused by the presence of the needle. This is reflected by a poorer fit relative to static contact angle measurements. However, the consistency of static measurements was fairly low, possibly due to unpredictable pinning effects of the advancing drop front during deposition. Advancing/receding values are therefore expected to be more relevant in the analysis of changes in surface chemistry in this system.

2.12 Peptide synthesis

A cell-adhesive peptide (DGEA, a collagen-I based fragment) was synthesized in the anticipation of future experiments on the bioactivity of functionalized PCL scaffolds. A cysteine, C, (which provides a thiol group for coupling to the epoxy groups present on the PGMA brush) was added to the peptide fragment via a flexible spacer (GGG). On the other end of the peptide, a Lysine, K, was added to provide an attachment point for a fluorescent fluorescein marker.

Thus, the resulting peptide to be synthesized had the structure

$$C\text{-}G_3\text{-}DGEA\text{-}K$$

Peptide synthesis was carried out using standard Fmoc-protected solid phase peptide synthesis (SPSS) protocols. Here, amino acids are coupled to each other (by reaction of the carboxyl group of one with the amine group of another) one-by-one to grow the peptide while attached to a solid polystyrene bead.

9-Fluorenylmethyloxycarbonyl (Fmoc) protected resin (0.25mmol) was used in this case. Resin was shaken with DCM inside a peptide synthesis vessel for 30mins, followed by deprotection in 20% piperidine in dimethylformaide (DMF) for 10 minutes. The latter step was repeated twice. After rinsing twice with DMF and DCM, successful deprotection was confirmed using a standard

ninhydrin test on a small sample of the beads. If the test was negative (i.e. showing no blue colour), deprotection was repeated.

In each subsequent attachment step, the Fmoc-protected amino acid in question was weighed out in 4x excess with respect to the resin, and the coupling aid 2-(1H-benzotriazol-1-yl)-1,1,3,3,-tetramethyluronium hexafluorophosphate (HBTU) in 3.95x excess. The two solids were dissolved in 25ml DMF alongside 260µl of N,N-Diisopropylethylamine (DIPEA), which acts to activate the carboxyl on the Fmoc-protected amino acid. The resin was then shaken with the coupling mixture for 3 hours, after which the vessel is drained and washed with DMF (x3) and DCM (x2). A ninhydrin test was then carried out to determine success of the coupling reaction. If the test indicated the presence of free NH_2 groups, the coupling reaction was repeated.

After each coupling step, any remaining free amines were capped: The resin was shaken with a solution of DMF with 5% acetic anhydride and 2.5% DIPEA (v/v) for ten minutes. After draining, the process was repeated for another 5 minutes, followed by washing with DCM (x4) and DMF (x2). Successful capping was confirmed via a ninhydrin test.

This process was repeated until the complete peptide is constructed, after which it was cleaved off the resin by shaking it for 3.5 hours with a solution of 95% TFA, 2.5% triisopropylsilane (TIS), 2.5% diH_2O (v/v and 1g of dithiothreitol (DTT). The vessel was drained into a round bottom flask, and the resin rinsed (again into the flask) with DCM.

After removing the solvents under reduced pressure, the peptide was precipitated in cold diethyl ether. The sample was then centrifuged at 6500rpm / 4°C for 10 minutes and the solvent drained. This process was repeated twice with fresh ether. The final product was dried in vacuo, and subsequently stored at -20°C until further use.

In a separate synthesis run, fluorescein was attached to the amine group present on the lysine (K) before the final cleavage step. After the full peptide was synthesised and capped, the lysine's amine group was deprotected by shaking the resin with 2% trifluoroacetic acid (TFA) in DCM (v/v) for 2min, followed by

successive rinsing with DCM, DMF, DCM, DMF + DIPEA, DMF and DCM. A spatula-tip of fluorescein N-hydroxysuccinimide ester (fluorescein-NHS) was then added to the vessel alongside 25ml DMF and 260µl DIPEA and left in darkness for 2 hours. The samples was then washed with DMF and DCM, coupling confirmed via ninhydrin test, and the peptide cleaved and purified as described above.

Substance		**Protected Mol. Weight**	**Weight (g)**
A - Alanine	Fmoc-Ala-OH	311.3	0.311
D – Aspartic Acid	Fmoc-Asp(OtBu)-OH	411.5	0.412
C – Cysteine	Fmoc-Cys(Trt)-OH	585.7	0.586
E – Glutamic Acid	Fmoc-Glu(OtBu)-OH	425.5	0.426
G – Glycine	Fmoc-Gly-OH	297.3	0.297
K - Lysine	Fmoc-Lys(Boc)-OH	468.6	0.469
HBTU		379.3	0.379
DIPEA (1.5 mmol)		129.2	0.1938
Resin		**Functionalization (mmole/g)**	**Weight (g)**
Rink Amide MBHA (0.25 mmol)		0.37	0.676

Table 1 - Peptide synthesis specifications. All products purchased from AGCT Bioproducts. Adapted from the masters thesis submitted by Lucia Podhorska.

2.13 High-performance liquid chromatography (HPLC)

HPLC (using a Gilson instrument) was used to purify the synthesised peptides. The instrument uses a UV detector to track sample elution.

The peptide was purified in acidic conditions: The mobile phase (95% water, 4.9% acetonitrile) and organic solvent (water/acetonitrile) both contain 0.1% TFA (v/v). The crude product was dissolved in the mobile phase at 5mg/ml and injected into the HPLC. Collected fractions corresponding to the same peaks in the HPLC trace were pooled, each pooled sample then frozen at -80°C and subsequently freeze-dried for 2 days. Samples are stored at -20°C until further use.

2.14 MALDI characterization of peptides

Matrix-assisted laser desorption/ionisation (MALDI) mass spectroscopy was used to analyse the different peptide fractions collected from the HPLC. 0.5mg of each phase were dissolved in a solution of 4-hydroxy-α-cynocinnamic acid (HCCA) in a 1:1 v/v solution of water and acetonitrile.

Samples were then analyised using a Micromass MALDI micro MX, operating in reflectron positive mode.

2.15 Thrombin generation assay

Electrospun scaffolds with surface-initiated PMPC brushes were analysed for haemocompatibility using a thrombin generation assay provided by HaemoProbe according to the instructions provided alongside the kit (accessible here: https://www.dropbox.com/s/u6g5u1b454qhu54/TGA%20kit%20insert.pdf).

Four wells were used for each material.

Data was read using a SoftMax Pro plate reader. Calibration yielded a relationship of Optical Density = 0.0059 * concentration + 0.0148, with concentration in mU / ml; This was used to calculate thrombin concentration from the optical density calculated as the difference between values recorded at 405 and 540nm.

3 Results

3.1 Optimised manufacture of electrospun scaffolds

3.1.1 Design of a dynamic spinning rig for more even fibre distribution

Electrospinning of PCL fibres was carried out based on modifications of established protocols. Failure stress in the range of 10-30MPa and elastic modulus of the order of 100MPa (values previously determined by Dr Seth McCullen) compare relatively favourably to the maximum values of found in the human supraspinatus tendon (16 and 270 MPa respectively) and are in excess of those found in weaker portions of the tendon.[23]

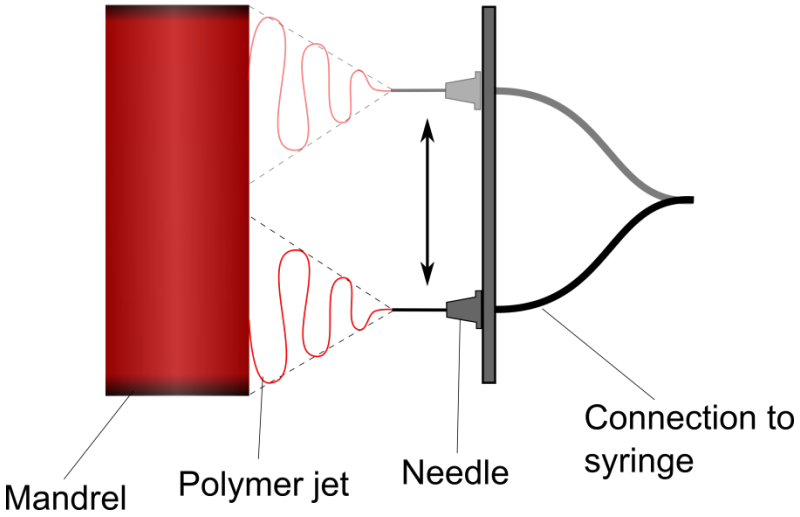

Figure 12: Concept drawing of the reciprocating fanner used to create more even fibre mats.

To improve the output of samples of consistent thickness, several modifications to the existing electrospinning setup were undertaken. All components were manufactured in the Departmental "Advanced Manufacturing Facility" according to our CAD drawings (Figure 13 (a)). The large existing mandrel (20 cm diameter) was replaced by a smaller one (6.35 cm diameter) to allow the production of smaller batches of samples, especially valuable for costly polymers such as PLLA and poly (γ-glutamic acid) (PγGA) used by other members of the group. Another goal was to spin fibre mats with a more even thickness across the mandrel, which would result in greater consistency in experiments employing samples collected from different positions across the

mandrel. To this end, a fanner was developed which can move the needle (from which the polymer is ejected) back and forth across the width of the mandrel by means of a crank mechanism connected to a DC motor. The needle is connected to the syringe (mounted on a syringe pump) via elastic silicone tubing through a series of PTFE adapters. Small bore diameters are employed to limit the amount of polymer solution lost in the apparatus to below 0.5 ml. The concept is depicted in Figure 12, with the complete setup shown in Figure 13 (b).

(a)

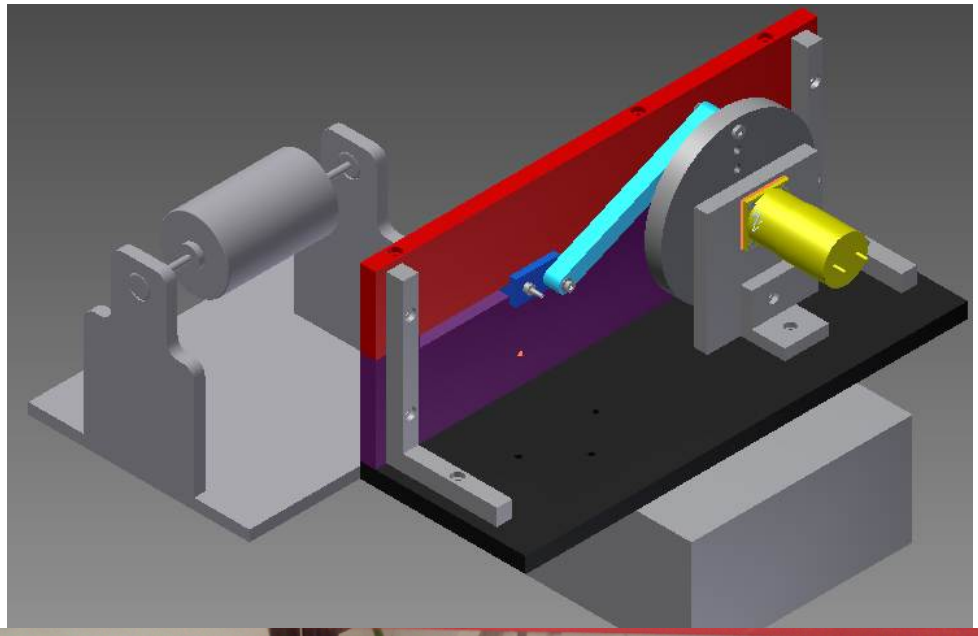

(b)

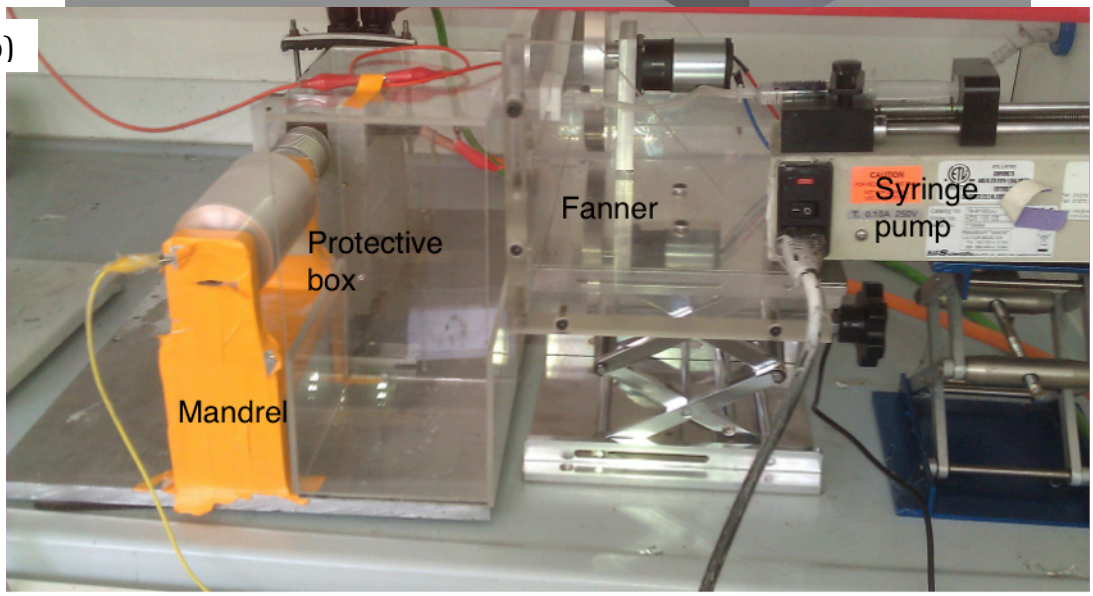

Figure 13: Concept drawing of the reciprocating fanner used to create more even fibre mats.

A video of the reciprocating fanner can be accessed here:
https://www.dropbox.com/s/a0yvkdl3a8gqu5i/Fanner1.avi

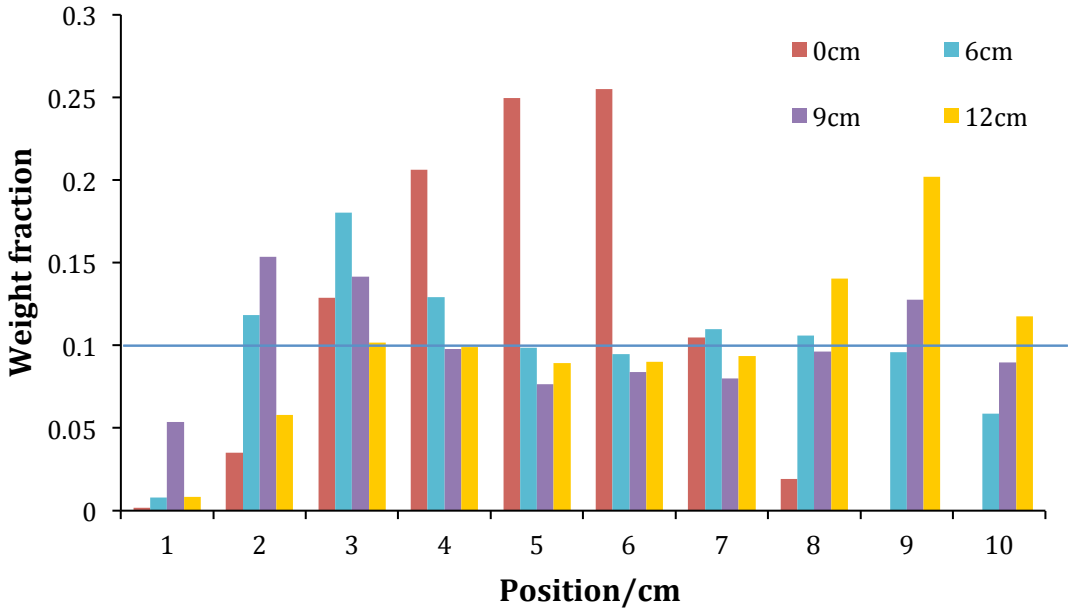

Figure 14: Distribution of electrospun fibres across the mandrel for different experimental setups (relative mass for each 1 cm-wide strip across the 10cm mandrel width). Results for the large and small mandrel with a static needle are shown in purple and red respectively. The distributions for the needle reciprocating at 55 rpm across the mandrel are shown blue and green for respective path lengths of 12 and 9 cm. (n=1)

The results of a preliminary trial comparing the evenness of deposition for PCL are shown in Figure 14. It can be seen that choosing a reciprocating path length just below the width of the mandrel results in significant improvements with a central region of 4-6 cm width showing little variation in deposited amount. In further studies the deposition of various polymers using the full range of possible path lengths will be evaluated. It should be noted at this point that, when the fanner is not used, the deposition of PγGA and PLLA seems to be more even than that of PCL for unknown reasons.

Furthermore, collection on the larger mandrel is more even than on the smaller one. This can be explained by the fact that the larger cylinder protrudes farther towards the needle, reducing the effect of stray fields originating from the surrounding metal. Further possible improvements should address the

increased isolation of the polymer jet from both stray fields and air-flow, both of which can significantly affect the electrospinning process.

3.1.2 Improving porosity of electrospun scaffolds

(a)

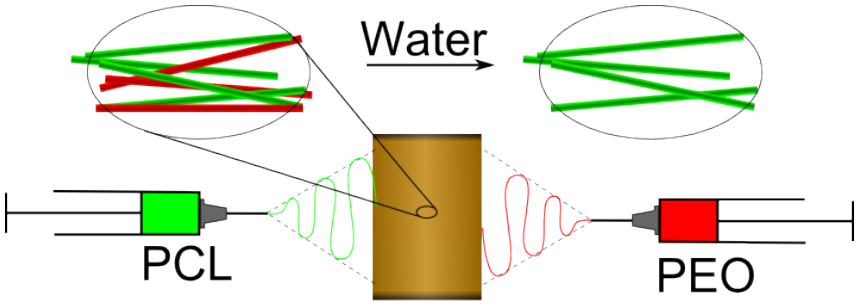

(b)

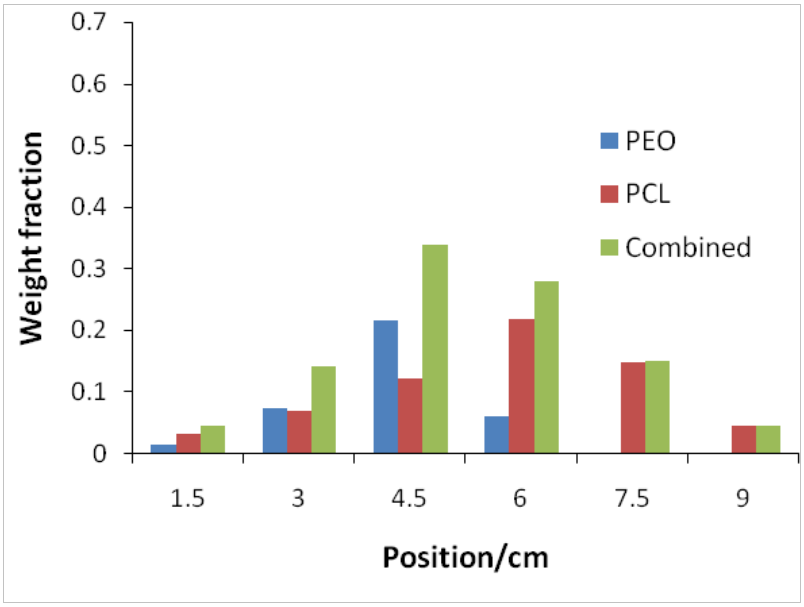

Figure 15: (a) Schematic depiction of co-spinning approach. (b)PCL, PEO and combined distribution by ight (relative mass of 1.5 cm-wide strips) across the mandrel. The large mandrel was used in this case.

Finally, attempts were made to improve the porosity of the electrospun mat by co-spinning PCL and PEO fibres, the latter of which can then be removed in water, leaving a distribution of relatively large pores (as depicted in Figure 15(a)). This is in an attempt to improve cellular infiltration of the electrospun scaffold, which is generally suboptimal in electrospun structures. This approach has previously been executed successfully by e.g. Baker *et al.*[149] Using the old setup without the fanner, the distributions of both PEO and PCL were too uneven to provide any useful samples. This is illustrated in Figure 15(b) by the

individual and combined weight distributions across the mandrel. To complete this project successfully, construction of a second would be required.

3.2 Creating a 2D model system for surface-functionalization of polymers

3.2.1 Spin-coated PCL on silicon as a model substrate

The effect of the two most readily variable spin coating parameters on film thickness and integrity was evaluated as depicted in Figure 16. Equation (2) shows the theoretical dependence of thickness d on spinning velocity ω and concentration c.[150] In contrast to this, the effect of spinning velocity was found to be negligible. However, the film thickness d was found to be proportional to the polymer concentration c, with a certain offset c_0, as expected.

$$d \propto \omega^{-\frac{1}{2}}(c - c_0) \qquad (2)$$

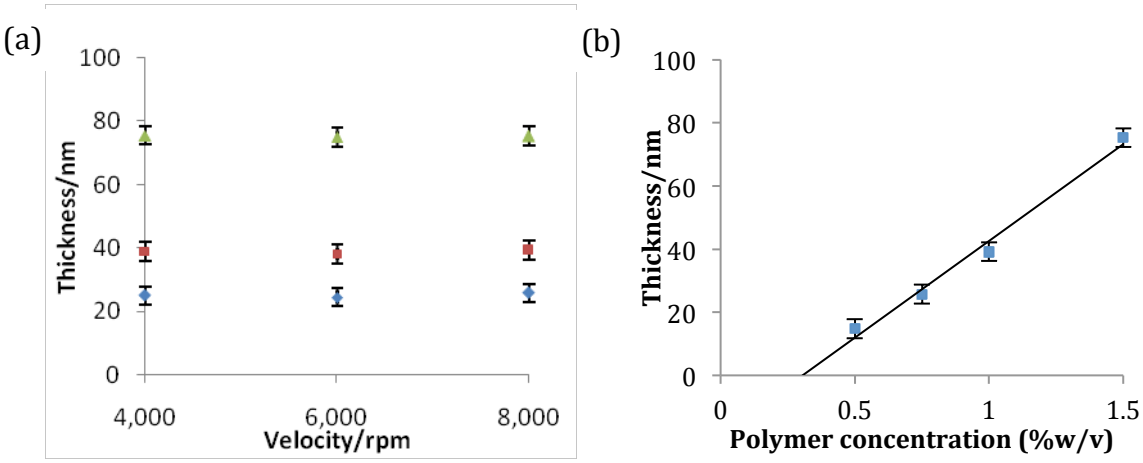

Figure 16: Effect on film thickness (as determined by ellipsometry) of (a) spinning velocity for polymer solution concentrations of 0.75%w/v (blue diamonds), 1%w/v (red squares) and 1.5%w/v (green triangles) and (b) polymer concentration at 8000rpm. The black line represents a linear fit with R^2=0.98. Error bars based on maximum intra-batch variation of 3nm.

Film thicknesses are typically consistent within at least ~1nm for each individual film at different positions and ~2 nm for each batch of films (prepared at the same time under the same conditions) on both instruments. Variations between batches were found to be significantly higher, which is most likely caused by differences in the polymer concentration due to both weighing errors and evaporation of solvent over time. By averaging over multiple measurements on the Woollam ellipsometer, precision could theoretically be increased further. While this is deemed unnecessary for the time being, this method will be used for definitive measurements once working experimental parameters have been established for each step of the functionalization scheme.

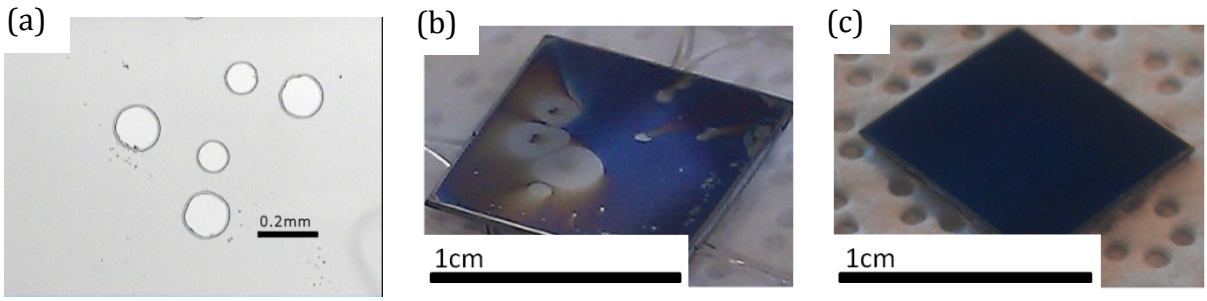

Figure 17: (a) Reflected light micrograph of holes in PCL film and photographs of a (b) heavily flawed and (c) near-perfect sample.

Several experimental parameters were found to have profound effects on film quality. A large number of microscopic bubbles, and subsequently holes (see Figure 17(a)) were produced when filtering the solution as well as when depositing it too forcefully on the silicon wafer. Additionally, the use of Plastipak® syringes rather than a micropipette with Starlab TipOne tips resulted in heavily flawed samples in some cases, as depicted in Figure 17(b). One possible explanation for this may be the leaching of chemicals from the syringe material into the solution. While the rigorous use of careful and clean experimental conditions was found to result in near-perfect films most of the time, consistency of results is somewhat limited by the lack of a clean-room environment and the unavoidable variations in temperature and humidity associated with a general laboratory environment.

PCL hydrolysis for creation of hydroxyl groups

As the first step of the functionalization scheme, a large number of hydroxyl groups need to be created on the film surface. Xu *et al.*[19] used base-catalyzed hydrolysis for 24-48h in aqueous NaOH at pH 12, corresponding to a 0.01 M solution. However, immersion of the spin-coated samples in 0.01 M NaOH resulted in delamination of the PCL film after ca. 2 minutes. Since the film itself was not destroyed and could be observe intact in solution, attempts at solving this issue were undertaken under the assumption that the interface between the hydrophilic silicon surface and hydrophobic polymer film was the reason for the rapid delamination. Several attempts, which are listed below, were therefore made to increase the hydrophobicity of the silicon surface:

Baking the films at 100^0C for 2 h to remove some of the hydroxyl groups which cap the silicon wafer's oxide layer after cleaning in piranha solution: While a slight increase in static contact angle to 10-15^0 (from values too small to observe) was detected, adhesion was not improved.

Silanization with triethoxy octlysilane (TEOS): The reaction scheme for the formation of a covalently bonded hydrophobic silane layer on the hydroxyl-terminated oxide layer of a silicon substrate is shown in Figure 18. Coating with TEOS raises the static contact angle to ca. 40^0 and delamination occurs after approximately one hour. It should be noted that the low contact angle indicates imperfect coverage of the silicon surface by the silane. Adhesion is not significantly improved further by annealing the films at 50^0C, although this could be expected to promote interdiffusion between the PCL and the silane's alkyl chain.

Silanization with octadecyl trichlorosilane (OTS): The formation of a near-ideal self-assembled monolayer (SAM) is indicated by ellipsometry and contact angle measurements. The measured static contact angle of $\sim 112^0$ and silane layer thickness of 2.5±1 nm fall within the range described in literature.[151,152] It was however found that the spin-coating solvent (tetrachloroethane) was unable to wet this surface, making spin-coating impossible using the current conditions. To solve this problem, a variety of other solvent will be evaluated. Toluene especially has been shown to allow spin coating onto hydrophobic silane SAMs.[153]

In parallel to these attempts, alternative ways to create a surface coverage of hydroxyl groups were sought. Films were found to be significantly more stable in acidic solutions. With TEOS pre-treatment, only minor degradation was observed after 18 h in 1 M aqueous HCl solution. Advancing and decreasing contact angles decrease with time as depicted in Figure 19. The receding angle does this in a more consistent manner, which may be due to inherent limitations of the setup where the relatively large needle is kept in the drop during measurements.

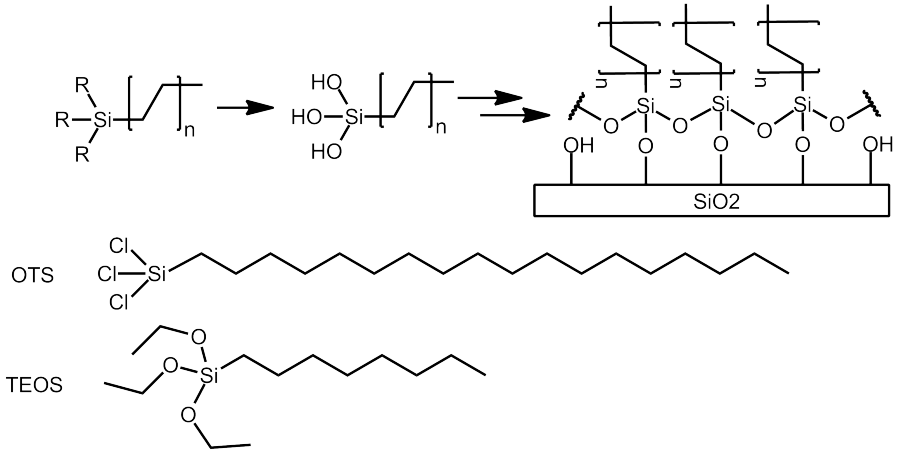

Figure 18: Idealized depiction of silane SAM formation.

While these results seem to suggest that the use of acid-catalyzed hydrolysis is the preferable method, hydrolysis is unlikely to be constrained only to the surface. This would make it unsuitable for use with fibrous scaffolds due to the expected negative impact of bulk chain scission on the mechanical properties on the scaffold. The reasons why base- and acid-catalysis likely result in surface- and bulk-hydrolysis respectively are discussed in detail by Croll *et al.*[102] Briefly, base-catalyzed chain scission consumes the active species (hydroxyl ions) and leaves a negatively charged carboxyl group which hinders diffusion of hydroxyl ions into the polymer bulk. In acid catalysis on the other hand, the active species (protons) is regenerated and the reaction products are uncharged. In addition, the protons are significantly smaller than hydroxyl ions, further aiding their diffusion into the bulk.

Lastly, the use of low-molecular-weight PCL represents an alternative similar to acid hydrolysis (short chains throughout the bulk), but with better control over hydroxyl group spacing. Increased hydrophilicity (advancing and receding contact angles of 71 ± 3^0 and 59 ± 3^0 respectively) was observed, indicative of the decreased spacing of hydroxyl groups, when choosing a molecular weight of 10 kDa (rather than 80 kDa as used before, which yielded advancing and receding contact angels of 78 ± 3^0 and 62 ± 3^0 respectively). Rough calculations suggest an average of one hydroxyl group per 7 nm^2 for the 10 kDa polymer, assuming that the fraction of the surface taken up by hydroxyl groups is equal to their fraction of the molecular weight and that their size is

approximately (0.15 nm)^2. This is in a similar range to the area occupied by each grafted chain in a dense polymer brush (2 nm^2) quoted by Xu *et al.*[19]

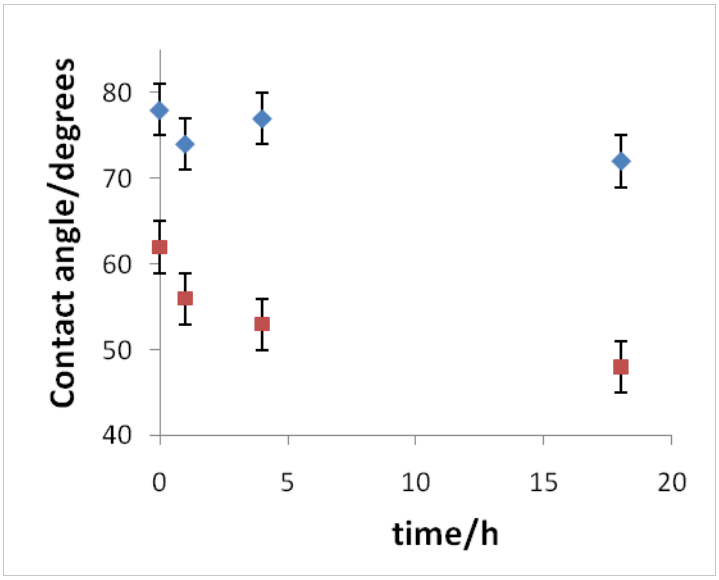

Figure 19: Advancing (blue diamonds) and receding (red squares) contact angles of PCL films (80kDa) immersed in 1 M aqueous HCl for various times.

Evaluation of suitability of spin-coated substrates

Trials of the subsequent functionalization steps were carried out using films composed of the shorter PCL. Rapid delamination was observed under the conditions required for immobilization of the initiator (BIBB) as well as the graft polymerization reaction both with and without pre-treatment with TEOS. Annealing of the films on TEOS-treated silicon resulted in significant improvements, leaving films essentially unchanged in the polymerization reaction mixture. With the current conditions for BIBB-immobilization however, films are still damaged significantly, eventually resulting in (partial) delamination. A thick layer of white crystals is seen to nucleate on the film surface, which may be associated with the observed damage. Potential remedies are a lower concentration of reagents and/or an improved way of agitating the reaction mixture.

3.2.2 Covalent immobilisation of PCL on silicon

The delamination problem described above is solved by attaching the PCL chains covalently to the underlying silicon substrate. This is achieved via a silane containing an isocyanato end-group, which is designed to react with the polymer's terminal OH-groups as depicted in Figure 20.[154] In this context it should however be noted that the silicon-oxygen bond, through which the silane is attached to the silicon surface, is itself hydrolyzable in basic conditions.[155] Therefore, a lower molecular-weight PCL (10kDa, rather than 80) is chosen – this will present a greater density of hydroxyl groups for both attachment to the silane, but also for subsequent functionalization, removing the need for any hydrolysis treatment.

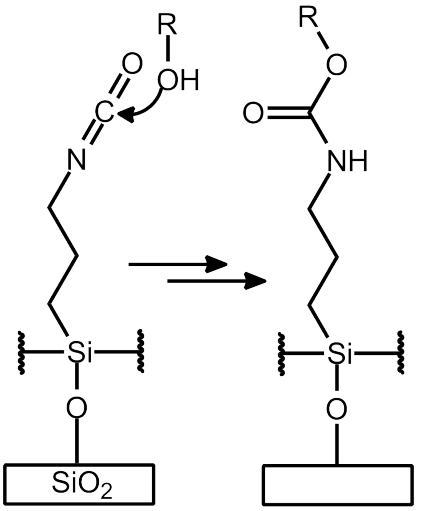

Figure 20: Immobilization of PCL via an isocyanatosilane. "R" denotes a PCL chain.

The covalent attachment of short-chain PCL to the silicon substrate from the melt was proven to be a reliable way of creating polymer substrates of thickness around 10nm, with a sufficient density of exposed chain ends for direct functionlisation with an ATRP initiator (BIBB), and subsequent surface-initiated ATRP of various polymers. As described above for spin-coated samples, the density of exposed chain ends can be calculated to be more than sufficient for full surface coverage of the polymer brush.

As an alternative, even simpler 2D sample, monolayers of amine-terminated silane (APTES) can be immobilised directly onto the silicon. The amine groups react with the BIBB initiator in the same way as the hydroxyl groups above, creating a dense coverage of initiation sites for surface-initiated ATRP.

3.2.3 Growth of functional polymer brushes on 2D surfaces

In this section the ultimate results of a range of optimised protocols for 2D sample preparation and subsequent surface-initiated ATRP of a range of different polymer brushes are presented.

The ultimate aim of this part of the project was to create a set of samples tailored towards effective, and specific subsequent reaction between epoxy-groups contained within the brush, and reactive groups (amine, thiol) on relevant biomolecules. Such a system would allow the creation of a dense coating of biomolecules on PCL polymer surfaces, turning the material from biocompatible to bioactive. These could therefore be used to tailor the PCL surface in such as way as to stimulate the adhesion/differentiation of specific cells in specific locations, facilitating the manufacture of sophisticated tissue engineering scaffolds.

The basis of the wider exploration of the parameter space shown here is the concept of using PGMA brushes on PCL, as per the original work by Xu et al. described in the introduction. The epoxy groups react quite aggressively with nucleophiles such as amines and thiols, which are commonly found in biomolecules. This basic approach presents certain problems however, which are partially addressed in the work shown here:

- The epoxy-nucleophile reaction is not inherently specific to a single nucleophile, raising the possibility of non-specific covalent bonding.
- ATRP reactions are quite sensitive to environmental parameters, especially oxygen. There is also the possibility of reactions between growing chains, whereby e.g. two radical chain ends combine. Well-controlled (i.e. linear) growth of chain length requires careful tailoring of experimental conditions.
- As PGMA is not water soluble, it will be impossible for any reactions to occur anywhere but in the surface monolayer of the polymer brush. This means the vast majority of epoxy groups will not be available for biomolecule immobilisation.

- Unless a flexible linker is engineered into the biomolecule to be attached, the molecule will be very tightly bound to the surface. This reduces the bioavailability of the immobilised species, as interactions with cells usually only occur if the biomolecule is in the correct orientation relative to a certain cell receptor.

To circumvent these problems, a brush that has wider gaps between polymer chains, but also contains a second monomer, which makes it water-soluble, was designed. The brush can thus swell when in aqueous solutions, theoretically allowing attachment of biomolecules along the length of the brush. Furthermore, the functionalised brush then represents a highly flexible linker to the underlying surface, which means cells can interact with the bioactive molecules in the relevant orientation.

Figure 21 depicts the growth of simple PGMA brushes via ATRP on a simple reference surface (initiators directly bound to the silicon surface via an silane (APTES) monolayer), as well as on the model PCL surface described in the previous section. While there is significant inter-sample variation (most likely due to oxygen contamination of some of the samples), linear growth of the brush was observed in both cases, based on ellipsometeric thickness measurements. This serves to validate the design of our 2D model system for further tuning of the brush.

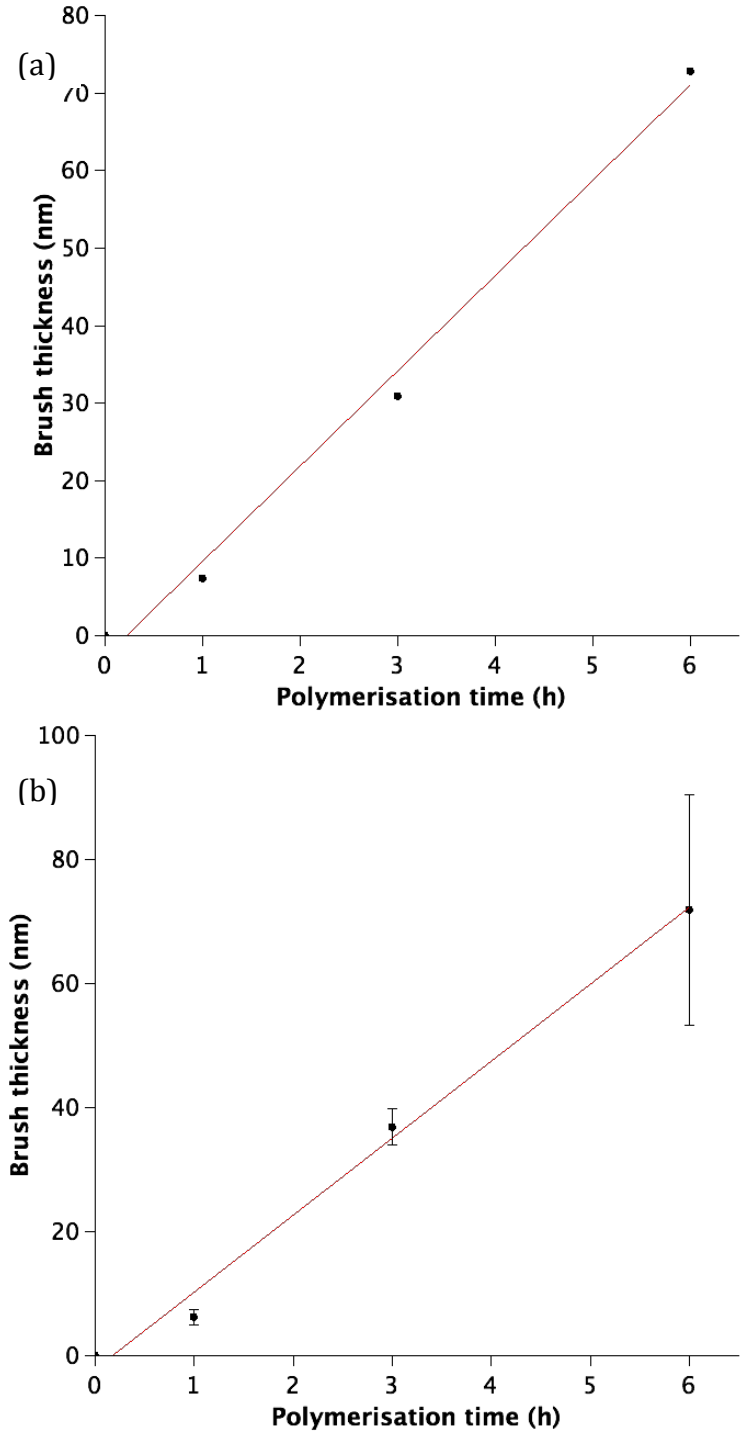

Figure 21: Graphs depicting the evaluation of controlled growth of simple PGMA polymer brushes on 2D surfaces. (a) Shows the growth of brushes from initiators bound to a silicon surface functionalised with APTES (n=2), while (b) shows the growth of the same brush from functionalised PCL covalently bound to a silicon surface (n=4).[A]

[A]Note: The full range of optimisation experiments to establish procedures, and end-to-end design of the experiments to be carried out were completed by Gabriel Mecklenburg. The final set of experiments (for which data is shown in the graphs above) has however been carried out by Lucia Podhorska.

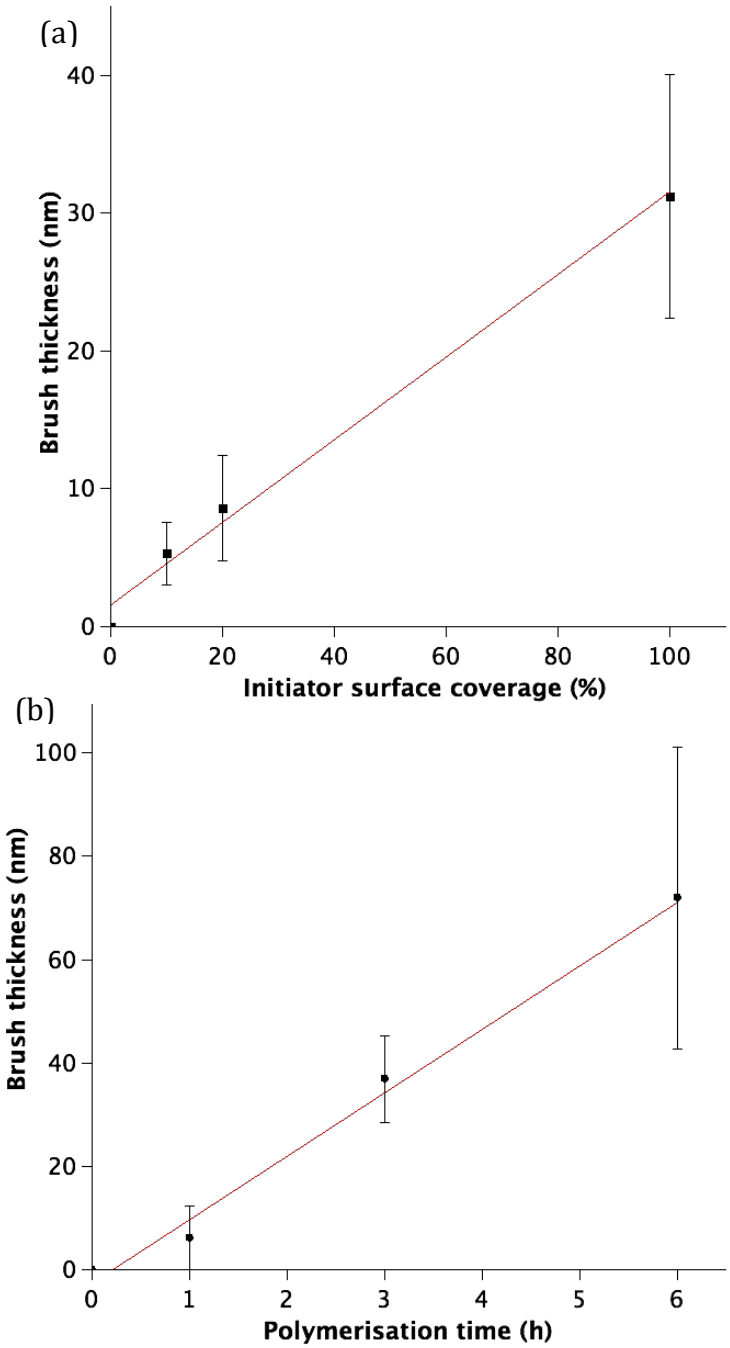

Figure 22: Graphs showing the growth of polymer brushes on 2D surfaces modified to improve efficiency of subsequent attachment of functional molecules. (a) shows the effect of varying the concentration of surface-bound initiator (BIBB), n=6). All samples were PGMA brushes grown for 3hours on PCL surfaces. (b) shows the growth over time of a co-polymer brush, incorporating GMA and HEMA monomers in equal proportions, grown on a surface coated with 100% BIBB (n=4).[B]

[B] Note: The full range of optimisation experiments to establish procedures, and end-to-end design of the experiments to be carried out were completed by Gabriel Mecklenburg. The final set of experiments (for which data is shown in the graphs above) has however been carried out by Lucia Podhorska.

Following on from this, several modifications of the brush system are carried out as outlined at the beginning of this section. Figure 22 shows the characterisation of the brushes created using these methods.

In the first instance, the spacing between polymer chains in the growing brush is increased. This is achieved by reacting the PCL surface with a mixture of the ATRP initiator (BIBB) and a blank equivalent (PIB). The latter reacts with the exposed hydroxyl groups in the same way as BIBB, but lacks the ATRP initiator functionality. This way the density of initiation sites can be tailored very simply. The effectiveness of this approach can be tracked simply via the thickness of the resulting brush – since the brush will lie flat in the dry state, where thickness is measured, a sparser brush will directly translate into a thinner brush. As can be seen in Figure 22 (a), increased brush spacing can indeed be achieved in this way in a straightforward and repeatable fashion.

Figure 22 (b) in turn depicts the linear, controlled growth of a PGMA-co-HEMA brush. In this system, the reactive GMA monomer is randomly copolymerised with water-soluble HEMA - This results in a water-swellable brush. As can be seen, growth in this system is not as tightly controlled as for pure PGMA, but linear growth is on average observed nevertheless.

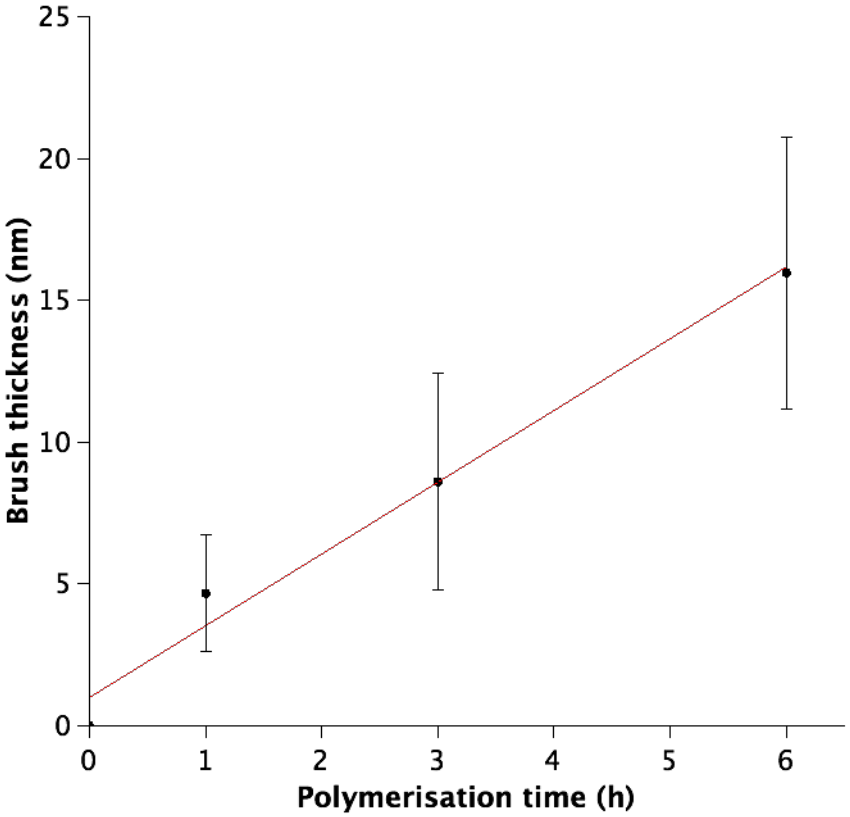

Figure 23: Growth curve for the optimised brush. The concentration of initiator is lowered to 20% surface coverage, and the brush consists of equal proportions of HEMA and GMA (n=4). [C]

Lastly, the two modification approaches were combined into the final system. Shown in Figure 23 is the well-controlled growth of PGMA-co-HEMA on a PCL surface with 20% coverage by the BIBB initiator.

[C] Note: Initial experiments to establish procedures and end-to-end design of the experiments to be carried out were completed by Gabriel Mecklenburg. The final set of experiments (for which data is shown in the graphs above) has however been carried out by Lucia Podhorska.

3.2.4 Immobilising molecules on functional polymer brushes

In the course of this project, a range of exploratory experiments were carried out to validate the design of the optimised reactive brush system described in the previous section. To achieve this, a variety of 2D samples were immersed in different solutions of reactive molecules.

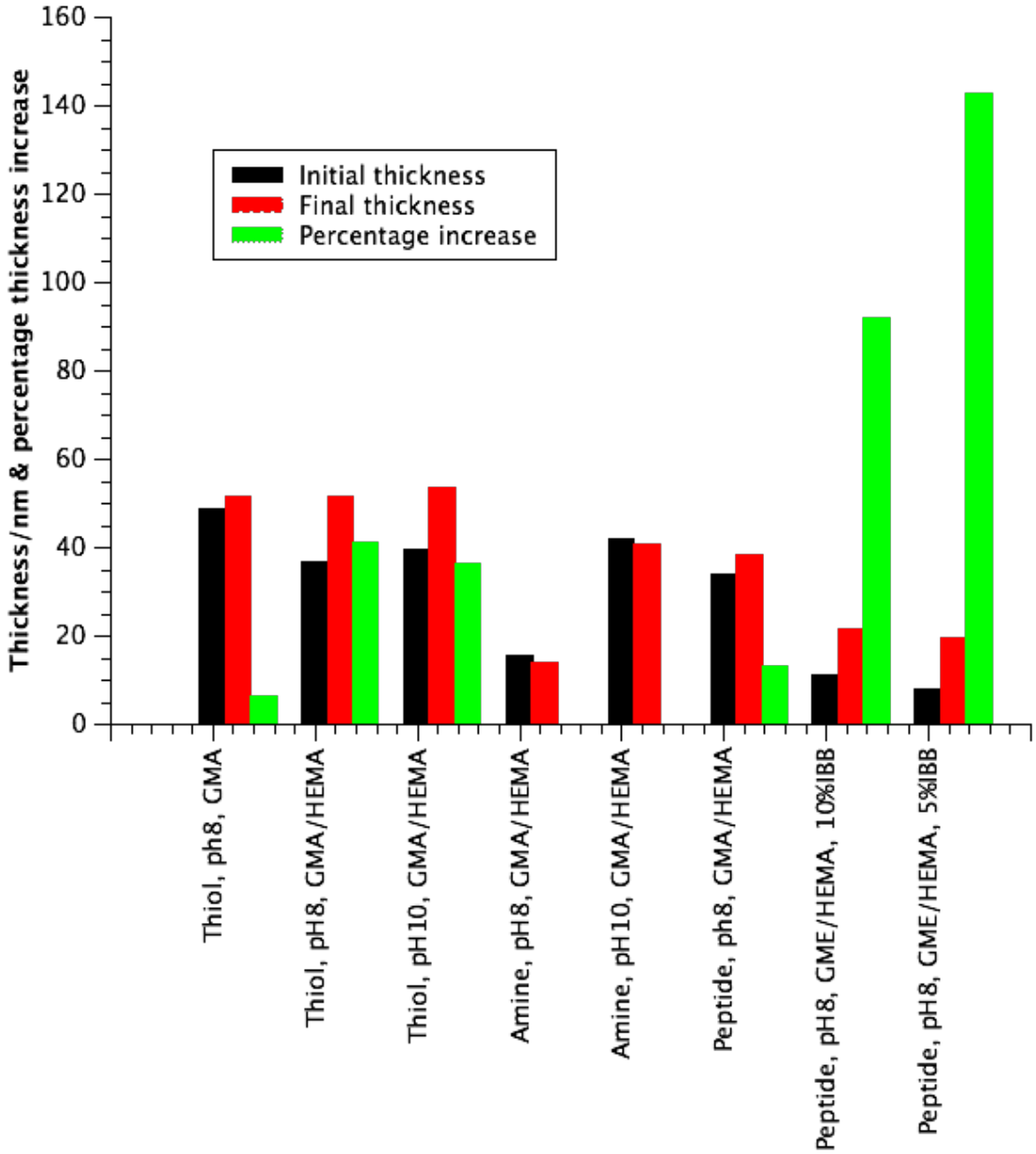

Figure 24: Exploratory experiments to find an effective system for attachment of active molecules to a surface-bound polymer brush. Shown are the thickness of different brush types before and after immersion in solutions of different reactive molecules, as well as the corresponding percentage increases. All experiments n=1.

In theory, it is possible to create the environment for a specific epoxy-nucleophile reaction. The epoxy-group reacts preferentially for SH, NH_2 and OH repectively, when in buffered solutions with pH 7.5-8.5, 9-11, >11.[156] As such, when at pH 8, only thiols should react with an epoxy-containing polymer brush, while at pH, amines (and potentially thiols) should react. If proven correct, this would allow specific attachment of biomolecules to the reactive polymer brush via a thiol linker, most relevantly a cysteine for proteins/peptides.

To test this hypothesis, both pure PGMA and PGMA-co-HEMA brushes were immersed in solutions of small molecules containing thiol and amine groups respectively, each at both pH8 and 10. The pure PGMA brushes did not achieve thickness increases noticeably outside the margin of measurement error in any of the four conditions. On the other hand, the addition of HEMA to the polymer brush results in thickness increases of the order of 40% for the thiol molecules at both pH values. This indicates the co-polymer brushes were able to react with a water-borne molecule to a greater extent, meaning that the addition of a water-soluble monomer improves the brush's ability to immobilise molecules from solution.

Interestingly however, the amine is found to not react with the PGMA-co-HEMA brush at either pH value. While this is surprisingly in light of the theoretical considerations laid out above, it does mean that a thiol linker can be expected to react specifically with the epoxy groups, without interference from any amine groups that may be present on the relevant biomolecule.

The last experiment involves the reaction of different polymer brushes with a thiol-containing peptide (CGGGKKK). While a reasonable thickness increase can be observed for a standard PGMA-co-HEMA increase, a dramatic effect of reducing the brush density can be observed. Reducing the coverage of ATRP initiator from 100 to 10 and 5% results not only in a an order-of-magnitude increase in the percentage thickness increase observed, but also a noticeable increase in the total thickness increase, despite a reduction in the initial thickness of the reactive brush.

3.3 Creation of biomolecule gradients on electrospun fibre mats

This section will describe preliminary experiments carried out to lay the groundwork for the translation of the 2D results outlined above into the tailorable functionalization of electrospun PCL scaffolds.

3.3.1 Covalent immobilization of marker molecules on electrospun PCL

At the start of the project a number of proof-of concept studies for the functionalization of fibrous PCL scaffolds via graft polymerization were carried out. The main goal was to determine the usefulness of a variety of materials characterization techniques for future optimization of the process, and to provide an initial assessment of the feasibility of the project. For this reason only a small number of different reaction conditions were evaluated, without trying to draw explicit conclusions about their effect. A number of techniques were employed to follow the reaction progress and changes in scaffold properties throughout the functionalization scheme.

In a first experiment, Hydrolysis conditions were varied to differing extents in the course of sample preparation for each technique while PGMA grafting time was kept constant at 2h.

In a second experiment, ATRP was carried out for different lengths of time without any hydrolysis, relying instead on already exposed hydroxyl groups on the fibre surfaces.

3.3.1.1 Analysis of scaffold microstructure

Scaffolds were studied at each step using scanning electron microscopy (SEM) to evaluate gross changes in mesh structure and fibre morphology. No significant differences between steps were observed as shown in Figure 25. Together with GPC results (see below) this suggests that degradation of the fibre mesh due to the different reaction steps is negligible. No differences could be observed between scaffolds hydrolysed in 0.2, 0.5 and 1 M aqueous solutions of NaOH (data not shown) at any point during the functionalization process, which consisted of hydrolysis, attachment of BIBB, ATRP (2h) of PGMA, and subsequent immersion in a 1mg/ml solution of type I collagen.

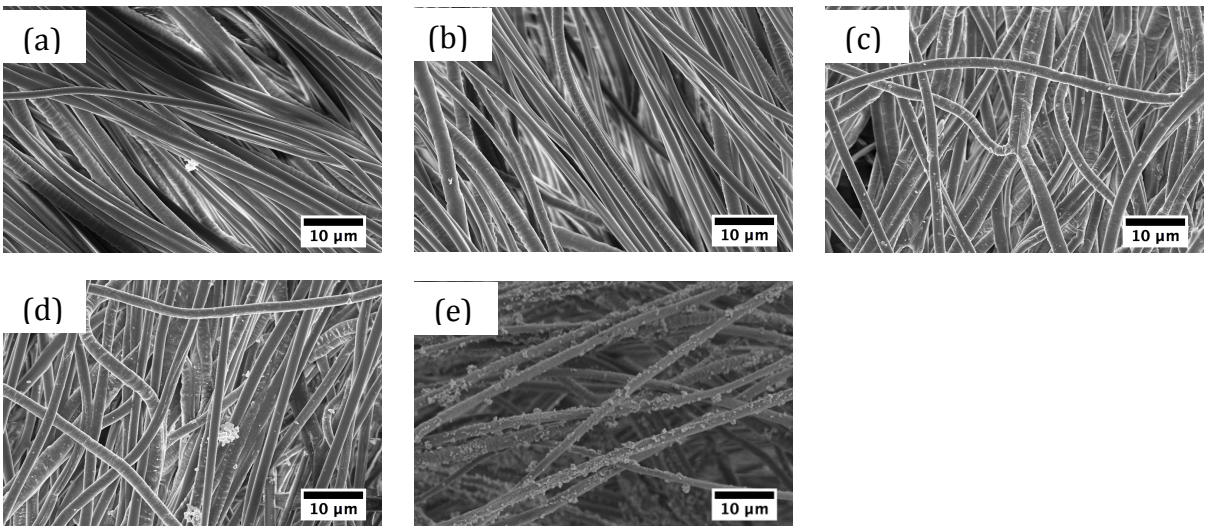

Figure 25: SEM images of PCL scaffolds: (a) pristine, (b) after 24h in 0.5M NaOH, and after subsequent attachment of (c)BIBB, (d) PGMA and (e) type 1 collagen.[D]

The experiment was subsequently repeated after optimization of the protocol in the 2D model system. Electrospun PCL scaffolds were functionalised with BIBB at a 20% surface coverage, followed by growth of a PGMA-co-HEMA brush for 1, 3 and 6 hours. Samples were then immersed in a 1mg/ml peptide solution overnight. None of the reaction steps resulted in meaningful morphological changes, indicating that the chosen reaction conditions would be well-suited to the functionalization of 3D scaffolds, without a negative effect on microstructure.

[D] Experiments carried out by Gabriel Mecklenburg. SEM images shown in this figure collected by Dr Lesley Chow.

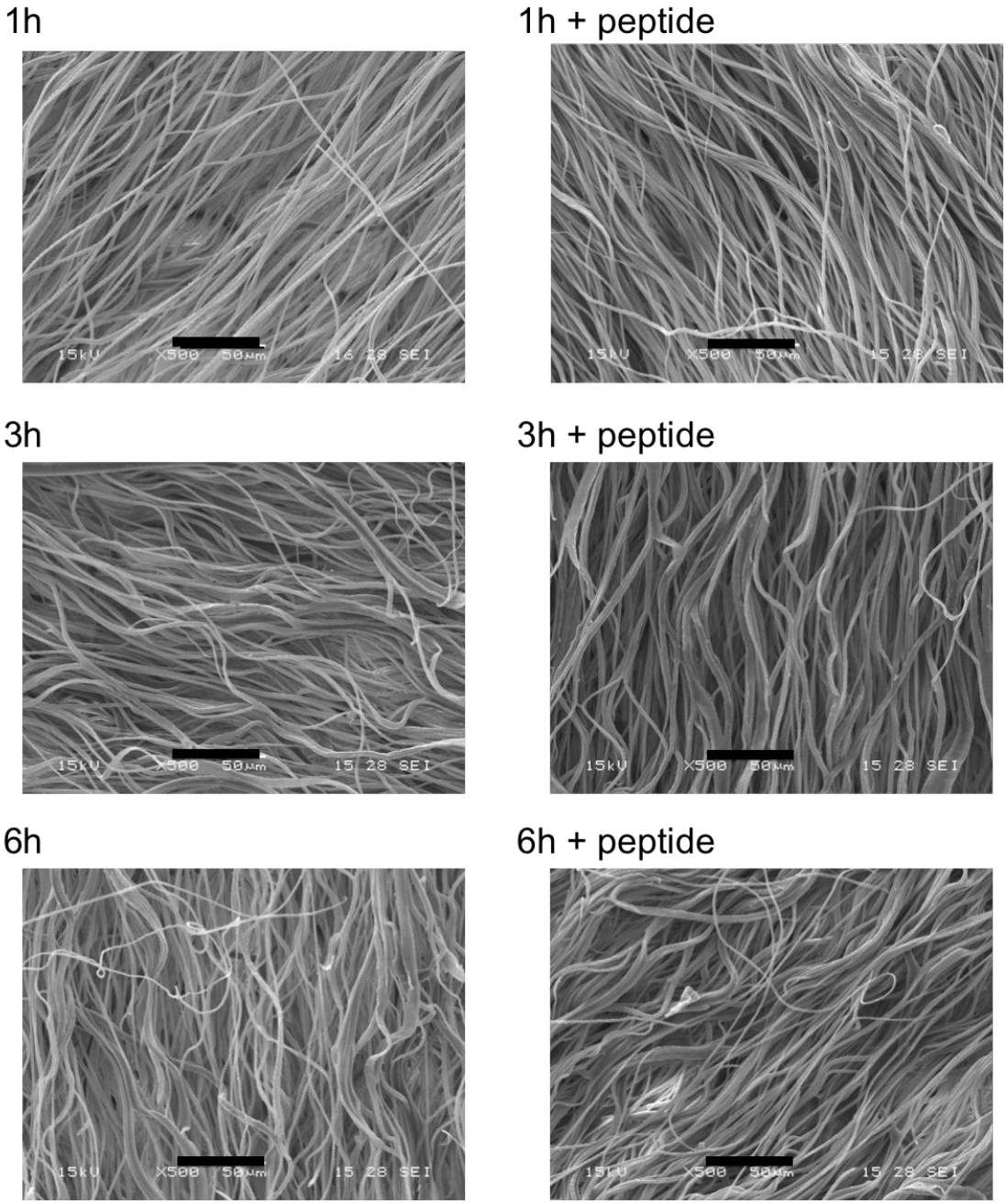

Figure 26: SEM images of PCL scaffolds, upon which surface-initiated ATRP has been carried out for 1,3 and 6 hours respectively. Samples are shown before and after immersion in a solution of a peptide to be attached to the reactive brush. Scale bar = 50μm.

3.3.1.2 Molecular weight changes during hydrolysis step

Electrospun scaffolds were hydrolyzed for 24h in 1, 0.5 and 0.2 M NaOH and for 6 h in 0.2 M NaOH and their gel permeation chromatography (GPC) traces compared to that of an non-hydrolyzed sample, as shown in Figure 27. The observable differences are too small to deduce any meaningful results. This

is not entirely unexpected, as chain scission should be confined to the surface and small polymer fragments are expected to be lost into solution.

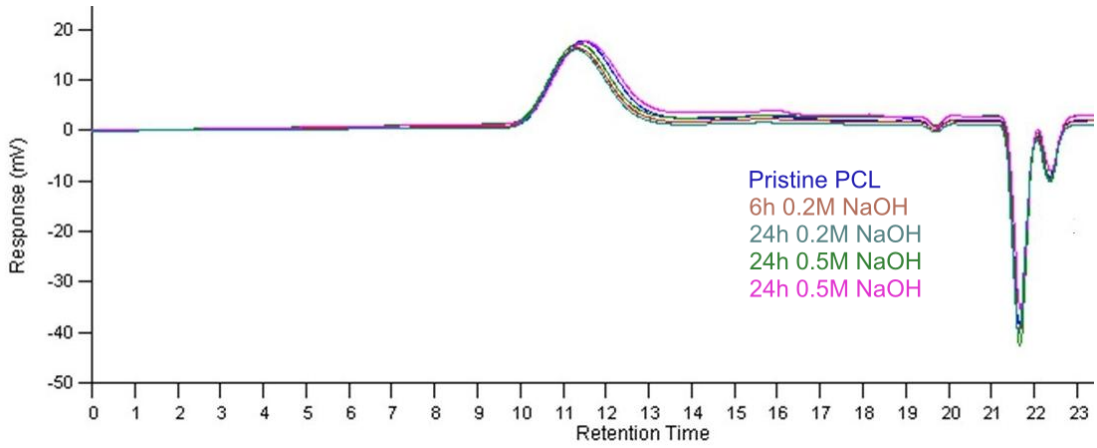

Figure 27: GPC trace of PCL scaffolds hydrolyzed in aqueous NaOH of varying molarity for different times (with prisitine PCL for comparison). Increasing retention time corresponds to lower molecular weight.[E]

3.3.1.3 Determination of PGMA graft yield

The chemical composition of the scaffolds was analyzed at each step using ^{1}H-NMR spectroscopy after dissolution of samples in $CDCl_3$ as well as attenuated total reflection Fourier transform (ATR-FTIR) spectroscopy. Changes due to hydrolysis and initiator attachment were found to be below the detection limit (data not shown).

[E] Experiments and subsequent sample preparation carried out by Gabriel Mecklenburg. GPC data collection courtesy of Dr Min Tang.

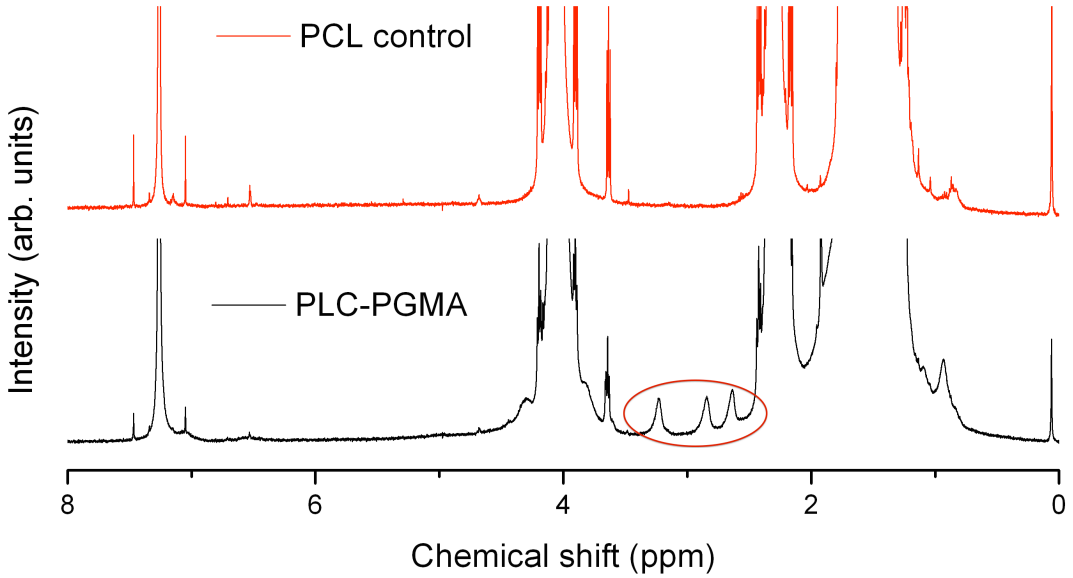

Figure 28: NMR data of PCL sample with grafted PGMA brush grown for 2h after 6h hydrolysis in 0.2M NaOH. The peaks characteristic of the epoxy group are circled in red.

Using the characteristic peaks corresponding to PGMA's epoxy ring (see Figure 8 for relevant structural drawings) in the ^{1}H-NMR spectra, 1 mol% of PGMA could be detected in graft-functionalized scaffolds, which was unaffected by varying the hydrolysis conditions during the first step from 6 to 24 h in 0.2 M NaOH. The spectra of the 6 h sample and a pristine scaffold are depicted in Figure 28, with the epoxy peaks circled in red. It is not entirely unexpected that no difference due to this change in hydrolysis conditions can be detected, since Xu *et al.*[19] found a denser-than-necessary distribution of hydroxyl-groups was already created in much milder conditions (24 h in 0.01 M NaOH). One issue to consider is that a portion of the epoxy groups may have already reacted with nucleophiles (most likely water) present during the grafting and washing processes. For the PGMA synthesized in bulk, the fraction of reacted epoxy groups was found to be close to 20%. Such detailed analysis is however impossible or at least very difficult to perform on the small fraction of PGMA grafted onto the PCL scaffolds. Because of this problem and since only unopened epoxy rings are important for subsequent biomolecule attachment we will continue to quantify the graft yield directly via these characteristic epoxy peaks.

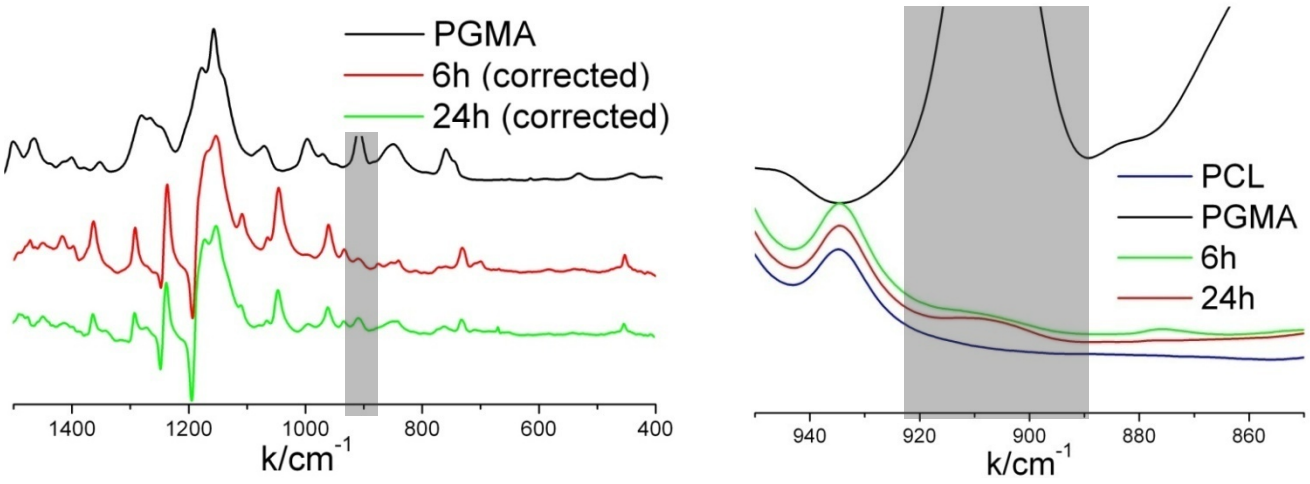

Figure 29: ATR-FTIR data of PCL grafted with PGMA as well as bulk PCL and PGMA. Curves marked "corrected" refer to PCL-PGMA signals with the PCL signal subtracted.

ATR-FTIR spectroscopy provides the means for rapid semi-quantitative analysis of the chemical make-up of the scaffolds without requiring sample preparation. Samples functionalized under the same conditions as for the NMR studies were used to facilitate comparison between the techniques. A peak around 910 cm^{-1} characteristic of the PGMA epoxy group is used for quantification, since there are no peaks in this region in the spectrum of pure PCL. An increase in peak height is visible when comparing the raw spectrum of the 24 h to the one of the 6 h sample (Figure 29(b)). The spectra resulting from normalization (using the prominent peak corresponding to the ester C=O bond stretch) of the spectra and subtraction of the pristine PCL spectrum are shown in Figure 29(a). The area of the epoxy peak is measured to have roughly doubled in the 24 h sample. Since the signals collected in ATR-FTIR spectroscopy originate from less than ~10 µm below the surface,[148] and no change in average PGMA content was found by NMR, this result seems to indicate uneven distribution of PGMA throughout the scaffold. This would not be entirely unexpected, since wetting of the fibrous mats in the NaOH solutions could be observed to progress rather slowly from the outer layers inwards. This effect can be attributed to the hydrophobic surface of the non-hydrolyzed PCL fibre surfaces and the small pore size, which reduce the rate of penetration of the aqueous solution into the mesh.

The non-hydrolysed samples were similarly analysed using NMR. The percentage ratios of PGMA to PCL were found to range from 2-4%,

corresponding to estimated brush thickness of 5-10nm. There was no direct correlation between polymerisation time and calculated brush thickness. This implies that the 3D system requires significantly more optimisation of the functionalization protocol.

3.3.1.4 Analysis of biomolecule immobilization

The incorporation of amine-modified fluorescein after grafting of PGMA was confirmed by fluorescence light microscopy. Samples hydrolysed for 16h in 0.2, 0.5 and 1 M aqueous NaOH solutions with subsequent PGMA grafting and fluorescein immobilization were compared. The results are depicted in Figure 30. As very intense fluorescence was observed, the possibility of fluorescence quenching makes even semi-quantitative statements comparing the different PCL-PGMA scaffolds impossible: The observed decreasing trend in intensity with harsher hydrolysis conditions can be due to decreased attachment or increased quenching. However, only very weak fluorescence was observed on thoroughly washed samples without PGMA attachment, proving that covalent attachment through the grafted PGMA occurred.

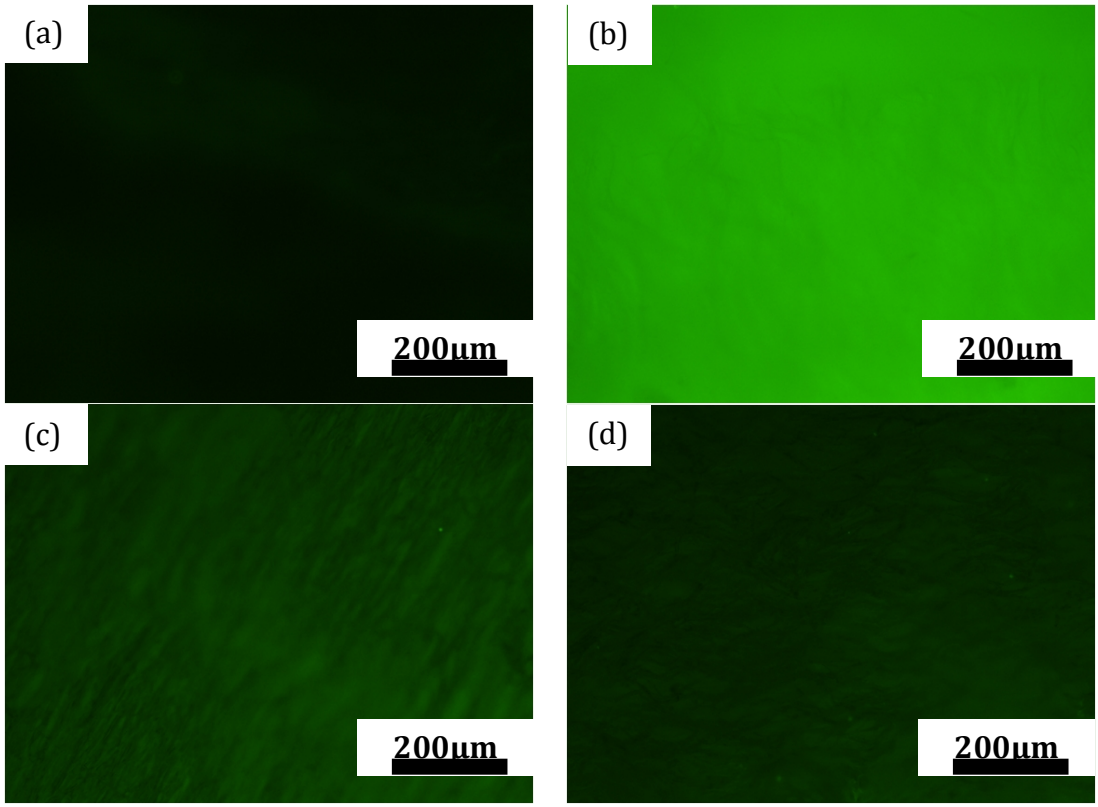

Figure 30: Fluorescence images of PCL scaffolds after treatment with fluorescein-amine. (a) Pristine scaffold and with grafted PGMA after initial hydrolysis for 24 h in (b)0.2 M, (c)0.5 M, (d)1 M NaOH.

3.3.2 Creation of covalently bound gradients on electrospun PCL via "controlled filling"

A limited proof-of-concept study evaluating the feasibility of covalent incorporation of a biochemical gradient into electrospun PCL scaffolds was performed. A gradient of fluorescein-amine persisting for at least one week could be created along a 5cm strip of electrospun PCL by the "controlled filling method" discussed before (as depicted in Figure 31). This was achieved with the following conditions: The strip was pre-wet with PBS to minimize wicking of the solution into the scaffold, which was previously shown to occur rapidly. To this end the vial was also closed to minimize evaporation of PBS from the pre-wet strip. The vial was filled at a rate of 5 ml/h, meaning the strip was immersed over the course of approximately 3 h, corresponding to a rate of 17 mm/h. Immediate thorough washing was found to prevent gradient formation, indicating that mainly physisorption occurred in the initial phase of attachment. To allow the gradient to achieve a state of covalent attachment, the strip was

confined between two cover slips for 5 h after a brief rinse and only then washed more thoroughly.

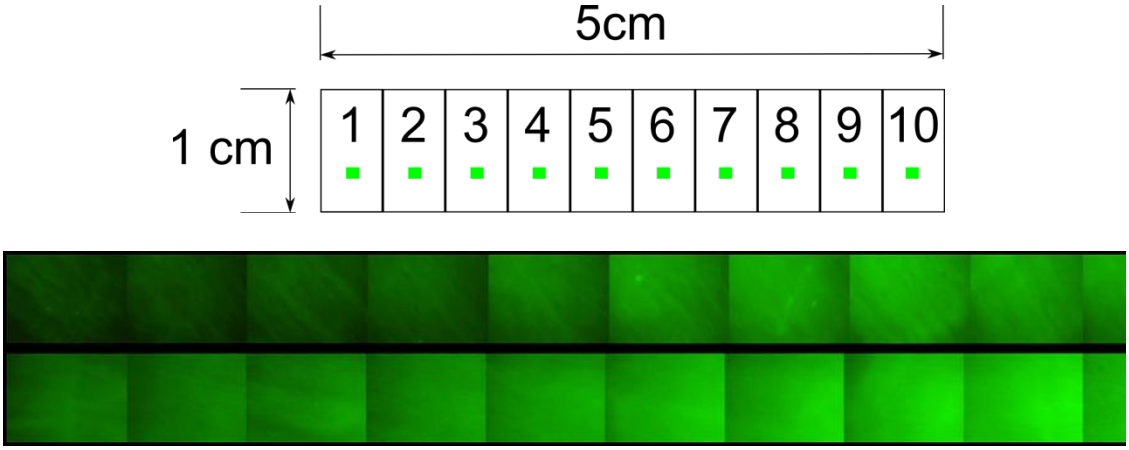

Figure 31: Fluorescence images collected along an immobilized fluorescein-amine gradient after immersion in PBS for 18 h and one week respectively. Individual images are approximately 900μm in width and are collected at 5mm intervals along a sample 5cm in length as depicted as depicted in (a), where the 10 green rectangles correspond to the 10 images making up each of the composite images in (b). Scale bar = 100microns.

3.3.3 Peptide synthesis

An obviously important consideration for the design of a tissue scaffold to be made bioactive via surface functionalization is the choice of biomolecule to be attached. A good candidate for this type of bioactive material are short peptides derived from fragments of extracellular matrix (ECM) proteins. Many ECM proteins contain amino acid sequences that interact with cell receptors and provide important instructions, such as what cell type a stem cell should differentiate into.

The chosen fragment in this case is DGEA, which is derived from collagen I. DGEA is a cell-adhesive motif that has been shown to strongly induce osteogenic differentiation in mesenchymal stem cells.[157,158] As such, it is a good candidate for functionalization of the bone-contacting half of the proposed gradient scaffold.

To create a usable molecule, a cysteine, C, (which provides a thiol group for specific coupling to the epoxy groups present on the PGMA brush) is added to

the peptide fragment via a flexible spacer (GGG). On the other end of the peptide, a Lysine, K, is added to provide an attachment point for a fluorescein marker (via an NHS ester linkage), to visualise the attachment of the peptide throughout the scaffold. The full structure of the molecule to be used is thus CGGGDGEAK-fluorescein. The peptide is synthesised using standard solid phase techniques with Fmoc chemistry. An attempt was made to attach the fluorescein, again in the solid phase, by coupling the amine group on the lysine (K) to the NHS ester group attached to the fluorescein.

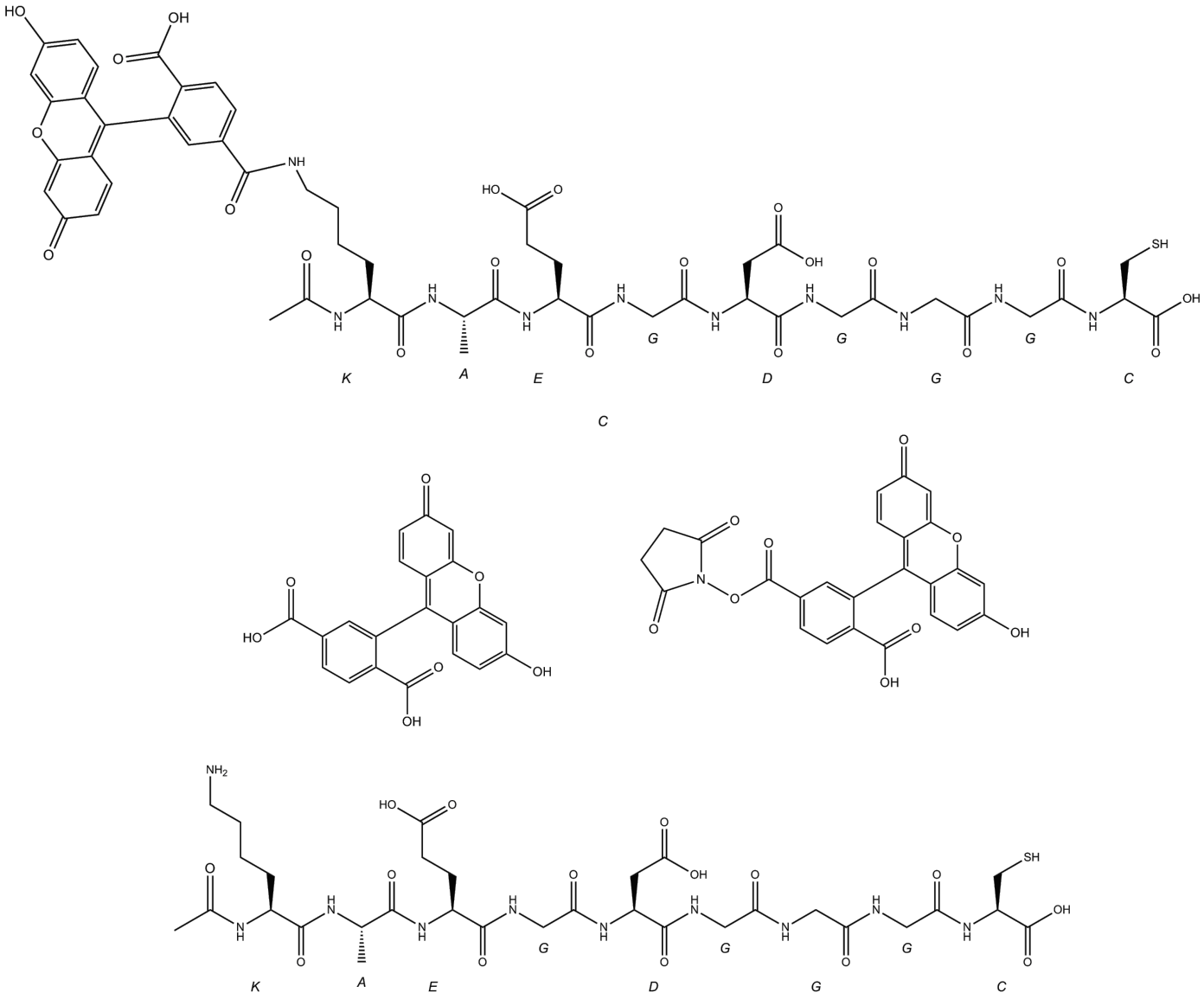

Figure 32: Structural drawing depicting the relevant chemical entities. The top shows the peptide with attached fluorescein, while the bottom shows the pure peptide. The middle row depicts fluorescein (left) and fluorescein-NHS (right).

The result of the peptide synthesis is shown below in the form of mass spectrometry traces of the peptide both with and without the attached fluorescein. While this part of the project was not pursued further, it is clear that standard solid phase synthesis methods are well suited to manufacture biologically relevant peptide fragments with fluorescent tracer groups, at least at experimental scale.

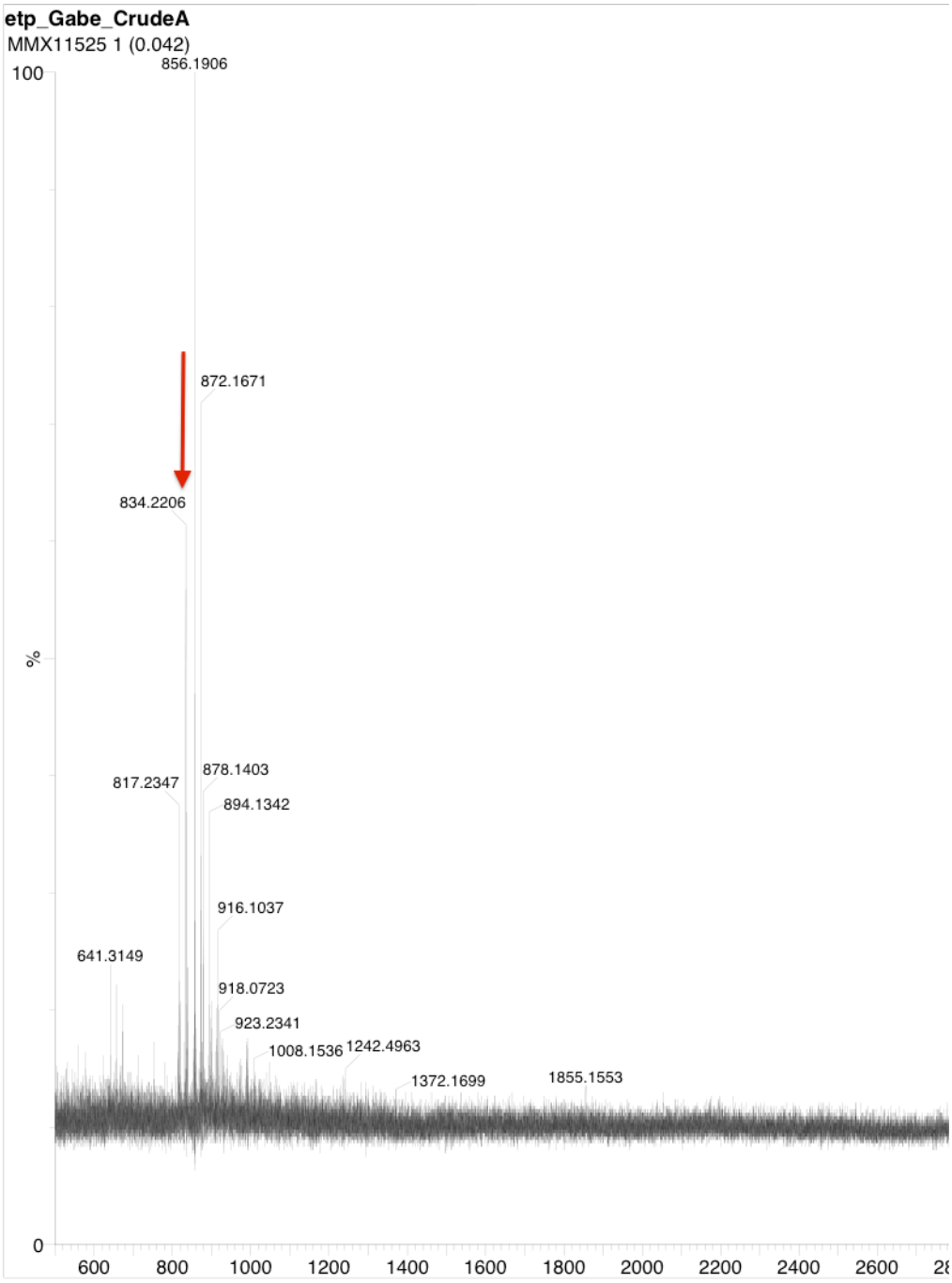

Figure 33: MALDI traces showing the molecular weight distributions in the synthesised peptide, with the peak at 834g/mol corresponding to the target peptide (CGGGDGEAK) without attached fluoresceine. (b) shows the peptide with attached fluorescein, which corresponds to the peak at 1192g/mol.

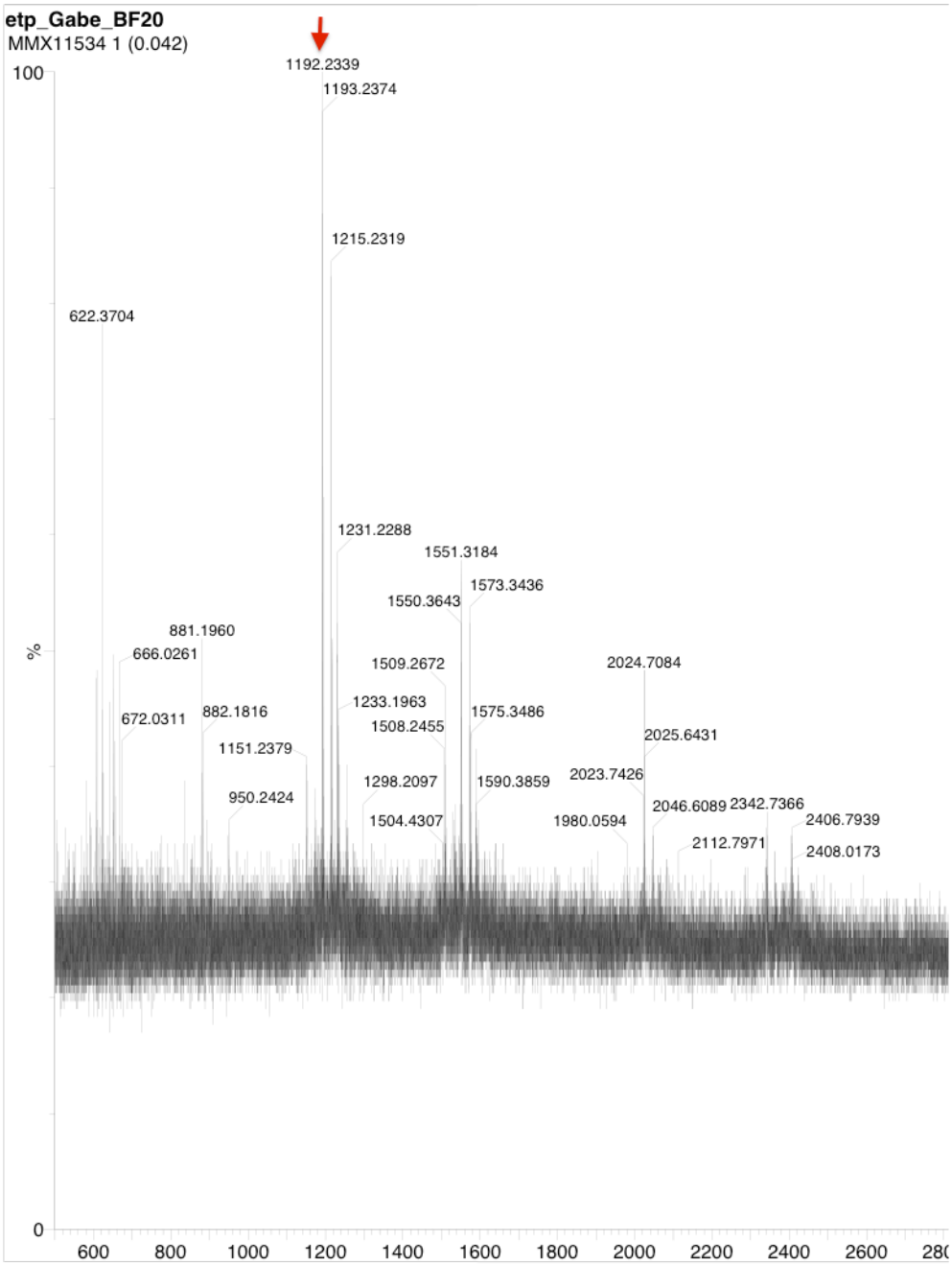

Figure 34: MALDI traces showing the molecular weight distributions in the synthesised peptide, with the peak at 1192g/mol corresponding to the target peptide (CGGGDGEAK) with attached fluorescein.

3.4 Electrospun scaffolds with covalently bound PMPC-coatings for heart valve tissue engineering

One of the major reasons for the careful optimisation of the 2D model system carried out in this project is the versatility of the use of surface-initiated ATRP for functionalization of polymer fibres. Apart from providing reactive epoxy groups (via the GMA-based brushes described above), there are many other methacrylate monomers that can be attached to electrospun fibres for a range of biomedical applications.

One such monomer is 2-Methacryloyloxyethyl phosphorylcholine (MPC). The zwitterionic side-chains on the resulting polymer (PMPC) mimic chemical structures found in the cell membrane, and have been shown to dramatically improve the hemocompatibility of artificial materials.[138,139]

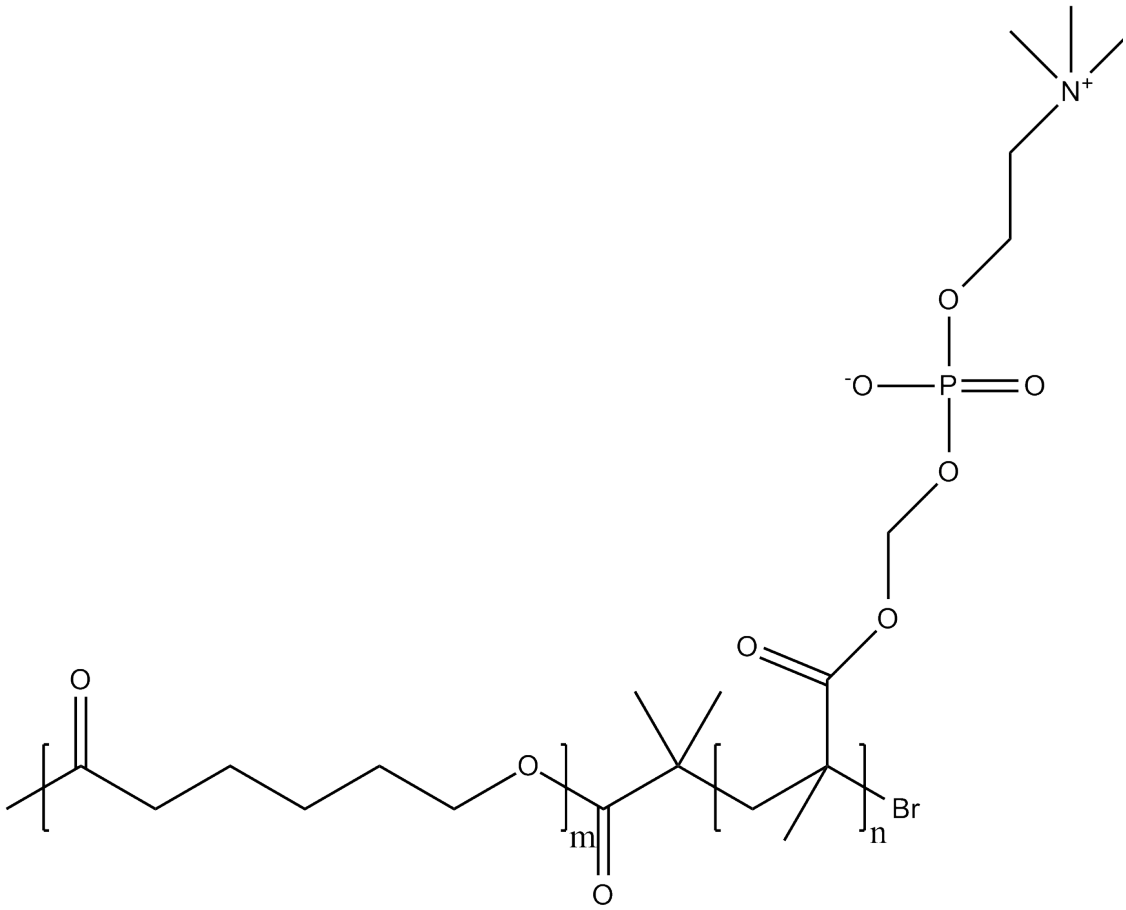

Figure 35: Schematic depiction of PMPC (right) grafted to the terminal hydroxyl group of the PCL (left) substrate.

As such, grafting PMPC on electrospun PCL is an interesting material to explore for the design of blood-contacting, semi-permanent tissue engineering scaffolds. Specifically, the microstructure and mechanical properties of such a non-woven PCL construct could be tailored to match those of a venous valve. By immobilising PMPC brushes on the PCL surface, formation of blood clots, traditionally a problem with all blood-contacting artificial materials, could be largely suppressed. As shown in previous sections, the properties of the underlying scaffold would hardly be affected by the graft polymer coating.

Shown in Figure 36 below are the results of exploratory experiments evaluating the growth of PMPC brushes on PCL, in both the 2D model system established previously, and on electrospun PCL fibres. While the results are very preliminary, it is not unreasonable to assume that the well-controlled, linear growth of PMPC brushes can be reliably achieved using a protocol closely related to that established for the GMA/HEMA system.

To test the hypothesis of improved haemocompatibility, a thrombin gene (b) ssay was carried out on electrospun PCL scaffolds with various thicknesses of PMPC coating, and compared to both blank PCL and a variety of reference materials provided in the assay kit.

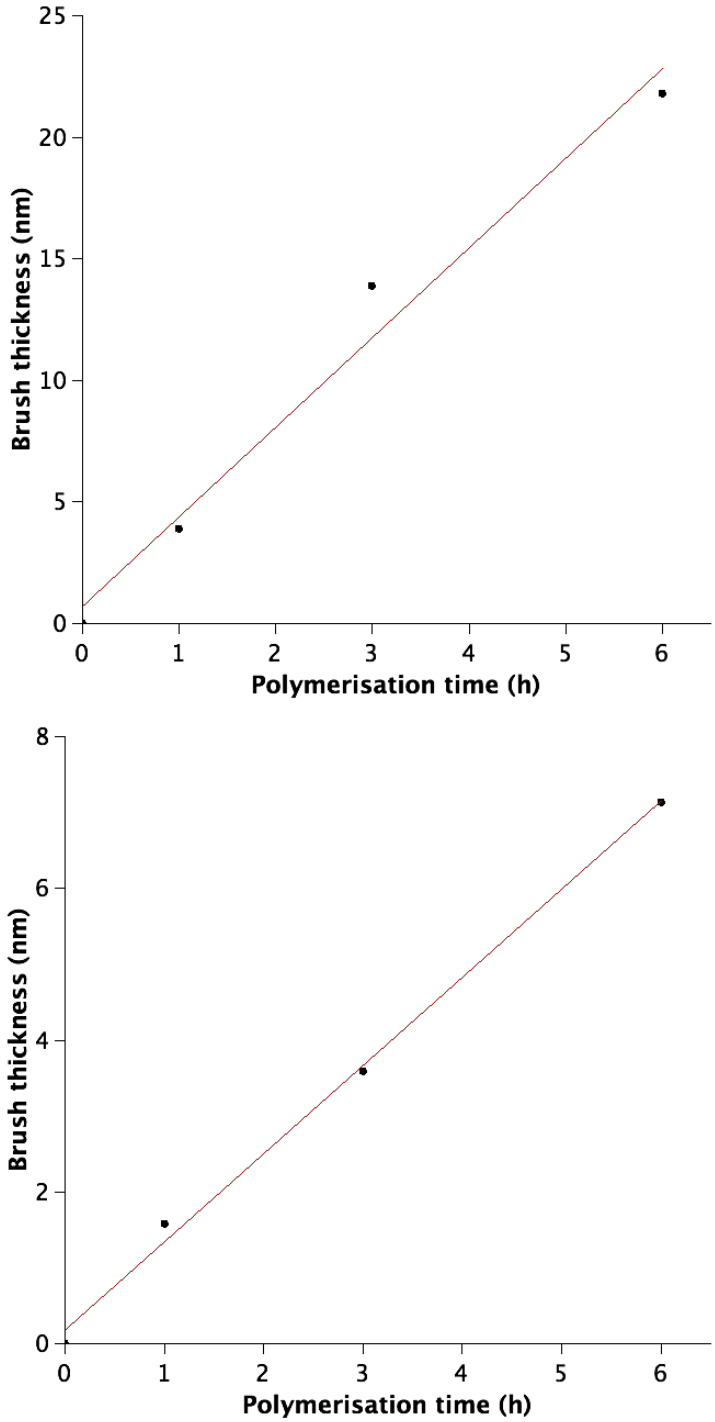

Figure 36: Results of exploratory experiments evaluating the growth of PMPC brushes. (a) shows brush thickness on a 2D PCL surface, covalently immobilised on silicon, determined using ellipsometry, while (b) shows the brush thickness on electrospun PCL, calculated from NMR analysis of dissolved scaffolds (both n = 1).

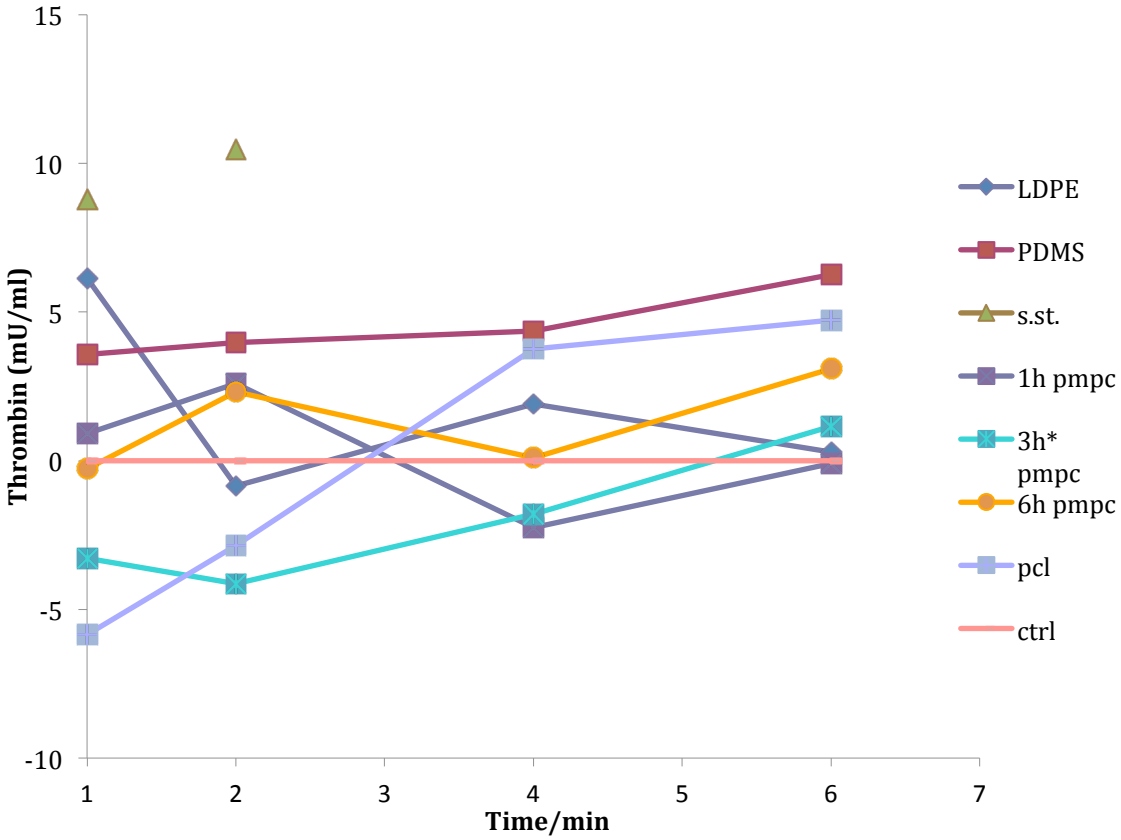

Figure 37: Results of the thrombin generation assay carried out on electrospun PCL scalffolds with surface-bound PMPC brushes grown for 1, 3, and 6h respectively as well as a range of controls: low density polyethylene (LDPE), stainless steel (s.st.), PDMS, a blank electrospun scaffold. All values are corrected by subtracting the values from an empty well (ctrl).[F]

3.5 Surface initiated polymerization of dapsone-methacrylate on electrospun PCL for anti-bacterial and –inflammatory membranes

In a similar vein to the PMPC-project outlined above, it was attempted to create surface coated with a polymerised version of the anti-microbial drug dapsone.[159] The starting material for this was dapsone-methacrylate, where one of the primary amine groups is modified with a methacrylate group (material kindly supplied by Luis Rojo del Olmo). Polymerised forms of drugs have previously shown to retain a degree of efficacy,[160] making surface-initiated drug polymer brushes a prime candidate for modification of surfaces of medical devices, sutures, bandages, etc.

[F] Experiments carried out jointly with Hayley Moore.

A range of different ATRP protocols were employed in the attempt to create controlled growth of the dapsone-polymer on 2D PCL surfaces, centering on the choice of different, more active catalyst systems. Following on from these unsuccessful experiments, it was further attempted to protonate the remaining free primary amine. This is because free amines are only in very rare cases compatible with any of the controlled radical polymerisation techniques (ATRP, RAFT, NMP).[161] However, simple protonation using TFA (see below) was not successful.

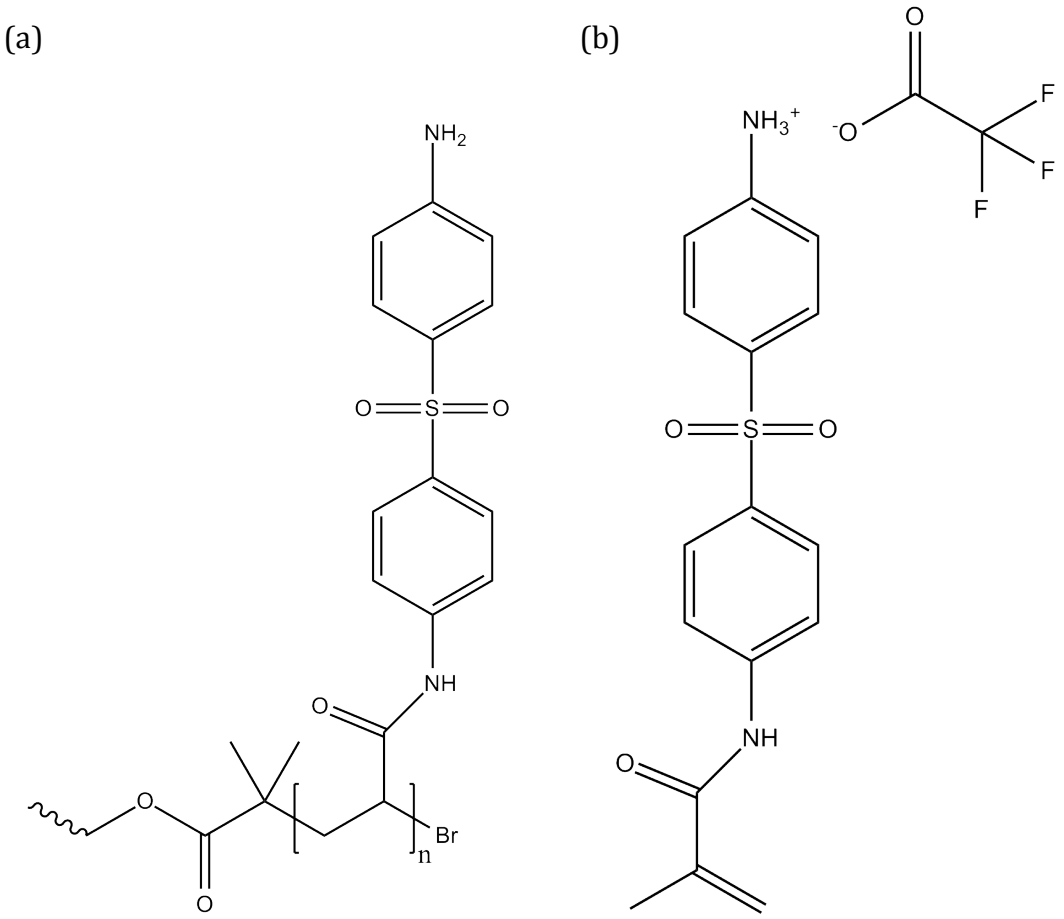

Figure 38: Schematic depiction of (a) poly(dapsone-MA) grafted to the hydroxyl group of a PCL substrate and (b) the dapsone-MA monomer protonated by reaction with TFA.

4 Discussion

4.1 Major findings

Most importantly, the results of the project presented in this thesis demonstrate the promise of the use of polymer brushes grown on electrospun polymers via surface-initiated ATRP for biomedical applications. At the same time, it is clear that there is ample scope for future work to more robustly validate and quantify the methods developed herein.

A robust, reliable and easy-to-characterise 2D model system based on PCL films covalently immobilised onto monocrystalline silicon was established. By using such a system, it was possible to use ellipsometeric thickness measurements to track nanometer-scale thickness changes in the polymer brushes grafted onto the PCL surface. The covalently immobilised PCL as well as the PCL chip were found to be stable and inert in all relevant reaction conditions explored. This system can thus be used to rapidly optimise the reaction conditions required for controlled growth of a wide variety of different polymer brushes on PCL.

Further, the versatility of the approach was demonstrated by successfully grafting two different homopolymers (based on Glycidyl Methacrylate, GMA, and 2-Methacryloyloxyethyl phosphorylcholine, MPC) and one co-polymer (based on GMA with Hydroxyethyl Methacrylate, HEMA) onto these 2D surfaces. All of these brushes could be grown with good control over the polymerisation progress, tracked via ellipsometric thickness. Furthermore, the reaction conditions for the MPC and GMA-co-HEMA brushes were established with only minor modifications of the protocol originally developed for GMA and rapidly optimised. Lastly, some successful initial steps were made to translate these results to electrospun PCL samples, where some graft brush growth was shown, albeit with poor control.

An established system of PGMA brushes on PCL for biomolecule immobilisation was also successfully optimised by increasing the spacing between brush polymer chains, and increasing the brushes water-swellability. While the results presented require more rigorous validation, they do suggest

the biomolecule attachment scheme is both effective (i.e. molecules are attached through the thickness of the brush) and selective (i.e. a certain functional group can be targeted for attachment to the brush). This is achieved by three key modifications to the original scheme:

1. Using a pH-dependent, selective epoxy-thiol linkage for biomolecule attachment to the reactive brush. In this context it was established that at moderate pH values (8-10), the epoxy groups on a P(GMA-co-HEMA) brush react selectively with thiol groups, but not amine groups. This could be used to form the basis of a specific attachment scheme via thiol linkers in certain locations on the biomolecule to be attached.

2. Adding a water-soluble component to the brush to improve penetration by the biomolecule. It was shown that the addition of HEMA to a GMA-based brush resulted in the thickness-increase resulting from incorporation of a small-molecule thiol to increase from 5 to 40% of the original brush thickness.

3. Reducing the surface coverage of the initiator, to create a less dense brush, and again improve penetration by the biomolecule. By reducing the surface coverage from 100 to 10 and 5%, the thickness increase of a P(GMA-co-HEMA) brush caused by incorporation of a thiol-containing peptide was shown to increase in absolute terms, despite a significant decrease in the original brush thickness. The results were even more dramatic when considered in percentage-increase terms, where the brush grown from 5% initiator coverage increased in thickness by 140%.

The results of the 2D optimisation have also been translated into early, exploratory work on electrospun samples: The effective incorporation of a model molecule (fluorescein) into electrospun scaffold, both uniformly and in for the form of a linear gradient was demonstrated. The effective immobilisation of fluorescein-amine is somewhat surprising in light of the results of the 2D studies, which showed negligible covalent attachment of amine-groups to PGMA brushes. Two possible explanations for this might be:

- Poor control over the 3D functionalization protocol resulting in non-covalent incorporation of the fluorescein-amine.
- Detection of the fluorescent signal on 3D scaffolds can be achieved at much lower brush functionalization percentages than detection of a thickness increase in the 2D system.

Taken together, the optimisation of the attachment scheme in the 2D model, and the promising initial results on electrospun fibres indicate that the use of a PGMA-co-HEMA brush with increased inter-chain spacing for immobilisation of biomolecules on electrospun PCL via thiol-epoxy coupling could be an effective biofunctionalisation scheme.

Furthermore, the versatility of the underlying approach was demonstrated by grafting PMPC brushes onto PCL, both in the 2D model system, and using electrospun PCL. Preliminary results indicate that the resulting fibre membrane shows promise as a highly haemocompatible material for cardiovascular tissue engineering, such as the reconstruction of venous valves (see Figure 37). It is obviously difficult to draw meaningful conclusions from a single repeat of a fairly complex assay, but all the PMPC-coated samples performed on par with the highly haemocompatible reference provided (LDPE), and outperformed the less haemocompatible PDMS and stainless steel. However, it is difficult deduce an improvement over uncoated PCL without more statistically significant data. Overall, early results of this project have been promising, especially considering that PMPC-grafted surfaces have previously been demonstrated to be effective.

4.2 Comparison to previous work

While the presented results are only preliminary, they do imply that the chosen functionalization approach compares favourably with previous work on a number of levels.

Most of the existing work on orthopaedic interfacial tissue engineering has focused on the creation of stratified scaffolds, rather than smooth gradients (such as Helen Lu's work on ACL repair [68,78,79]). This affords obvious advantages in manufacturing, as the final scaffold can be created by joining several

homogeneous scaffolds. However, it can be expected that a smoother gradient of scaffold properties will result in a final construct that more closely approximates the graded (rather than abruptly stratified) properties found in the natural enthesis connecting ligament/tendon to bone. Some limited efforts have been made to create smoother gradients, using e.g. PLGA microspheres with encapsulated growth factors[90] - these approaches can ben expected to gain in popularity as the sophistication of available biofunctionalisation techniques grows.

Of course, its versatility means that the use of surface initiated ATRP has been evaluated by a number of groups for a range of biomedical applications. As discussed in a thorough review by Jiang *et al.,* even biofunctionalisation of surfaces using such polymer brushes has been studied extensively.[120] Common functional groups incorporated into the polymer brush for subsequent conjugation to groups on the biomolecules to be immobilised include epoxy, carboxyl, hydroxyl, cationic, aldehyde, and primary amine groups. Various chemistries based on these groups have been used to immobilised anything from short peptide fragments to complete proteins and DNA strands on a range of polymer and inorganic surfaces. However, none of these approaches went significantly beyond simple homopolymer brushes – both the incorporation of a water-swellable moiety into the reactive brush and the increase of brush spacing represent novel approaches for increasing the amount of immobilized biomolecules and improving their bioavailability. Specifically, this represents a significant improvement over the original work by Xu et al., which forms the foundation for the work presented here.[19]

One important advantage of the 2D model system described in this thesis is the ability to perform precise high-throughput optimisation studies for novel monomer systems. Rather than relying on imprecise methods such as weighing (as employed by Xu et al.) to quantify brush growth on polymer films, the use of ellipsometry allows rapid, precise and reliable measurements of both brush growth and subsequent functionalization. While 2D results are obviously not directly translatable to functionalization of microfibrous polymers, the 2D

system can certainly be used to optimise reaction conditions before further detailed study on more relevant 3D scaffolds.

4.3 Limitations and future work

Obviously, the results presented here only represent a first step towards the ultimate goal of using ATRP to create a wide range of biofunctionalised materials, focusing especially on the creation of biochemical gradients for orthopaedic interfacial tissue engineering.

Further work should focus on the thorough characterisation of incorporation of different biomolecules into reactive brushes in the 2D system. This should be followed by more rigorous translation of these 2D results to electrospun fibres, as well as the characterisation of cellular response to immobilised osteogenic/tenogenic molecules (such as the successfully synthesised collagen I-derived fragment DGEA). In addition, the experimental setup for gradient creation needs to be fine-tuned. This should include more efficient means for suspending the scaffold. In order to minimize the amount of costly biomolecules needed for further studies, it might also be sensible to construct a custom chamber similar to the one described by Shi *et al.*[20]

Another remaining untested hypothesis is that the brush will present the attached biomolecules to contacting cells more effectively, by acting as a flexible linker to the substrate. This will require cell culture experiments to be carried out, where surfaces modified with the same biomolecule, via a direct linker and a flexible brush respectively, would be compared.

Unfortunately, the constraints of the ATRP technique prevented the successful synthesis of brushes comprising a modified version of the antibacterial drug dapsone. The only real possibility for the creation of graft polymer brushes with dapsone functionality would thus be the use of a protecting group on the free amine (such as Fmoc, which is commonly used in peptide synthesis). However, this may well introduce undue complexity into the manufacturing process, which would essentially negate the benefit of the simple ATRP-based functionalization approach. At the same time, this does not preclude the systems usefulness for creating surfaces covalently coated with other

polymeric drugs, assuming they do not include functional groups that are incompatible with ATRP.

4.4 Wider implications

As stated before, the key aspect of the presented work is the development of a versatile system for developing and optimising ATRP-based functionalization schemes for polymer scaffolds. The applications for this are nearly endless, only limited by the availability of methacrylate polymers (and their compatibility with the ATRP reaction). These brushes can in principle grown on any kind of polyester, meaning the underlying mechanical and degradation properties can be tailored independently from the surface functionality. Possible applications include a wide range of tissue engineering scaffolds, functional wound dressings, water filters, etc.

Focusing again on the application that originally motivated this work, the prevalence of rotator cuff supraspinatus tendon tears (present in roughly 30% of the population over the age of 60[4]) is rapidly increasing as the population ages, while the supply of suitable donor tissue is highly limited. Combined with the fact that most people are expecting to be able to stay active much later into their lives, this makes the development of suitable synthetic tissue engineering scaffolds for these applications an increasingly urgent requirement.

One interesting consideration to mention in the context of the ultimate clinical application is the actual tissue engineering strategy to be employed. In terms of adoption by clinicians, a fully synthetic product that can be implanted into the patient directly off the shelf would obviously be ideal, as it would represent the least amount of change to clinical practice. However, this requires the scaffold to be able to recruit and sustain local cell populations from the damaged tissues around the tear site. Especially on the tendon side (where tissue degradation is common), this will likely present significant problems. More likely (especially in the short term) is a situation whereby the scaffold is seeded in vitro with stem cells harvested from the patient, grown into a construc more closely resembling the native tissue, and subsequently implanted.

5 Conclusions

In summary, a robust workflow for optimising the growth of polymer brushes on PCL via surface-initiated ATRP was designed. The method revolves around rapid optimisation of an ATRP system in an easy-to-characterise 2D model system, followed by translation of these optimised results to usable 3D fibrous scaffolds.

Exploration of the use of this workflow to design an effective and selective biofunctionalisation scheme, as well as a new haemocaompatible cardiovascular tissue engineering scaffold, was begun. The immobilisation scheme involved the following key aspects:

- Incorporation of GMA into the surface-bound brush provided epoxy groups, which were shown to react selectively with thiol groups at certain pH values. This would allow the specific coupling of biomolecules to the brush via e.g. a cycteine incorporated into a peptide.
- By including water-soluble HEMA into the brush, the amount of attached molecules could be increased. This is hypothsised to be due to the fact that these molecules could reach GMA groups deeper in the water-swollen PGMA-co-HEMA brush than in the water-insoluble PGMA brush.
- Molecule incorporation could be further increased (both in relative and absolute terms) by increasing the spacing of the brush, by reducing the density of initiators on the underlying polymer surface.

Some initial promising results were generated in relation to translating the functionalisation scheme from the 2D model to 3D by incorporating even distributions as well as gradients of a fluorescent model molecule into electrospun fibrous PCL scaffolds.

This system should in the future enable rapid iteration in the design of related graft-polymer systems, both for biomedical and other applications. Most

directly, the work presented here should be continued towards the goal of creating counter-running dual gradients of osteogenic and tenogenic biomolecules on fibrous PCL scaffolds. These scaffolds could then be evaluated for their suitability as tissue engineering scaffolds for damaged orthopaedic interfaces such as torn rotator cuff tendons.

References

1. Yang, P. J. & Temenoff, J. S. Engineering orthopedic tissue interfaces. *Tissue Eng. Part B. Rev.* **15,** 127–41 (2009).

2. Phillips, J. E., Burns, K. L., Le Doux, J. M., Guldberg, R. E. & García, A. J. Engineering graded tissue interfaces. *Proc. Natl. Acad. Sci. U. S. A.* **105,** 12170–5 (2008).

3. Lu, H. H., Subramony, S. D., Boushell, M. K. & Zhang, X. Tissue engineering strategies for the regeneration of orthopedic interfaces. *Ann. Biomed. Eng.* **38,** 2142–54 (2010).

4. Sherman, S. L., Lyman, S., Koulouvaris, P., Willis, A. & Marx, R. G. Risk factors for readmission and revision surgery following rotator cuff repair. *Clin. Orthop. Relat. Res.* **466,** 608–13 (2008).

5. Cheung, E. V, Silverio, L. & Sperling, J. W. Strategies in biologic augmentation of rotator cuff repair: a review. *Clin. Orthop. Relat. Res.* **468,** 1476–84 (2010).

6. Lyman, S. *et al.* Epidemiology of anterior cruciate ligament reconstruction: trends, readmissions, and subsequent knee surgery. *J. Bone Joint Surg. Am.* **91,** 2321–8 (2009).

7. O'Neill, D. B. D. B. Arthroscopically assisted reconstruction of the anterior cruciate ligament - A prospective randomized analysis of three techniques. *J. Bone Jt. Surg.* **78A,** 803–813 (1996).

8. Reilly, P. *et al.* Passive tension and gap formation of rotator cuff repairs. *J. Shoulder Elb. Surg.* **13,** 664–667 (2004).

9. Boileau, P. *et al.* Arthroscopic repair of full-thickness tears of the supraspinatus: does the tendon really heal? *J. Bone Joint Surg. Am.* **87,** 1229–40 (2005).

10. Lu, H. H. & Jiang, J. Interface Tissue Engineering and the Formulation of Multiple-Tissue Systems. *Adv Biochem Engin/Biotechnol* **102,** 91–111 (2006).

11. Longo, U. G., Lamberti, A., Maffulli, N. & Denaro, V. Tissue engineered biological augmentation for tendon healing: a systematic review. *Br. Med. Bull.* 1–29 (2010). doi:10.1093/bmb/ldq030

12. Tsiridis, E., Velonis, S., Limb, D. & Giannoudis, P. V. Tissue engineering approaches to rotator cuff tendon deficiency. *Connect. Tissue Res.* **49,** 455–63 (2008).

13. Moffat, K. L. *et al.* Novel nanofiber-based scaffold for rotator cuff repair and augmentation. *Tissue Eng. Part A* **15,** 115–26 (2009).

14. Vaquette, C. *et al.* Aligned poly(L-lactic-co-e-caprolactone) electrospun microfibers and knitted structure: a novel composite scaffold for ligament tissue engineering. *J. Biomed. Mater. Res. A* **94,** 1270–82 (2010).

15. Rokkanen, P. *et al.* Absorbable devices in the fixation of fractures. *J. Trauma* **40,** S123–7 (1996).

16. Sutures: Absorbable | ETHICON PRODUCT CATALOG. at <http://www.ecatalog.ethicon.com/sutures-absorbable>

17. Gunatillake, P. a & Adhikari, R. Biodegradable synthetic polymers for tissue engineering. *Eur. Cell. Mater.* **5,** 1–16; discussion 16 (2003).

18. Braunecker, W. & Matyjaszewski, K. Controlled/living radical polymerization: Features, developments, and perspectives. *Prog. Polym. Sci.* **32,** 93–146 (2007).

19. Xu, F. J., Wang, Z. H. & Yang, W. T. Surface functionalization of polycaprolactone films via surface-initiated atom transfer radical polymerization for covalently coupling cell-adhesive biomolecules. *Biomaterials* **31,** 3139–47 (2010).

20. Shi, J. *et al.* Incorporating protein gradient into electrospun nanofibers as scaffolds for tissue engineering. *ACS Appl. Mater. Interfaces* **2,** 1025–30 (2010).

21. Benjamin, M. in *Regen. Med. Biomater. Repair Connect. Tissues* (Archer, C. & Ralphs, J.) 351–374 (Woodhead Publishing Limited, 2010).

22. Saamanen, A.-M., Arokoski, J. P. A., Jurvelin, J. S. & Kiviranta, I. in *Regen. Med. Biomater. Repair Connect. Tissues* (Charles, A. & Ralphs, J.) 1–38 (Woodhead Publishing Limited, 2010).

23. Itoi, E. *et al.* Tensile properties of the supraspinatus tendon. *J. Orthop. Res.* **13,** 578–584 (1995).

24. James, R., Kesturu, G., Balian, G. & Chhabra, a B. Tendon: biology, biomechanics, repair, growth factors, and evolving treatment options. *J. Hand Surg. Am.* **33,** 102–12 (2008).

25. Pryce, B. a *et al.* Recruitment and maintenance of tendon progenitors by TGFbeta signaling are essential for tendon formation. *Development* **136,** 1351–61 (2009).

26. Taylor, E. D., Nair, L. S., Nukavarapu, S. P., McLaughlin, S. & Laurencin, C. T. Novel nanostructured scaffolds as therapeutic replacement options for rotator cuff disease. *J. Bone Joint Surg. Am.* **92 Suppl 2,** 170–9 (2010).

27. Liu, Y., Ramanath, H. S. & Wang, D.-A. Tendon tissue engineering using scaffold enhancing strategies. *Trends Biotechnol.* **26,** 201–9 (2008).

28. Funk, L. Rotator Cuff Biomechanics. (2005). at <http://www.shoulderdoc.co.uk/education/rotator_cuff_mechanics.pdf>

29. Benjamin, M. & Ralphs, J. R. Fibrocartilage in tendons and ligaments--an adaptation to compressive load. *J. Anat.* **193 (Pt 4,** 481–94 (1998).

30. Stevens, M. M. Biomaterials for bone tissue engineering. *Mater. today* **11,** 18–25 (2008).

31. Fallon, J., Blevins, F. T., Vogel, K. & Trotter, J. Functional morphology of the supraspinatus tendon. *J. Orthop. Res.* **20,** 920–6 (2002).

32. Langer, R. & Vacanti, J. Tissue engineering. *Science* **260,** 920–926 (1993).

33. Lee, M. & Wu, B. M. in *Regen. Med. Biomater. Repair Connect. Tissues* (Archer, C. & Raalphs, J.) 419–436 (Woodhead Publishing Limited, 2010).

34. Goh, J. C. H. & Sahoo, S. in *Regen. Med. Biomater. Repair Connect. Tissues* (Archer, C. & Ralphs, J.) 452–469 (2010).

35. Ge, Z., Yang, F., Goh, J. C. H., Ramakrishna, S. & Lee, E. H. Biomaterials and scaffolds for ligament tissue engineering. *J. Biomed. Mater. Res. Part A* **94A,** 639–651 (2006).

36. Longo, U. G. *et al.* Synthetic Grafts for Anterior Cruciate Ligament Reconstruction. *Curr. Stem Cell Res. Ther.* **8,** 429–437 (2013).

37. Ricchetti, E. T., Aurora, A., Iannotti, J. P. & Derwin, K. A. Scaffold devices for rotator cuff repair. *J. Shoulder Elbow Surg.* **21,** 251–65 (2012).

38. Kuo, C. K. & Tuan, R. S. Mechanoactive tenogenic differentiation of human mesenchymal stem cells. *Tissue Eng. Part A* **14,** 1615–27 (2008).

39. Juncosa-Melvin, N. *et al.* Effects of mechanical stimulation on the biomechanics and histology of stem cell-collagen sponge constructs for rabbit patellar tendon repair. *Tissue Eng.* **12,** 2291–300 (2006).

40. Shen, W. *et al.* The effect of incorporation of exogenous stromal cell-derived factor-1 alpha within a knitted silk-collagen sponge scaffold on tendon regeneration. *Biomaterials* **31,** 7239–49 (2010).

41. Longo, U. G., Lamberti, A., Maffulli, N. & Denaro, V. Tendon augmentation grafts: a systematic review. *Br. Med. Bull.* **94,** 165–88 (2010).

42. Derwin, K. a, Badylak, S. F., Steinmann, S. P. & Iannotti, J. P. Extracellular matrix scaffold devices for rotator cuff repair. *J. Shoulder Elbow Surg.* **19,** 467–76 (2010).

43. Kishore, V., Bullock, W., Sun, X., Van Dyke, W. S. & Akkus, O. Tenogenic differentiation of human MSCs induced by the topography of electrochemically aligned collagen threads. *Biomaterials* **33,** 2137–44 (2012).

44. Nair, L. & Laurencin, C. Biodegradable polymers as biomaterials. *Prog. Polym. Sci.* **32,** 762–798 (2007).

45. Cao, Y. *et al.* Bridging tendon defects using autologous tenocyte engineered tendon in a hen model. *Plast. Reconstr. Surg.* **110,** 1280–9 (2002).

46. Sahoo, S., Ouyang, H., Goh, J. C.-H., Tay, T. E. & Toh, S. L. Characterization of a novel polymeric scaffold for potential application in tendon/ligament tissue engineering. *Tissue Eng.* **12,** 91–9 (2006).

47. Xie, J. *et al.* "Aligned-to-random" nanofiber scaffolds for mimicking the structure of the tendon-to-bone insertion site. *Nanoscale* **2,** 923–6 (2010).

48. Cooper, J. a *et al.* Biomimetic tissue-engineered anterior cruciate ligament replacement. *Proc. Natl. Acad. Sci. U. S. A.* **104,** 3049–54 (2007).

49. Petrigliano, F. a *et al.* The effects of local bFGF release and uniaxial strain on cellular adaptation and gene expression in a 3D environment: implications for ligament tissue engineering. *Tissue Eng.* **13,** 2721–31 (2007).

50. Ma, B., Xie, J., Jiang, J., Shuler, F. D. & Bartlett, D. E. Rational design of nanofiber scaffolds for orthopedic tissue repair and regeneration. *Nanomedicine (Lond).* **8,** 1459–81 (2013).

51. Downes, S. & Bosworth, L. A. Tissue Repair Scaffold. (2010).

52. Yokoya, S. *et al.* Rotator cuff regeneration using a bioabsorbable material with bone marrow-derived mesenchymal stem cells in a rabbit model. *Am. J. Sports Med.* **40,** 1259–68 (2012).

53. Yin, Z. *et al.* The regulation of tendon stem cell differentiation by the alignment of nanofibers. *Biomaterials* **31,** 2163–75 (2010).

54. Erisken, C., Zhang, X., Moffat, K. L., Levine, W. N. & Lu, H. H. Scaffold fiber diameter regulates human tendon fibroblast growth and differentiation. *Tissue Eng. Part A* **19,** 519–28 (2013).

55. Hayami, J. W. S., Surrao, D. C., Waldman, S. D. & Amsden, B. G. Design and characterization of a biodegradable composite scaffold for ligament tissue engineering. *J. Biomed. Mater. Res. A* **92,** 1407–20 (2010).

56. Xu, Y. *et al.* Fabrication of electrospun poly(L-lactide-co-ε-caprolactone)/collagen nanoyarn network as a novel, three-dimensional, macroporous, aligned scaffold for tendon tissue engineering. *Tissue Eng. Part C. Methods* **19,** 925–36 (2013).

57. Sahoo, S., Toh, S. L. & Goh, J. C. H. A bFGF-releasing silk/PLGA-based biohybrid scaffold for ligament/tendon tissue engineering using mesenchymal progenitor cells. *Biomaterials* **31,** 2990–8 (2010).

58. James, R., Kumbar, S. G., Laurencin, C. T., Balian, G. & Chhabra, a B. Tendon tissue engineering: adipose-derived stem cell and GDF-5 mediated regeneration using electrospun matrix systems. *Biomed. Mater.* **6,** 025011 (2011).

59. Chainani, A. *et al.* Multilayered electrospun scaffolds for tendon tissue engineering. *Tissue Eng. Part A* **19,** 2594–604 (2013).

60. Agarwal, S., Wendorff, J. H. & Greiner, A. Progress in the field of electrospinning for tissue engineering applications. *Adv. Mater.* **21,** 3343–51 (2009).

61. Beachley, V. & Wen, X. Polymer nanofibrous structures: Fabrication, biofunctionalization, and cell interactions. *Prog. Polym. Sci.* **35,** 868–892 (2010).

62. Bayer, M. L. *et al.* Release of tensile strain on engineered human tendon tissue disturbs cell adhesions, changes matrix architecture, and induces an inflammatory phenotype. *PLoS One* **9,** e86078 (2014).

63. Subramony, S. D. *et al.* The guidance of stem cell differentiation by substrate alignment and mechanical stimulation. *Biomaterials* **34,** 1942–53 (2013).

64. Riehl, B. D., Park, J.-H., Kwon, I. K. & Lim, J. Y. Mechanical stretching for tissue engineering: two-dimensional and three-dimensional constructs. *Tissue Eng. Part B. Rev.* **18,** 288–300 (2012).

65. Dormer, N. H., Berkland, C. J. & Detamore, M. S. Emerging techniques in stratified designs and continuous gradients for tissue engineering of interfaces. *Ann. Biomed. Eng.* **38,** 2121–41 (2010).

66. Moffat, K. L., Wang, I.-N. E., Rodeo, S. a & Lu, H. H. Orthopedic interface tissue engineering for the biological fixation of soft tissue grafts. *Clin. Sports Med.* **28,** 157–76 (2009).

67. Farnebo, S., Woon, C. Y., Kim, M., Pham, H. & Chang, J. Reconstruction of the tendon-bone insertion with decellularized tendon-bone composite grafts: comparison with conventional repair. *J. Hand Surg. Am.* **39,** 65–74 (2014).

68. Spalazzi, J. P. *et al.* In vivo evaluation of a multiphased scaffold designed for orthopaedic interface tissue engineering and soft tissue-to-bone integration. *J. Biomed. Mater. Res. A* **86,** 1–12 (2008).

69. Seidi, A., Ramalingam, M., Elloumi-Hannachi, I., Ostrovidov, S. & Khademhosseini, A. Gradient biomaterials for soft-to-hard interface tissue engineering. *Acta Biomater.* **7,** 1441–51 (2011).

70. Singh, M., Berkland, C. & Detamore, M. S. Strategies and applications for incorporating physical and chemical signal gradients in tissue engineering. *Tissue Eng. Part B. Rev.* **14,** 341–66 (2008).

71. Smith, L., Xia, Y., Galatz, L. M., Genin, G. M. & Thomopoulos, S. Tissue-engineering strategies for the tendon/ligament-to-bone insertion. *Connect. Tissue Res.* **53,** 95–105 (2012).

72. Lu, H. H. & Thomopoulos, S. Functional attachment of soft tissues to bone: development, healing, and tissue engineering. *Annu. Rev. Biomed. Eng.* **15,** 201–26 (2013).

73. Zhang, X., Bogdanowicz, D., Erisken, C., Lee, N. M. & Lu, H. H. Biomimetic scaffold design for functional and integrative tendon repair. *J. Shoulder Elbow Surg.* **21,** 266–77 (2012).

74. Seidi, A. & Ramalingam, M. Impact of Gradient Biomaterials on Interface Tissue Engineering. *J. Biomater. Tissue Eng.* **2,** 89–99 (2012).

75. Ker, E. D. F. *et al.* Engineering spatial control of multiple differentiation fates within a stem cell population. *Biomaterials* **32,** 3413–3422 (2011).

76. Sharma, R. I. & Snedeker, J. G. Biochemical and biomechanical gradients for directed bone marrow stromal cell differentiation toward tendon and bone. *Biomaterials* **31,** 7695–7704 (2010).

77. Zhu, Y., Mao, Z. & Gao, C. Control over the gradient differentiation of rat BMSCs on a PCL membrane with surface-immobilized alendronate gradient. *Biomacromolecules* **14,** 342–9 (2013).

78. Spalazzi, J. P., Doty, S. B., Moffat, K. L., Levine, W. N. & Lu, H. H. Development of controlled matrix heterogeneity on a triphasic scaffold for orthopedic interface tissue engineering. *Tissue Eng.* **12,** 3497–508 (2006).

79. Wang, I. E. *et al.* Role of Osteoblast – Fibroblast Interactions in the Formation of the Ligament-to-Bone Interface. *J. Orthop. Res.* **25,** 1609–1620 (2007).

80. Ma, J. *et al.* Morphological and functional characteristics of three-dimensional engineered bone-ligament-bone constructs following implantation. *J. Biomech. Eng.* **131,** 101017 (2009).

81. Lee, J. *et al.* Enhanced regeneration of the ligament-bone interface using a poly(L-lactide-co-ε-caprolactone) scaffold with local delivery of cells/BMP-2 using a heparin-based hydrogel. *Acta Biomater.* **7,** 244–57 (2011).

82. O'Shea, T. M. & Miao, X. Bilayered scaffolds for osteochondral tissue engineering. *Tissue Eng. Part B. Rev.* **14,** 447–64 (2008).

83. Keeney, M. & Pandit, A. The osteochondral junction and its repair via bi-phasic tissue engineering scaffolds. *Tissue Eng. Part B. Rev.* **15,** 55–73 (2009).

84. Tampieri, A. *et al.* Design of graded biomimetic osteochondral composite scaffolds. *Biomaterials* **29,** 3539–46 (2008).

85. Xie, J., Ma, B., Michael, P. L. & Shuler, F. D. Fabrication of nanofiber scaffolds with gradations in fiber organization and their potential applications. *Macromol. Biosci.* **12,** 1336–41 (2012).

86. Bonani, W., Motta, A., Migliaresi, C. & Tan, W. Biomolecule gradient in micropatterned nanofibrous scaffold for spatiotemporal release. *Langmuir* **28,** 13675–87 (2012).

87. Liverani, L. *et al.* Simple fabrication technique for multilayered stratified composite scaffolds suitable for interface tissue engineering. *Mater. Sci. Eng. A* **557,** 54–58 (2012).

88. Erisken, C., Kalyon, D. M. & Wang, H. Functionally graded electrospun polycaprolactone and beta-tricalcium phosphate nanocomposites for tissue engineering applications. *Biomaterials* **29,** 4065–73 (2008).

89. Ozkan, S., Kalyon, D. M., Yu, X., McKelvey, C. a & Lowinger, M. Multifunctional protein-encapsulated polycaprolactone scaffolds: fabrication and in vitro assessment for tissue engineering. *Biomaterials* **30,** 4336–47 (2009).

90. Dormer, N. H. *et al.* Osteochondral interface regeneration of the rabbit knee with macroscopic gradients of bioactive signals. *J. Biomed. Mater. Res. A* **100,** 162–70 (2012).

91. Li, X. *et al.* Nanofiber scaffolds with gradations in mineral content for mimicking the tendon-to-bone insertion site. *Nano Lett.* **9,** 2763–8 (2009).

92. Samavedi, S., Guelcher, S. A., Goldstein, A. S. & Whittington, A. R. Response of bone marrow stromal cells to graded co-electrospun scaffolds and its

implications for engineering the ligament-bone interface. *Biomaterials* **33,** 7727–35 (2012).

93. Kolluru, P. V *et al.* Strong and tough mineralized PLGA nanofibers for tendon-to-bone scaffolds. *Acta Biomater.* **9,** 9442–50 (2013).

94. Vepari, C. P. & Kaplan, D. L. Covalently immobilized enzyme gradients within three-dimensional porous scaffolds. *Biotechnol. Bioeng.* **93,** 1130–7 (2006).

95. Lee, K., Silva, E. A. & Mooney, D. J. Growth factor delivery-based tissue engineering: general approaches and a review of recent developments. *J. R. Soc. Interface* (2010). doi:10.1098/rsif.2010.0223

96. Yoo, H. S., Kim, T. G. & Park, T. G. Surface-functionalized electrospun nanofibers for tissue engineering and drug delivery. *Adv. Drug Deliv. Rev.* **61,** 1033–42 (2009).

97. Casper, C. L., Yamaguchi, N., Kiick, K. L. & Rabolt, J. F. Functionalizing electrospun fibers with biologically relevant macromolecules. *Biomacromolecules* **6,** 1998–2007 (2005).

98. Gentsch, R. *et al.* Modular Approach toward Bioactive Fiber Meshes Carrying Oligosaccharides. *Macromolecules* **43,** 9239–9247 (2010).

99. Sun, X.-Y., Shankar, R., Börner, H. G., Ghosh, T. K. & Spontak, R. J. Field-Driven Biofunctionalization of Polymer Fiber Surfaces during Electrospinning. *Adv. Mater.* **19,** 87–91 (2007).

100. Gentsch, R. *et al.* Single-Step Electrospinning to Bioactive Polymer Nanofibers. *Macromolecules* **44,** 110110072713076 (2011).

101. Yoo, H. S., Kim, T. G. & Park, T. G. Surface-functionalized electrospun nanofibers for tissue engineering and drug delivery. *Adv. Drug Deliv. Rev.* **61,** 1033–42 (2009).

102. Croll, T. I., O'Connor, A. J., Stevens, G. W. & Cooper-White, J. J. Controllable surface modification of poly(lactic-co-glycolic acid) (PLGA) by hydrolysis or aminolysis I: physical, chemical, and theoretical aspects. *Biomacromolecules* **5,** 463–73 (2004).

103. Delaittre, G., Greiner, A. M., Pauloehrl, T., Bastmeyer, M. & Barner-Kowollik, C. Chemical approaches to synthetic polymer surface biofunctionalization for targeted cell adhesion using small binding motifs. *Soft Matter* **8,** 7323 (2012).

104. Zhu, Y., Gao, C., Liu, X. & Shen, J. Surface modification of polycaprolactone membrane via aminolysis and biomacromolecule immobilization for

promoting cytocompatibility of human endothelial cells. *Biomacromolecules* **3,** 1312–9 (2002).

105. Gough, J. E., Scotchford, C. a & Downes, S. Cytotoxicity of glutaraldehyde crosslinked collagen/poly(vinyl alcohol) films is by the mechanism of apoptosis. *J. Biomed. Mater. Res.* **61,** 121–30 (2002).

106. Chang, K.-Y., Hung, L.-H., Chu, I.-M., Ko, C.-S. & Lee, Y.-D. The application of type II collagen and chondroitin sulfate grafted PCL porous scaffold in cartilage tissue engineering. *J. Biomed. Mater. Res. A* **92,** 712–23 (2010).

107. Sun, H. & Onneby, S. Facile polyester surface functionalization via hydrolysis and cell-recognizing peptide attachment. *Polym. Int.* **55,** 1336–1340 (2006).

108. Hartman, O. *et al.* Biofunctionalization of electrospun PCL-based scaffolds with perlecan domain IV peptide to create a 3-D pharmacokinetic cancer model. *Biomaterials* **31,** 5700–18 (2010).

109. Zhang, H., Migneco, F., Lin, C. & Hollister, S. J. Chemically-conjugated bone morphogenetic protein-2 on three-dimensional polycaprolactone scaffolds stimulates osteogenic activity in bone marrow stromal cells. *Tissue Eng. Part A* **16,** 3441–8 (2010).

110. Zhang, H., Lin, C.-Y. & Hollister, S. J. The interaction between bone marrow stromal cells and RGD-modified three-dimensional porous polycaprolactone scaffolds. *Biomaterials* **30,** 4063–9 (2009).

111. El Habnouni, S. *et al.* Toward potent antibiofilm degradable medical devices: a generic method for the antibacterial surface modification of polylactide. *Acta Biomater.* **9,** 7709–18 (2013).

112. Dunlop, I. E. *et al.* Interactions Between Polymer Brushes: Varying the Number of End-Attaching Groups. *Macromol. Chem. Phys.* **205,** 2443–2450 (2004).

113. Borner, H. G., Kuhnle, H. & Hentschel, J. Making "' Smart Polymers '" Smarter : Modern Concepts to Regulate Functions in Polymer Science. *J. Polym. Sci. Part A Polym. Chem.* **48,** 1–14 (2010).

114. Ju, Y. M. *et al.* Beneficial effect of hydrophilized porous polymer scaffolds in tissue-engineered cartilage formation. *J. Biomed. Mater. Res. B. Appl. Biomater.* **85,** 252–60 (2008).

115. Yao, C., Li, X., Neoh, K. G., Shi, Z. & Kang, E. T. Surface modification and antibacterial activity of electrospun polyurethane fibrous membranes with quaternary ammonium moieties. *J. Memb. Sci.* **320,** 259–267 (2008).

116. Klein Gunnewiek, M. *et al.* Thin polymer brush decouples biomaterial's micro-/nanotopology and stem cell adhesion. *Langmuir* **29,** 13843–52 (2013).

117. Hou, J. *et al.* Aqueous-based immobilization of initiator and surface-initiated ATRP to construct hemocompatible surface of poly (styrene-b-(ethylene-co-butylene)-b-styrene) elastomer. *Colloids Surf. B. Biointerfaces* **111C,** 333–341 (2013).

118. Yuan, W. *et al.* Hemocompatible surface of electrospun nanofibrous scaffolds by ATRP modification. *Mater. Sci. Eng. C. Mater. Biol. Appl.* **33,** 3644–51 (2013).

119. Qian, X., Fan, H., Wang, C. & Wei, Y. Preparation of high-capacity, weak anion-exchange membranes by surface-initiated atom transfer radical polymerization of poly(glycidyl methacrylate) and subsequent derivatization with diethylamine. *Appl. Surf. Sci.* **271,** 240–247 (2013).

120. Jiang, H. & Xu, F.-J. Biomolecule-functionalized polymer brushes. *Chem. Soc. Rev.* **42,** 3394–426 (2013).

121. Yuan, L., Wei, W. & Liu, S. Label-free electrochemical immunosensors based on surface-initiated atom radical polymerization. *Biosens. Bioelectron.* **38,** 79–85

122. Wang, X. *et al.* Preparation of a novel immunosensor for tumor biomarker detection based on ATRP technique. *J. Mater. Chem. B* **1,** 2132 (2013).

123. Chen, W. *et al.* Strategy for the Modification of Electrospun Fibers that Allows Diverse Functional Groups for Biomolecular Entrapment. *Chem. Mater.* **22,** 6212–6214 (2010).

124. Yao, F., Xu, L., Lin, B. & Fu, G.-D. Preparation and applications of functional nanofibers based on the combination of electrospinning, controlled radical polymerization and "Click Chemistry". *Nanoscale* **2,** 1348–57 (2010).

125. Jeong, S. I. *et al.* Preparation and Characterization of Temperature-Sensitive Poly(N-isopropylacrylamide)-g-Poly(L-lactide-co-ε-caprolactone) Nanofibers. *Macromol. Res.* **16,** 139–148 (2008).

126. Hu, Y., Zhao, N. N., Li, J. S., Yang, W. T. & Xu, F. J. Temperature-responsive porous polycaprolactone-based films via surface-initiated ATRP for protein delivery. *J. Mater. Chem.* **22,** 21257 (2012).

127. Klein Gunnewiek, M. *et al.* Controlled Surface Initiated Polymerization of N-Isopropylacrylamide from Polycaprolactone Substrates for Regulating Cell Attachment and Detachment. *Isr. J. Chem.* **52,** 339–346 (2012).

128. Barbey, R., Kauffmann, E., Ehrat, M. & Klok, H.-A. Protein microarrays based on polymer brushes prepared via surface-initiated atom transfer radical polymerization. *Biomacromolecules* **11,** 3467–79 (2010).

129. Iwasaki, Y., Omichi, Y. & Iwata, R. Site-specific dense immobilization of antibody fragments on polymer brushes supported by silicone nanofilaments. *Langmuir* **24,** 8427–30 (2008).

130. Rao, S. V., Anderson, K. W. & Bachas, L. G. Oriented immobilization of proteins. *Mikrochim. Acta* **128,** 127–143 (1998).

131. Bergan, John J., M. D. *et al.* Chronic venous disease. *N. Engl. J. Med.* **355,** 488–498 (2006).

132. Beckman, J. a. Diseases of the Veins. *Circulation* **106,** 2170–2172 (2002).

133. Teebken, O. E. *et al.* Preclinical development of tissue-engineered vein valves and venous substitutes using re-endothelialised human vein matrix. *Eur. J. Vasc. Endovasc. Surg.* **37,** 92–102 (2009).

134. Wei, Z., Liu, C., Zhou, M. & Qiao, W. [Comparison between canine decellularized venous valve stent combined with endothelial progenitor cells and native venous valve on venous valve closure mechanism in normal physiological conditions]. *Chinese J. reparative Reconstr. Surg.* **23,** 1260–3 (2009).

135. Buttafoco, L. *et al.* Electrospinning of collagen and elastin for tissue engineering applications. *Biomaterials* **27,** 724–34 (2006).

136. Stitzel, J. *et al.* Controlled fabrication of a biological vascular substitute. *Biomaterials* **27,** 1088–94 (2006).

137. Balguid, A. *et al.* Tailoring fiber diameter in electrospun poly(epsilon-caprolactone) scaffolds for optimal cellular infiltration in cardiovascular tissue engineering. *Tissue Eng. Part A* **15,** 437–44 (2009).

138. Liu, P.-S., Chen, Q., Wu, S.-S., Shen, J. & Lin, S.-C. Surface modification of cellulose membranes with zwitterionic polymers for resistance to protein adsorption and platelet adhesion. *J. Memb. Sci.* **350,** 387–394 (2010).

139. Yan, L. & Ishihara, K. Graft copolymerization of 2-methacryloyloxyethyl phosphorylcholine to cellulose in homogeneous media using atom transfer radical polymerization for providing new hemocompatible coating materials. *J. Polym. Sci. Part A Polym. Chem.* **46,** 3306–3313 (2008).

140. Edmondson, S., Nguyen, N. T., Lewis, A. L. & Armes, S. P. Co-nonsolvency effects for surface-initiated poly(2-(methacryloyloxy)ethyl phosphorylcholine) brushes in alcohol/water mixtures. *Langmuir* **26,** 7216–26 (2010).

141. Morse, A. J. *et al.* Biocompatible polymer brushes grown from model quartz fibres: synthesis, characterisation and in situ determination of frictional coefficient. *Soft Matter* **6,** 1571 (2010).

142. Chen, B., Pernodet, N., Rafailovich, M. H., Bakhtina, A. & Gross, R. a. Protein immobilization on epoxy-activated thin polymer films: effect of surface wettability and enzyme loading. *Langmuir* **24,** 13457–64 (2008).

143. Elwing, H. Protein absorption and ellipsometry in biomaterial research. *Biomaterials* **19,** 397–406 (1998).

144. Follows, D. *et al.* Co-adsorption of β-casein and calcium phosphate nanoclusters (CPN) at hydrophilic and hydrophobic solid–solution interfaces studied by neutron reflectometry. *Food Hydrocoll.* **25,** 724–733 (2011).

145. Li, D. & Xia, Y. Electrospinning of Nanofibers: Reinventing the Wheel? *Adv. Mater.* **16,** 1151–1170 (2004).

146. Yan, M., Bartlett, M. & Hamish, B. UV Induced Attachment of Ultrathin Polymer Films on Silicon Wafers. in *8th Int. Symp. Adv. Packag. Mater.* 311–316 (2002).

147. *Handbook of Ellipsometry*. (Springer, 2005).

148. Hecht, E. *Optics*. (Addison Wesley Longman, Inc., 1998).

149. Baker, B. M. *et al.* The potential to improve cell infiltration in composite fiber-aligned electrospun scaffolds by the selective removal of sacrificial fibers. *Biomaterials* **29,** 2348–58 (2008).

150. Schubert, D. W. & Dunkel, T. Spin coating from a molecular point of view: its concentration regimes, influence of molar mass and distribution. *Mater. Res. Innov.* **7,** 314–321 (2003).

151. Rozlosnik, N., Gerstenberg, M. C. & Larsen, N. B. Effect of Solvents and Concentration on the Formation of a Self-Assembled Monolayer of Octadecylsiloxane on Silicon (001). *Langmuir* **19,** 1182–1188 (2003).

152. Fragneto, G., Thomas, R. K., Rennie, a R. & Penfold, J. Neutron reflection study of bovine beta-casein adsorbed on OTS self-assembled monolayers. *Science* **267,** 657–60 (1995).

153. Okerberg, B. C. *et al.* Competition between crystallization and dewetting fronts in thin polymer films. *Soft Matter* **5,** 562 (2009).

154. Gelest. Silane Coupling Agents: Connecting Across Boundaries. (2006).

155. Wasserman, S. R., Tao, Y. T. & Whitesides, G. M. Structure and reactivity of alkylsiloxane monolayers formed by reaction of alkyltrichlorosilanes on silicon substrates. *Langmuir* **5,** 1074–1087 (1989).

156. Hermanson, G. T. Bioconjugation techniques. *Acad. Press* **10,** 0123705010 (2008).

157. Hennessy, K. M. *et al.* The effect of collagen I mimetic peptides on mesenchymal stem cell adhesion and differentiation, and on bone formation at hydroxyapatite surfaces. *Biomaterials* **30,** 1898–909 (2009).

158. Culpepper, B. K., Bonvallet, P. P., Reddy, M. S., Ponnazhagan, S. & Bellis, S. L. Polyglutamate directed coupling of bioactive peptides for the delivery of osteoinductive signals on allograft bone. *Biomaterials* **34,** 1506–13 (2013).

159. ZUIDEMA, J., HILBERSMODDERMAN, E. & MERKUS, F. CLINICAL PHARMACOKINETICS OF DAPSONE. *Clin. Pharmacokinet.* **11,** 299–315

160. Suárez, P., Rojo, L., González-Gómez, Á. & Román, J. S. Self-assembling gradient copolymers of vinylimidazol and (acrylic)ibuprofen with anti-inflammatory and zinc chelating properties. *Macromol. Biosci.* **13,** 1174–84 (2013).

161. Janoschka, T., Teichler, A., Krieg, A., Hager, M. D. & Schubert, U. S. Polymerization of free secondary amine bearing monomers by RAFT polymerization and other controlled radical techniques. *J. Polym. Sci. Part A Polym. Chem.* **50,** 1394–1407 (2012).